JAERI-Data/Code
2001-015

THE GEM CODE — A SIMULATION PROGRAM FOR THE EVAPORATION AND THE FISSION PROCESS OF AN EXCITED NUCLEUS —

March 2001

Shiori FURIHATA*, Koji NIITA*, Shin-ichiro MEIGO,
Yujiro IKEDA and Fujio MAEKAWA

日本原子力研究所
Japan Atomic Energy Research Institute

本レポートは、日本原子力研究所が不定期に公刊している研究報告書です。
入手の問合わせは、日本原子力研究所研究情報部研究情報課（〒319-1195　茨城県那珂郡東海村）あて、お申し越し下さい。なお、このほかに財団法人原子力弘済会資料センター（〒319-1195　茨城県那珂郡東海村日本原子力研究所内）で複写による実費頒布を行っております。

This report is issued irregularly.
Inquiries about availability of the reports should be addressed to Research Information Division, Department of Intellectual Resources, Japan Atomic Energy Research Institute, Tokai-mura, Naka-gun, Ibaraki-ken 〒319-1195, Japan.

編集兼発行　日本原子力研究所

JAERI−Data/Code 2001−015

The GEM Code – A Simulation Program for the Evaporation and the Fission Process of an Excited Nucleus –

Shiori FURIHATA*, Koji NIITA**, Shin-ichiro MEIGO, Yujiro IKEDA and Fujio MAEKAWA

Center for Neutron Science
Tokai Research Establishment
Japan Atomic Energy Research Institute
Tokai-mura, Naka-gun, Ibaraki-ken

(Received February 5, 2001)

The GEM code is a simulation program which describes the de-excitation process of an excited nucleus, which is based on the Generalized Evaporation Model and the Atchison fission model. It has been shown that the combination of the Bertini intranuclear cascade model and GEM accurately predicts the cross sections of light fragments, such as Be produced from the proton-induced reactions. It has also been shown that the use of the reevaluated parameters in the Atchison model improves predictions of cross sections of fission fragments produced from the proton-induced reaction on Au.

In this report, we present details and the usage of the GEM code. Furthermore, the results of benchmark calculations are shown by using the combination of the Bertini intranuclear cascade model and the GEM code (INC/GEM). Neutron spectra and isotope production cross sections from the reactions on various targets irradiated by protons are calculated with INC/GEM. Those results are compared with experimental data as well as the calculation results with LAHET. INC/GEM reproduces the experiments of double differential neutron emissions from the reaction on Al and Pb. The isotopic distributions for He, Li, and Be produced from the reaction on Ag are in good agreement with experimental data within 50%, although INC/GEM underestimates those of heavier nuclei than O. It is also shown that the predictions with INC/GEM for isotope production of light fragments, such as Li and Be, are better than those calculation with LAHET, particularly for heavy target. INC/GEM also gives better estimates of the cross sections of fission products than LAHET.

Keywords: GEM Code, Evaporation, High Energy Fission,
Light Fragment Productions, Proton-induced Reactions

*Mitsubishi Research Institute Inc.
**Research Organization for Information Science and Technology

JAERI－Data/Code 2001－015

GEM コード
－蒸発および核分裂過程シミュレーション計算コード－

日本原子力研究所東海研究所中性子科学研究センター
降旗 志おり*・仁井田 浩二**・明午 伸一郎・池田 裕二郎・前川 藤夫

(2001 年 2 月 5 日 受理)

GEM コードは励起原子核の脱励起を記述するシミュレーションプログラムである．このコードは GEM (Generalized Evaporation Model) と Atchison の核分裂モデルから成り立つ．Bertini の核内カスケードモデルと GEM とを組み合わせた計算モデルにより，陽子入射における Be のような軽いフラグメント生成断面積を精度良く予測できることが示された．また，Atchison モデルに使用されているパラメータを再評価することにより，Au に陽子を入射する場合に生成する核分裂片の断面積を改善することが示された．

本レポートでは，GEM コードの詳細と使用方法について記述し，Bertini 核内カスケードモデルと GEM コード組み合わせた計算 (INC/GEM) によるベンチマーク計算の結果を示す．様々なターゲットに陽子を照射した場合における中性子スペクトルおよび同位体生成断面積を INC/GEM を用いて計算した．これらの計算結果を実験値と比較するとともに，LAHET による計算結果との比較も行った．その結果 INC/GEM による計算は，Al と Pb の中性子放出の二重微分断面積の実験値を再現することがわかった．Ag から生成される同位体は O より重いフラグメントの生成が過小評価されるものの，He, Li, Be の生成については 50 %以内で実験と良い一致を示すことがわかった．また，Li や Be 等の軽核の生成断面積は，特に重いターゲット核において LAHET による計算結果より良い一致を示すことがわかった．さらに，INC/GEM による計算は LAHET による計算よりも核分裂片生成断面積の予測精度が良いことが示された．

東海研究所：〒 319-1195 茨城県那珂郡東海村白方白根 2-4
*(株) 三菱総合研究所
**(財) 高度情報科学技術研究機構

Contents

目次

1 Introduction

The GEM code is a simulation program for an evaporation and a fission process of an excited nucleus. The code is based on the Furihata's generalized evaporation model[1] and the Atchison's fission model.

The generalized evaporation model [1] is based on the Weisskopf-Ewing model [2]. The model is similar to the Dostrovsky's evaporation model [3] except that: (1) it is assumed that 66 nuclides up to Mg, not only in their ground states but also in their excited states, can be emitted from an excited nucleus during evaporation process; (2) the accurate level density function is used instead of an approximate expression for deriving the decay width of a particle emission. It has been shown [1] that the estimates of ^{7}Be produced from proton induced reactions are drastically improved by the use of GEM in the simulation instead of EVAP [4] subsequent to intranuclear cascade calculations.

GEM includes as user options two parameter sets for the Atchison's fission model. One is the original parameter set of mass, charge, and kinetic energy distributions of fission fragments derived by Atchison. And the other is the parameter set evaluated by Furihata [5]. The use of the Furihata's parameter set in the Atchison model improves predictions of cross sections for fission fragments produced from the proton-induced reaction on Au [5].

In this report, we present details of GEM and determine the capability of the code. Section 2 describes details of the generalized evaporation model and parameters used in the model. The section also contains the description of the Atchison's fission model and the parameter set derived by Furihata. In section 3, benchmark calculations of neutron spectra, isotopic distributions, and activation yields produced from proton induced reaction are presented. Since GEM simply simulates a decaying process of an excited nucleus, we use the Bertini intranuclear cascade model implemented in LAHET [6] for first non-equilibrium stage of the interaction, to simulate whole reaction. The estimates are compared with experimental data as well as those calculated using LAHET. The user's manual of GEM is shown in section 4.

2 The Models

2.1 Generalized Evaporation Model

2.1.1 Decay Width

The generalized evaporation model proposed by Furihata [1] is based on the Weisskopf-Ewing's formulation [2]. According to the formulation, the decay probability P_j for the emission of a particle j from a parent nucleus i with total kinetic energy in the center-of-mass system between ϵ and $\epsilon + \mathrm{d}\epsilon$ is

$$P_j(\epsilon)d\epsilon = g_j\sigma_{inv}(\epsilon)\frac{\rho_d(E-Q-\epsilon)}{\rho_i(E)}\epsilon d\epsilon, \tag{1}$$

where E[MeV] is excitation energy of a parent nucleus i with mass A_i charge Z_i, and d denotes a daughter nucleus with mass A_d and charge Z_d produced after the emission of ejectile j with mass A_ji and charge Z_j in its ground state; σ_{inv} is the cross section for the inverse reaction, ρ_i and ρ_d are level densities [MeV^{-1}] of the parent and the daughter nucleus, respectively; g_j is expressed as $g_j = (2S_j+1)m_j/\pi^2\hbar^2$, with the spin S_j and the mass m_j of the emitted particle j; The Q-value is calculated using the excess mass $M(A,Z)$ as $Q = M(A_j,Z_j)+M(A_d,Z_d)-M(A_i,Z_i)$. In GEM, four mass tables are used to calculate Q-values, according to the following priority: (1) Audi-Wapstra's mass table [7]; (2) theoretical masses calculated by Moller *et al.* [8]; (3) theoretical masses calculated Comay *et al.* [9]; (4) the excess mass calculated by using Cameron's formula. Cameron's mass formula is expressed as:

$$M(A,Z) = 8.071323A - 0.782354Z + E_v + E_s + E_c + E_{ex} + S,$$

where E_v, E_s, E_c, E_{ex} are the volume energy, the symmetry energy, the Coulomb energy, and the Coulomb exchange energy given by the following expressions:

$$\begin{aligned}
E_v &= -17.0354A(1 - 1.84619\frac{(A-2Z)^2}{A^2},) \\
E_s &= 25.8357A^{2/3}\left(1 - 1.71219\frac{(A-2Z)^2}{A^2}\right)\left(1 - \frac{0.62025}{A^{2/3}}\right)^2, \\
E_c &= 0.779\frac{Z(Z-1)}{A^{1/3}}\left(1 - \frac{1.5849}{A^{2/3}} + \frac{1.2273}{A} + \frac{1.5772}{A^{4/3}}\right), \\
E_{ex} &= -0.4323\frac{Z^{4/3}}{A^{1/3}}\left(1 - \frac{0.57811}{A^{1/3}} - \frac{0.14518}{A^{2/3}} + \frac{0.49597}{A}\right).
\end{aligned}$$

The shell correction S is expressed as a sum of separate contributions from neutrons and protons, i.e., $S = S(Z_d) + S(N_d)$ listed in Table 1.

The cross section for the inverse reaction σ_{inv} is expressed as

$$\sigma_{inv}(\epsilon) = \begin{cases} \sigma_g c_n\,(1 + b/\epsilon) & \text{for neutrons} \\ \sigma_g c_j\,(1 - V/\epsilon) & \text{for charged particles} \end{cases} \equiv \sigma_g\alpha\left(1 + \frac{\beta}{\epsilon}\right), \tag{2}$$

where $\sigma_g = \pi {R_b}^2$ [fm^2] is the geometric cross section, and $V = k_j Z_j Z_d e^2/R_c$ [MeV] is the Coulomb barrier. GEM includes two options for the parameter set of c_n, b, c_j, k_j, R_b, and R_c. The choices will be described in section 2.1.4.

The total decay width Γ_j can be calculated by integrating Eq. (1) with respect to the total kinetic energy ϵ from the Coulomb barrier V up to the maximum possible value $(E-Q)$. By using Eq. (2) for σ_{inv}, the total decay width for the particle emission is expressed as

$$\Gamma_j = \frac{g_j \sigma_g \alpha}{\rho_i(E)} \int_V^{E-Q} \epsilon \left(1 + \frac{\beta}{\epsilon}\right) \rho_d(E - Q - \epsilon) d\epsilon. \tag{3}$$

According to the Fermi-gas model, the total level density $\rho(E)$ is given by the expression [10]

$$\rho(E) = \begin{cases} \dfrac{\pi}{12} \dfrac{e^{2\sqrt{a(E-\delta)}}}{a^{1/4}(E-\delta)^{5/4}} & \text{for } E \geq E_x \\ \dfrac{\pi}{12} \dfrac{1}{T} e^{(E-E_0)/T} & \text{for } E < E_x \end{cases}, \tag{4}$$

where a [MeV^{-1}] is the level density parameter, and δ[MeV] is the pairing energy of the daughter nucleus. Gilbert and Cameron [10] determined E_x as $E_x = U_x + \delta$ where $U_x = 2.5 + 150/A_d$. The pairing energy δ is expressed as a sum of separate contributions from neutrons and protons, i.e. $\delta = P(Z_d) + P(N_d)$. In the code, the values by Cook *et al.* [11] are mainly used. For the values not evaluated by Cook *et al.* [11], those obtained by Gilbert and Cameron [10] are used. The paring energy $P(Z)$ and $P(N)$ are shown in Table 1. The nuclear temperature T is given by $1/T = \sqrt{a/U_x} - 1.5/U_x$, and E_0 is defined as $E_0 = E_x - T(\log T - 0.25 \log a - 1.25 \log U_x + 2\sqrt{aU_x})$.

By substituting Eq. (4) into Eq. (3), Eq. (3) is expressed as

$$\Gamma_j = \frac{\pi g_j \sigma_g \alpha}{12 \rho_i(E)} \begin{cases} \{I_1(t,t) + (\beta + V) I_0(t)\} & \text{for } E - Q - V < E_x \\ [I_1(t,t_x) + I_3(s,s_x) e^s + (\beta + V) \{I_0(t_x) + I_2(s,s_x) e^s\}] & \text{for } E - Q - V \geq E_x \end{cases} \tag{5}$$

where $t = (E - Q - V)/T$ and $t_x = E_x/T$, $s = 2\sqrt{a(E - Q - V - \delta)}$, and $s_x = 2\sqrt{a(E_x - \delta)}$. $I_0(t)$, $I_1(t, t_x)$, $I_2(s, s_x)$, and $I_3(s, s_x)$ are expressed as:

$$\begin{aligned}
I_0(t) &= e^{-E_0/T}(e^t - 1), \\
I_1(t,t_x) &= e^{-E_0/T} T \{(t - t_x + 1)e^{t_x} - t - 1)\}, \\
I_2(s,s_x) &= 2\sqrt{2} \left\{ s^{-3/2} + 1.5 s^{-5/2} + 3.75 s^{-7/2} - (s_x^{-3/2} + 1.5 s_x^{-5/2} + 3.75 s_x^{-7/2}) e^{s_x - s} \right\}, \\
I_3(s,s_x) &= (\sqrt{2}a)^{-1} \Big[2s^{-1/2} + 4s^{-3/2} + 13.5 s^{-5/2} + 60.0 s^{-7/2} + 325.125 s^{-9/2} - \Big\{ (s^2 - s_x^2) s_x^{-3/2} \\
&+ (1.5 s^2 + 0.5 s_x^2) s_x^{-5/2} + (3.75 s^2 + 0.25 s_x^2) s_x^{-7/2} + (12.875 s^2 + 0.625 s_x^2) s_x^{-9/2} \\
&+ (59.0625 s^2 + 0.9375 s_x^2) s_x^{-11/2} + (324.8 s^2 + 3.28 s_x^2) s_x^{-13/2} \Big\} e^{s_x - s} \Big].
\end{aligned}$$

In a Monte Carlo simulation, ejectile j is selected according to the probability distribution calculated as $p_j = \Gamma_j / \sum_j \Gamma_j$, where Γ_j is given by Eq. (5).

2.1.2 Kinetic Energy

The probability distribution of the total kinetic energy ϵ of an ejectile and a daughter nucleus is given by Eq. (1). Substituting Eq. (4) into Eq.(1), and normalizing yields

$$P_j(\epsilon) = \begin{cases} g_j \sigma_g \alpha(\epsilon+\beta) \dfrac{e^{(E-Q-\epsilon-E_0)/T}}{T} \dfrac{1}{\Gamma_j} & E-Q-E_x \le \epsilon \le E-Q \\ \\ g_j \sigma_g \alpha(\epsilon+\beta) \dfrac{e^{2\sqrt{a(E-Q-\delta-\epsilon)}}}{a^{1/4}(E-Q-\delta-\epsilon)^{5/4}} \dfrac{1}{\Gamma_j} & kV \le \epsilon \le E-Q-E_x \end{cases} . \quad (6)$$

The total kinetic energy ϵ is randomly chosen with respect to the probability given by Eq. (6). The direction of the motion $\boldsymbol{w}$ is randomly selected to be isotropic in the center of mass system. Then the excitation energy of the daughter nucleus is calculated as $E_d^* = E - Q - \epsilon$.

The kinetic energy of the ejectile in the laboratory system is calculated in the following manner: The momentum of the ejectile in the center of mass system $\boldsymbol{p_{cm}}$ is calculated by ϵ and the unit vector $\boldsymbol{w}$ of the direction of motion as

$$\boldsymbol{p_{cm}} = \boldsymbol{w}\sqrt{\epsilon^2 + \frac{2m_j m_d \epsilon}{m_j + m_d}}, \quad (7)$$

where m_j and m_d are the masses in MeV of the ejectile and the daughter nucleus, respectively. The momentum $\boldsymbol{p_j}'$ of the ejectile in the laboratory system are obtained by the Lorentz transformation as

$$\begin{aligned} \boldsymbol{p_j}' &= \boldsymbol{p_{cm}} + T_j \boldsymbol{V_i}, \\ \boldsymbol{p_d}' &= -\boldsymbol{p_{cm}} + T_d \boldsymbol{V_i}, \\ T_\ell &= \gamma\left\{\frac{\gamma}{\gamma+1}(\boldsymbol{p_{cm}}\cdot\boldsymbol{V_i}) + E_\ell\right\} \qquad \ell = j \text{ or } d, \end{aligned}$$

where $E_\ell = \sqrt{\boldsymbol{p_{cm}}^2 + m_\ell^2}$ ($\ell = j$ or d), $\gamma = 1/\sqrt{1-\boldsymbol{V_i}^2}$, and the velocity of the parent nucleus in the laboratory system $\boldsymbol{V_i} = \boldsymbol{u}\sqrt{E_r{}^2 + 2m_i E_r}/(E_r + m_i)$ with the recoil energy E_r of the parent nucleus and the direction of $\boldsymbol{u}$ (unit vector) in the laboratory system after the initial non-equilibrium stage. The kinetic energy in the laboratory system is calculated as $E_\ell' = \sqrt{\boldsymbol{p_\ell}'^2 + m_\ell^2}$ ($\ell = j$ or d).

2.1.3 Ejectiles

In GEM, 66 nuclides, not only in their ground states but also in their excited states, are treated as ejectiles. The selected ejectiles listed in Table 2 satisfy the following criteria: (1) isotopes with $Z_j \le 12$; (2) naturally existing isotopes or isotopes near the stability line; (3) isotopes with half-life longer than 1 ms.

If the mean lifetime of a resonance is longer than the decay width of the resonance emission, such a resonance can survive during the evaporation process. The excited state is included if its

half lifetime $T_{1/2}$ [sec] satisfies the following condition:

$$\frac{T_{1/2}}{\ln 2} > \frac{\hbar}{\Gamma_j^*}, \tag{8}$$

where Γ_j^* is the decay width of the resonance emission. Γ_j^* can be calculated in the same manner as for a ground state particle emission. The Q-value for the resonance emission is expressed as $Q^* = Q + E_j^*$, where E_j^* is the excitation energy of the resonance. The spin state of the resonance S_j^* is used in the calculation of g_j, instead of the spin of the ground state S_j. Although the mass of an excited state is different from that of the ground state, the ground state mass m_j is used, because the difference of the masses is negligible.

Instead of treating a resonance as an independent particle, the decay width of the ground state particle emission is simply enhanced. The decay width Γ_j is redefined as

$$\Gamma_j = \Gamma_j^0 + \sum_n \Gamma_j^n, \tag{9}$$

where Γ_j^0 is the decay width of the ground state particle j emission, and Γ_j^n is that of the nth excited state of the particle j emission which satisfies Eq. (8).

The total kinetic energy distribution of the excited particle emission is assumed to be the same as that of the ground state particle emission. S_j^*, E_j^*, and $T_{1/2}$ used in this study were extracted from the ENSDF database maintained by the National Nuclear Data Center [12].

2.1.4 Parameters of Coulomb Barrier and the Cross Section for Inverse Reaction

The cross section for inverse reaction σ_{inv} and the Coulomb barrier V are expressed as

$$\sigma_{inv}(\epsilon) = \begin{cases} \pi {R_b}^2 c_n (1 + b/\epsilon) & \text{for neutrons} \\ \pi {R_b}^2 c_j (1 - V/\epsilon) & \text{for charged particles} \end{cases}, \tag{10}$$

$$V = k_j \frac{Z_j Z_d e^2}{R_c}. \tag{11}$$

GEM includes two options for the parameter set in the above expressions. One is 'the simple parameter set', and the other is 'the precise parameter set'.

1. The simple parameter set
   The simple parameter set is given as $c_n = c_j = k_j = 1$, $b = 0$ and $R_b = R_c = r_0(A_j^{1/3} + A_d^{1/3})$ [fm]. User needs to input r_0.
2. The precise parameter set (default)
   The precise parameter set is the combination of parameters determined by Dostrovsky *et al.* [3] and Matsuse *et al.* [13]. Details are as follows:

   (a) For n, p, d, t, ^{3}He, and α emission
   Dostrovsky *et al.* [3] determined the parameters for n, p, d, t, ^{3}He, and α emissions by fitting the expression to the theoretical calculation done by Shapiro [14] and Blatt and

Weisskopf [15], so that the effect of overlapping wave functions was taken into account. The Dostrovsky's parameters are given as $c_n = 0.76 + 1.93A_d^{-1/3}$, $b = (1.66A_d^{-2/3} - 0.050)/(0.76+1.93A_d^{-1/3})$ (and $b = 0$ for $A_d \geq 192$), $c_p = 1+c$, $c_d = 1+c/2$, $c_t = 1+c/3$, $c_{^3\mathrm{He}} = c_\alpha = 0$, $k_p = k$, $k_d = k + 0.06$, $k_t = k + 0.12$, $k_{^3\mathrm{He}} = k_\alpha - 0.06$, where c, k, and k_α are listed in Table.3 for each Z_d. Between the Z_d values listed in Table.3, c_p, k_p, and k_α are interpolated linearly. The nuclear distances are given by $R_b = 1.5A_d^{1/3}$ for neutrons and protons, and $1.5(A_d^{1/3} + A_j^{1/3})$ for d, t, ^{3}He, and α. The nuclear distance for the Coulomb barrier is expressed as $R_c = R_d + R_j$ where $R_d = 1.7A^{1/3}$ and $R_j = 0$ for neutrons and protons, and $R_j = 1.2$ for d, t, ^{3}He, and α particles.

(b) For other particle emission

Matsuse *et al.* [13] analyzed the critical distance in the fusion reaction of heavy-ion systems. They compared the experimental and theoretical fusion cross sections, and determined the parameters as follows: $c_j = k = 1$, $R_b = R_0(A_j) + R_0(A_d) + 2.85$ [fm], $R_c = R_0(A_j) + R_0(A_d) + 3.75$ [fm], where $R_0(A) = 1.12A^{1/3} - 0.86A^{-1/3}$.

2.1.5 Level Density Parameter

GEM includes two options for the expression of the level density parameters a. One is the simple level density parameter, and the other is the Gilbert-Cameron-Cook-Ignatyuk(GCCI) level density parameter [16]. Details are as follows:

1. The simple level density parameter

   The simple level density parameter is given by $a = A_d/a_0$. User need to input a_0.

2. The GCCI level density parameter (default)

   For $Z_d \leq 98$ and $N_d \leq 150$, the GCCI level density parameter a[MeV^{-1}] is expressed as

$$a = \tilde{a}\frac{1-e^{-u}}{u} + a_I\left(1 - \frac{1-e^{-u}}{u}\right), \tag{12}$$

   where $u = 0.05(E-\delta)$, and

$$a_I = \left(0.1375 - 8.36\times10^{-5}A_d\right)\times A_d,$$

$$\tilde{a} = \begin{cases} A_d/8 & Z_d < 9 \text{ or } N_d < 9 \\ A_d(a' + 0.00917S) & \text{for others} \end{cases}.$$

   For deformed nuclei with $54 \leq Z_d \leq 78$, $86 \leq Z_d \leq 98$, $86 \leq N_d \leq 122$, or $130 \leq N_d \leq 150$, $a' = 0.12$ and $a' = 0.142$ for other nuclei. The shell correction S is expressed as a sum of separate contributions from neutrons and protons, i.e. $S = S(Z_d) + S(N_d)$. The shell corrections are tabulated in Table 1.

2.1.6 Option for CPU Time Saving

GEM needs more CPU time than other simulation programs for evaporation process, which do not include any ejectile heavier than He. In order to save CPU time of execution of GEM, the following technique is implemented: The major particles emitted from an excited nucleus are n, p, d, t, ^{3}He, and α. For most of the cases, total emission probability of particle heavier than α is negligible compared to those for the emissions of light ejectiles. Therefore, we make a criteria to determine whether to calculate emission probability for all 66-ejectiles or to calculate those for ejectiles lighter than α. Obtain the random number x, which is uniformly distributed from 0 to 1, to determine which ejectile is emitted. In the following cases, the calculations of the probabilities for the emission of particles heavier than α are skipped:

- $A_i > 40$ and $x < 0.95$;
- $30 < A_i \leq 40$ and $x < 0.93$;
- $20 < A_i \leq 30$ and $x < 0.7$.

Otherwise, probabilities are calculated for all 66 particle emissions. Above criteria are determined by the actual simulation.

2.2 Fission Model

For a heavy exited nuclus, the fission process is very important for a residual nucleus production. GEM employs the Atchison fission model [17] with two options for parameter set which gives mass, charge, and kinetic energy distribution of post fission fragments. One of them is an original parameter set in the Atchison model, and the other is a parameter set evaluated by Furihata [5].

2.2.1 Fission Probability

The Atchison fission model [17] is based on the assumption that fission competes with neutron emissions at all stage of nuclear de-excitation, with the fission probability P_f expressed as

$$P_f \approx \frac{\Gamma_f}{\Gamma_f + \Gamma_n} = \frac{1}{1 + \Gamma_n/\Gamma_f}, \tag{13}$$

where Γ_n is total width of neutron emission, and Γ_f is the total fission width. Whether a fission occurs or not is randomly selected with respect to P_f. Since the model does not describe the fission of a nucleus with Z< 70, fission is assumed to occur only for a nucleus with $A \geq 70$.

1. $89 \leq Z_i \leq 100$

   In the Atchison fission model [17], the following semi-empirical expression by Vandenbosch and Huizenga [18] is used to calculate the fission probability for a pre-fission nucleus with

$89 \leq Z_i \leq 100$.

$$\log(\Gamma_n/\Gamma_f) = \Phi(Z_i)(A_i - \Psi(Z_i)) \tag{14}$$

Φ and Ψ are tabulated as a function of Z in Table 4. The fission probability P_f is independent of the excitation energy of the pre-fission nucleus.

2. $70 < Z_i \leq 88$

For nuclei with $70 < Z_i \leq 88$, neutron emission width and fission width are calculated separately. The fission width Γ_f is given by

$$\Gamma_f = \frac{(s_f - 1)e^{s_f} + 1}{a_f} \tag{15}$$

where $s_f = 2\sqrt{a_f(E - B_f - \delta)}$ and $a_f = a_n\{1.09 + 0.011({Z_i}^2/A_i - 31.09)^2\}$, and the fission barrier B_f [MeV] is given as

$$B_f = Q_n + 321.2 - 16.7\frac{{Z_i}^2}{A} + 0.218\left(\frac{{Z_i}^2}{A_i}\right)^2. \tag{16}$$

The neutron emission width Γ_n for the calculation of P_f is expressed as [17]

$$\Gamma_n = 0.352\left(1.68J_0 + 1.93{A_i}^{1/3}J_1 + {A_i}^{2/3}(0.76J_1 - 0.05J_0)\right) \tag{17}$$

where J_0 and J_1 is the function of $s_n(= 2\sqrt{a_n(E - Q_n - \delta)})$ and $a_n(= (A_i - 1)/8)$ expressed as

$$\begin{aligned} J_0 &= \frac{(s_n - 1)e^{s_n} + 1}{2a_n} \\ J_1 &= \frac{(2s_n^2 - 6s_n + 6)e^{s_n} + s_n^2 - 6}{8a_n^2}. \end{aligned}$$

Although the neutron emission width Γ_n and the level density parameter a_n used in the above expression differs from the ones used in the evaporation model, we use the above Γ_n and a_n to maintain the accuracy of the Atchison model.

2.2.2 Mass Distribution

The selection of the mass of the fission fragments depends on whether the fission is symmetric or asymmetric. For a pre-fission nucleus with $({Z_i}^2/A_i) \leq 35$, only symmetric fission is allowed. For $({Z_i}^2/A_i) > 35$, both symmetric and asymmetric fission is allowed, depending on the excitation energy of the pre-fission nuclei. No new parameter is determined for asymmetric fission.

For nucleus with $({Z_i}^2/A_i) > 35$, whether the fission is symmetric or not is determined by the asymmetric fission probability P_{asy}

$$P_{asy} = \frac{4870e^{-0.36E}}{1 + 4870e^{-0.36E}}. \tag{18}$$

1. Asymmetric fission

   For asymmetric fission, the mass of one of the post-fission fragments A_1 is selected from a Gaussian distribution of mean $A_f = 140$ and width $\sigma_M = 6.5$. The mass of the other post-fission fragment is $A_2 = A_i - A_1$.

2. Symmetric fission

   For symmetric fission, A_1 is selected from the Gaussian distribution of mean $A_f = A_i/2$ and width σ_M. GEM has two options for σ_M.

   - Original σ_M in the Atchison model

     In the Atchison model, σ_M is given by

$$\sigma_M = \begin{cases} 3.97 + 0.425(E - B_f) - 0.00212(E - B_f)^2 & E - B_f < 100[MeV] \\ 25.27 & E - B_f \geq 100[MeV] \end{cases} \tag{19}$$

     where B_f obtained by Eq.(16) for pre-fission nucleus with $Z_i \leq 88$. For a pre-fission nucleus with $Z_i > 88$, the following expression for B_f given by Neuzil and Fairhall [19] is used.

$$B_f = C - 0.36({Z_i}^2/A_i) \tag{20}$$

     where C =18.8, 18.1, 18.1 and 18.5 for odd-odd, even-odd, odd-even, and even-even pre-fission nuclei, respectively.

   - σ_M evaluated by Furihata (default)

     Furihata [5] assumed the following expression of σ_M

$$\sigma_M = C_3(Z_i^2/A_i)^2 + C_4(Z_i^2/A_i) + C_5(E - B_f) + C_6, \tag{21}$$

     and obtained $C_3 = 0.122, C_4 = -7.77, C_5 = 3.32 \times 10^{-2}$ and $C_6 = 134.0$, by fitting the expression to experimental data collected in ref. [20] and ref. [21]. In above expression, the fission barrier B_f given by Myers and Swiatecki [22] is used. The excitation energy dependency and the Z^2/A dependency of σ_M are shown in Fig. 1.

2.2.3 Charge Distribution

The charge distribution of a fission fragment is assumed to the Gaussian distribution of mean Z_f and width σ_Z. Z_f is expressed as

$$Z_f = \frac{Z_i + Z_1' - Z_2'}{2}, \tag{22}$$

where

$$Z_\ell' = \frac{65.5A_\ell}{131 + {A_\ell}^{2/3}} \qquad \ell = 1 \text{ or } 2. \tag{23}$$

- The original σ_Z in the Atchison model

  In the Atchison model, $\sigma_Z = 2.0$ is used.

- σ_Z evaluated by Furihata (default)

  It is shown that the Atchison model with $\sigma_Z = 0.75$ produces better results than with $\sigma_Z = 2.0$ [23]. Therefore, $\sigma_Z = 0.75$ is used in GEM as a default value.

2.2.4 Kinetic Energy Distribution

The kinetic energy of the post-fission nuclei is determined by the Gaussian distribution with mean ϵ_f and width σ_{ϵ_f}.

- The original parameters in the Atchison model

  The parameters for the kinetic energy distribution are expressed as

$$\begin{aligned} \epsilon_f &= 0.133{Z_i}^2/{A_i}^{1/3} - 11.4 \\ \sigma_{\epsilon_f} &= 0.084\epsilon_f \end{aligned}$$

- The parameters evaluated by Furihata

  Rusanov *et al.* determined the ${Z_i}^2/{A_i}^{1/3}$ dependence of ϵ_f by fitting to experimental data as follows [20]:

$$\epsilon_f = \begin{cases} 0.131 Z_i^2/A_i^{1/3} & \text{for} \quad Z_i^2/A_i^{1/3} \le 900 \\ 0.104 Z_i^2/A_i^{1/3} + 24.3 & \text{for } 900 < \quad Z_i^2/A_i^{1/3} \le 1800 \end{cases} . \tag{24}$$

  Furihata fitted the following expression of σ_{ϵ_f} to the experimental data [24],

$${\sigma_{\epsilon_f}}^2 = \begin{cases} C_1\left(Z_i^2/A_i^{1/3} - 1000\right) + C_2 & \text{for } Z_i^2/A_i^{1/3} > 1000 \\ C_2 & \text{for } Z_i^2/A_i^{1/3} \le 1000 \end{cases} , \tag{25}$$

  and got $C_1 = 5.70 \times 10^{-4}$ and $C_2 = 86.5$. The experimental data used for fitting are the extrapolated values to the nuclear temperature 1.5 MeV by Itkis *et al.* [24]. The fitted result is compared with the experimental data as well as the original parameters in the Atchison model in Fig. 2.

3 Benchmark Calculation for Proton Induced Reactions

Neutron spectra, isotopic distributions, and activation yields for proton induced reactions are calculated by the combination of the Bertini intranuclear cascade (INC) model implemented in LAHET [6] and GEM ('INC/GEM'). No preequilibrium model is used in this benchmark calculation. The results are compared with various experimental data and those calculated using LAHET, to test the capability of GEM. Since the same INC model is used in both INC/GEM and LAHET calculation, the difference in the results of INC/GEM and LAHET shows the capability of the de-excitation models for prediction. The models and parameters used in both INC/GEM and LAHET are summarized in Table 5.

The Bertini model employed in LAHET is modified [25] from the original one. In the model implemented in LAHET, the randomized cutoff energy is used instead of fixed cutoff energy used in the original model [26]. The randomized cutoff energy for neutrons is determined by uniform distribution between zero and twice the mean binding energy. The Coulomb barrier is randomly distributed in a form simulating a Coulomb barrier transmission probability, and then the maximum value of the Coulomb barrier and the neutron cutoff is used as the proton cutoff. The other modification of the Bertini INC model in LAHET is energy correction for (n,p) and (p,n) reactions. The energy of an outgoing particle is corrected by the Q-value for these reactions.

The GEM code simulates the decay process of the excited nuclei whose distribution of mass A_i, charge Z_i, excited energy E, and the direction of recoil motion of the excited nuclei are determined by the Bertini INC model. The GCCI level density parameter, the precise parameter set for cross sections of inverse reactions, and the new parameter set for the Atchison fission model are used in the GEM calculations. In the LAHET calculation, all the default options are selected, i.e., the Fermi break-up model [27] is used for $A_i \leq 13$ and for $14 \leq A_i \leq 20$ with excitation energy below 44 MeV, otherwise Dresner's evaporation code, EVAP [4] with the GCCI level density parameter and the Atchison fission model with original parameter set is used. Since the EVAP code is also based on the Dostrovsky's evaporation model [3], both EVAP and GEM use the same parameters for cross sections of inverse reactions.

3.1 Neutron Spectra

Double differential cross sections of neutron productions for proton induced Al and Pb reactions at 113 MeV and 800 MeV are shown in Fig. 3 and Fig. 4. The results calculated using INC/GEM agree with the most of experimental data measured by Amian *et al.* [28] and Meier *et al.* [29] within 50 % accuracy except the cross sections at 30 and 60 degree for the 800 MeV protons on Al reaction. LAHET also reproduces the cross sections except those at 30 and 60 degree for 113 MeV proton incident on Al.

3.2 Isotopic Distributions

Isotopic distributions of light fragments produced from the 480 MeV proton induced Ag reaction are shown in Fig. 5. The calculated results by INC/GEM are compared with experimental data [30]. The estimates of He, Li, and Be productions by INC/GEM agree with experimental data with 50 % accuracy, however, INC/GEM underestimates the cross sections as a fragment mass increases.

Figure 6 $\sim$ Fig. 8 shows cross sections of spallation residues produced from the 1 GeV protons on ^{208}Pb reaction. The INC/GEM calculations are shown as well as the results calculated by LAHET. The calculations are compared with the experimental data measured by GSI [31]. The isotopic distributions predicted by INC/GEM are shifted towards proton-rich side compared to the estimates by LAHET. Both the simulations produce similar widths of distributions, and these widths are narrower than those of the measurements for isotopes with $Z < 79$. Although INC/GEM reproduces the magnitude of cross sections for heavy elements with $Z \geq 72$, it overestimates the cross sections for lighter elements. LAHET overestimates these cross sections more than INC/GEM does. The differences in the estimates are due to the effective Coulomb barrier used in GEM and EVAP. In EVAP, Coulomb barrier for an excited nucleus is reduced from the expression given as $V = k_j Z_j Z_d e^2 / R_c$. Because no such a Coulomb barrier reduction is used in GEM, more neutrons are emitted than protons. Thus GEM produces more proton-rich isotope than LAHET. Other differences between GEM and EVAP, i.e., the level density function used to derive particle emission probability, and whether including fragment emission or not, do not affect the results significantly. One of the reasons is that the difference between the accurate level density function and approximate one is small when the mass of an excited nuclei is large, and the other is that the probability of fragment emission is much less than those of proton and neutron emissions, particularly in the case of a heavy target.

3.3 Excitation Functions of Isotope Production

Excitation functions are calculated for proton induced ^{16}O, ^{27}Al, ^{nat}Fe, ^{93}Nb, ^{197}Au, and ^{238}U reactions. The estimates by INC/GEM are compared with experimental data as well as the calculated results by LAHET in Fig. 9 $\sim$ Fig. 56. The calculated cross sections are summed for all the cross sections of the nuclide and its progenitors when cross sections are measured as a cumulative yield. Table 6 shows the combination of a target and a nuclide which are compared with experimental data.

Experimental data are mainly collected from EXFOR database at National Nuclear Data Center [32] and ref. [33]. We also use ref. [34], which compiled a lot of production cross sections, as a source of experimental data. In Fig. 9 $\sim$ Fig. 56, the data extracted from EXFOR database are shown by EXFOR number which is indicated by an alphabet followed by 4 digits, such as 'C0235'. 'NEA' show those from ref. [34]. For the experimental data compiled in ref.

[33], the marks of the references used in ref. [33], such as 'Ber73', are denoted in the figures. The combination of 3 alphabets and 2 digits with asterisk, such as 'Pos71*', shows other sources of experimental data those listed in Appendix 4.6.

3.3.1 Oxygen Target

Reaction with a light target is very difficult to be described by a combination of an intranuclear cascade model and an evaporation model. INC assumed that nucleon density depends on region inside nucleus. This assumption does not hold for a small nucleus that has a clustering structure. Also, an evaporation model becomes less applicable for a light nucleus, because the mass of an ejectile can be comparable to the mass of a residual nucleus. Besides, even small excitation energy can be comparable to their total binding energy.

Despite these difficulties of applying INC/GEM to a light target, the results calculated by INC/GEM agrees well with the measurements as seen in Fig.9 and Fig.10. It is even surprising that INC/GEM produces similar results to those calculated using LAHET, in which the Fermi break-up model is implemented to describe decay of a light excited nucleus. Both calculations agree with most of experimental data within a factor of two to three. INC/GEM successfully reproduces the threshold reaction for Be productions. Although INC/GEM predicts the threshold energy for ^{13}N production slightly higher than that of the measurements, and it does not reproduce three peaks of the cross sections below 20MeV, it roughly reproduces the shape of the excitation function as well as LAHET. It is believed that an evaporation model can not describe de-excitation of a light nucleus as successful as the Fermi break-up model does, however, the results show that GEM can describe it. We consider the reason to be as follows: Two-body break-up is the main channel of disintegration of a light nucleus particularly at low excitation energy, and the probability of two-body break-up in the Fermi break-up model is similar to those in an evaporation model. The main differences in the expressions of the probability calculation are: (1) the Fermi break-up model does not use any inverse reaction cross section; (2) instead of using level density functions, experimental levels and spins are used for counting the number of states of post-decay fragments. Since the accurate level density function is used for the calculation of particle emission probability in GEM, and the difference between the accurate level density function and the approximate one is large for a light nucleus at low excited energy, the discrepancies in results caused by (2) might be improved from the evaporation model in which the level density parameter in an approximate form is used. Also, our previous study [1] showed that the excitation function for a light target calculated by INC/GEM were insensitive to the parameters of the inverse reaction cross section. Therefore (1) might not affect the results significantly.

3.3.2 Aluminum Target

Fig. 11 and Fig. 12 show the excitation function for the reaction on aluminum target induced by proton. INC/GEM predicts the triton and helium productions more accurately than LAHET. The use of the accurate level density function improves these particle emissions, particularly at low proton incident energy. The excitation function for ^{7}Be production calculated using INC/GEM agrees with the most of experimental data within 50 % of accuracy whereas LAHET produces no ^{7}Be below 100 MeV. INC/GEM also reproduces the shape of the excitation function for ^{10}Be production, although it underestimates them by a factor of two to five. GEM also improves the prediction of the cumulative cross section of ^{20}Ne production below 40 MeV. The excitation function calculated using INC/GEM has a peak around 20 MeV, whereas LAHET fails to reproduce the peak. According to the INC/GEM calculation, the peak of the cross section at 20 MeV is contributed by the ^{27}Al(p,2α)^{20}Ne reaction at threshold energy of emission of two α particles. As seen in the figure of the excitation function for α emission, since GEM improves the particle emission from a light target, it also describes the threshold reaction such as ^{27}Al(p,2α)^{20}Ne accurately. Both INC/GEM and LAHET produce similar results for the residuals whose masses are near the target.

3.3.3 Iron Target

The excitation function for the reaction of proton induced natural iron target are shown in Fig. 13 $\sim$ Fig. 18. The estimates of triton and helium production by INC/GEM agree with those by LAHET within a factor of two, except near the threshold energies. INC/GEM reproduces the threshold energy of an α particle emission better than LAHET. The predictions of beryllium productions are much improved by using INC/GEM. It reproduces both the excitation functions within 50 % to a factor of two, while LAHET underestimates them by more than one order of magnitude. INC/GEM predicts the threshold energies of light residual nuclei, such as Na, lower than LAHET, however, those of experimental data are much lower than the INC/GEM predictions. As already seen in the isotopic distribution produced from lead target, it is also shown in Fig. 14, 15, 17, and 18 that INC/GEM produces more proton-rich nuclei than LAHET. INC/GEM predicts more ^{28}Mg, ^{36}Ar, ^{44}Ti, ^{48}Cr, ^{52}Fe, and ^{55}Co productions from iron target than LAHET. In the excitation functions for the cumulative ^{51}Cr production and independent ^{54}Mn production (Fig. 17), there are peaks at proton incident energy below 20 MeV. INC/GEM reproduce these peaks but LAHET does not. According to the INC/GEM calculation, the ^{54}Fe(p,α)^{51}Cr reaction contributes to the cumulative ^{51}Cr production below 30 MeV, and ^{57}Fe(p,α)^{54}Mn does to the ^{54}Mn production below 20 MeV. Since INC/GEM reproduces the threshold of α emission, it also reproduces these reaction. The differences in the results calculated by INC/GEM and LAHET shows how much it improves the predictions to use the accurate level density function in an evaporation model, as already mentioned in previous

section. Both calculation procedures produce the similar excitation functions of other residuals.

3.3.4 Niobium Target

The excitation functions for nuclide production from the reaction of proton induced niobium target are shown in Fig. 19 ∼ Fig. 24. INC/GEM reproduce the excitation function for the ^{7}Be production within a factor of two in whole energy region while LAHET predicts no ^{7}Be from the reaction. There is a large discrepancy between the experimental data and the estimated excitation functions of ^{22}Na production below 2 GeV. Both INC/GEM and LAHET severely underestimate ^{22}Na production. It is not clear whether ^{22}Na is produced as a residual nucleus or an ejectile, however, irrespective of it, INC/GEM underestimates sodium productions from the reaction induced by low energy proton as shown in Fig.5 (the fragment productions from the reaction on Ag target induced by 480 MeV protons) and Fig. 14 (the ^{22}Na production from the reaction on Fe target). There are less differences in the predictions by both the calculation procedures of the threshold reactions of α particle emissions, such as ^{93}Nb(p,nα)^{89}Zr (Fig. 24) and ^{93}Nb(p,2nα)^{89}Zr (Fig. 23), in contrast to the estimates for the reaction on Al and Fe targets. Since the accurate level density function is used for $E^* < 2.5 + 150/A_d + \delta$, the difference of calculated probability decreases as A_d increases. Thus, whether using the accurate level density parameter or not does not affect the results significantly. For other nuclide, the differences in the results calculated by both methods are within a factor of two.

3.3.5 Gold Target

The excitation functions for the nuclide productions from the reaction on gold induced by protons are shown in Fig. 25 ∼ Fig. 36.

As seen in the results for other targets, INC/GEM reproduces ^{7}Be productions above 300 MeV, whereas LAHET severely underestimates them by more than one order of magnitude. The estimates of ^{18}F productions calculated by INC/GEM agree with experimental data above 1 GeV, while the discrepancies between the measurements and the estimates of ^{22}Na, ^{24}Na and ^{28}Mg productions are a factor of five or more. According to the calculations by INC/GEM, half of these particles are produced from evaporation process and the rest of them are fission products, however, it is hard to be decided from the experimental data how these particles are produced.

The nuclide with $30 < A < 130$ are fission fragments. Some predictions for fission products are drastically improved by using GEM. INC/GEM reproduces the excitation function of ^{82}Br, ^{88}Y, and ^{95}Nb productions whereas LAHET fails to reproduce the shapes of them. LAHET produce light fission fragments (^{46}Sc, ^{48}V, ^{54}Mn, and ^{59}Fe productions shown in Fig. 26 and 27) more than INC/GEM, from the reaction induced by low energy protons . Since LAHET uses the RAL fission model with the original parameter set, it produces wider mass distribution than

INC/GEM that uses the same model but with the parameter set derived by Furihata [5]. Of ^{84}Rb, ^{86}Rb, ^{95}Zr, and ^{103}Ru, although the estimates by INC/GEM agree with the experimental data better than those by LAHET on average, the shapes of the excitation functions are not perfectly reproduced by INC/GEM. The reason could be the imbalance of neutron and proton emission as shown in figures of the spallation products from the reaction on Pb induced by 1 GeV protons, or insufficient description in the fission model. For detail analysis, the calculation should be compared with forthcoming experimental data measured by GSI [35].

According to the calculation, nuclides with $125 < A \leq 140$ are produced from the reaction as fission products at low proton incident energies, and as spallation products at high energy. Therefore, the calculated excitation functions of these nuclides (Fig. 30) shows no clear threshold energy such that seen in the excitation function of a spallation product with $A > 140$.

INC/GEM and LAHET produce similar results for the spallation products with $A > 140$, except the threshold energies. INC/GEM estimates the threshold energies of deep spallation products higher than LAHET. Like the reaction on O, Al, Fe, and Nb, INC/GEM underestimates the neutron-rich nuclei, i.e., ^{148}Eu and ^{168}Tm shown in Fig. 31.

3.3.6 Uranium Target

The excitation functions for the fragments produced form the reaction on ^{238}U irradiated by protons are shown in Fig. 37 $\sim$ 56.

INC/GEM reproduces the excitation function for ^{9}Li production as well as those of ^{7}Be. Above 500 MeV, the estimates agree with experimental data within a factor of two to three. The cross sections of ^{16}C, ^{24}Na, and ^{28}Mg are not predicted by INC/GEM, as already seen in the results of the Nb and Au targets.

Use of different σ_M in the RAL fission model changes the resulting excitation functions for nuclides with $30 < A < 80$ or $140 < A < 200$. INC/GEM predicts the threshold energy of these nuclides higher than LAHET (^{45,47}Ca, ^{43,46,47,48}Sc, ^{47,48,49}V, ^{49,51}Cr, ^{66}Ni, ^{67}Cu, and ^{72,73}Ga) because the use of σ_M given by Eq. (21) in the fission model causes the narrower mass distribution for fission fragments produced at low proton incident energy. Fig. 27 shows that INC/GEM underestimates the cross sections of ^{67}Cu and ^{72}Ga below 100 MeV, however, the results calculated by INC/GEM are in good agreement with the measurements above 100 MeV. INC/GEM reproduces the excitation functions for the cumulative ^{66}Ni, ^{73}Ga, ^{153}Sm, and ^{156,157}Eu productions within a factor of two to three above 40 MeV. Fig. 40 $\sim$ Fig. 50 shows that the use of $\sigma_Z = 0.75$ in the RAL fission model improves the prediction of excitation functions of nuclides with $80 < A < 140$. It improves the accuracy of predictions for both neutron-rich and proton-rich nucleus, particularly below 200 MeV (see ^{86}Rb production in Fig. 28 and ^{97}Rb production in Fig.30 as examples).

The estimates for spallation products with $A > 200$ calculated using INC/GEM are similar to those by LAHET.

3.4 Conclusion of Benchmark Calculations

Neutron spectra, isotopic distributions, and excitation functions for the reaction on various targets irradiated by protons are calculated using the combination of the Bertini intranuclear cascade model (INC) and the generalized evaporation model (GEM). The results of INC/GEM are compared with experimental data as well as the estimates by LAHET.

Using GEM instead of EVAP improves the estimates of light particle productions. INC/GEM predicts the cross sections of a light fragment, such as ^{7}Be productions from the reaction on O to U targets with 50% accuracy on average. It is believed that only a fragmentation model can describe light particle productions, however, the results suggest that light fragments can be produced from evaporation process. INC/GEM can adequately describe threshold reaction of alpha particle emissions, since the accurate level density function is used in GEM. INC/GEM gives the better excitation function than LAHET, for α particle productions as well as that for residuals produced from the threshold reaction of α emission, such as cumulative ^{51}Cr production from ^{nat}Fe target. The use of new parameter set in a fission model improves the prediction of cross section of a fission product, such as ^{95}Nb from Au, and Rb from U.

GEM is not perfect still, however. INC/GEM underestimates the cross sections of a heavy fragment, such as ^{22}Na, produced from bombardment of a target with $A > 90$ by more than an order of magnitude. From the experimental data measured by GSI [35], it does not seem that sodium isotopes are produced as fission products. According to their experiment, which they measured cross sections for fission residues produced from the reaction on proton irradiated by 800 MeV/A ^{197}Au, the cross sections of fission products with $A < 40$ are less than 0.1 mb. The experimental data in Fig. 25 shows the cumulative cross section of ^{24}Na at 800 MeV is about 0.3 mb. Therefore, the main process which contributes the ^{24}Na production is not fission below 800 MeV. It may improve predictions to take the effect of the Coulomb barrier reduction between an ejectile and a highly excited nucleus into account in GEM, or to employ a multi-fragmentation model in the simulation.

INC/GEM also underestimates neutron-rich isotopes of spallation products. The new parameters of the inverse cross section, instead of those derived by Dostrovsky *et al.* [3], is needed to improve the underestimates, as pointed out by many authors [34, 36] that that is one of the problems in an evaporation model. The use of more accurate expression of the level density parameter may also improve predictions.

4 The GEM Code Users Manual

4.1 Introduction

GEM is a Fortran program for the Linux computer with g77 compiler. GEM simulates a decaying process of an excited nucleus, therefore you should use other computer programs to determine the excited nuclei produced after first non-equilibrium stage of a nuclear reaction, such as proton induced reaction. Also, you need to edit an output file of GEM to estimate cross sections.

4.2 File Structure

The following directories and files are included in the gem.tar file.

- for/

```
 1 -rw-r--r--   1      383 Nov  6 17:37 Makefile
 9 -rw-rw-r--   1     8784 Feb 10  2000 bd01.f
 3 -rw-rw-r--   1     2061 Feb 11  2000 bdejc.f
 2 -rw-rw-r--   1     1293 Feb 11  2000 dost.f
 5 -rw-rw-r--   1     4381 Feb 10  2000 drein1.f
 4 -rw-rw-r--   1     3285 Feb 10  2000 drein2.f
 2 -rw-rw-r--   1     1206 Feb 11  2000 ef.f
 3 -rw-rw-r--   1     2076 Jun 16 18:03 energy.f
 4 -rw-rw-r--   1     3969 Feb 23  2000 eye.f
20 -rw-rw-r--   1    19002 Jun 16 18:30 fiss.f
 7 -rw-rw-r--   1     7036 Feb 23  2000 fprob.f
 8 -rw-rw-r--   1     7882 Jun 16 18:32 gamma.f
 2 -rw-rw-r--   1     1042 Feb 24  2000 gaussn.f
 4 -rw-rw-r--   1     3357 Jun 16 18:32 geta.f
 1 -rw-rw-r--   1      913 Feb 12  2000 getime.f
 7 -rw-rw-r--   1     6404 Nov  6 14:46 main.f
 1 -rw-rw-r--   1      553 Feb 10  2000 paire.f
 4 -rw-rw-r--   1     4040 Feb 11  2000 pe.f
 2 -rw-rw-r--   1     1282 Feb 24  2000 ran.f
 2 -rw-rw-r--   1     1521 Jun 16 18:32 rb.f
 2 -rw-rw-r--   1     1119 Feb 10  2000 rho.f
 3 -rw-rw-r--   1     2777 Jun 16 18:19 setup.f
 6 -rw-rw-r--   1     5445 Feb 24  2000 stdcay.f
 2 -rw-rw-r--   1     1874 Jun 16 18:33 vcoul.f
```

- for/Data

```
 57 -rw-rw-r--   1     56968 Feb 12  2000 level.tbl
250 -rw-rw-r--   1    254696 Feb 12  2000 mass.tbl
197 -rw-rw-r--   1    200354 Feb 11  2000 shell.tbl
```

- Sample/

```
  1 -rw-rw-r--   1       682 Nov  6 14:55 in
  4 -rw-rw-r--   1      3440 Nov  6 13:33 nucl.in
  8 -rw-rw-r--   1      7668 Nov  6 13:33 sample.gem.out
```

4.3 Installation

1. Type the following command to extract files and directories from gem.tar file.

```
tar xvf gem.tar
```

2. Change the following three lines (line 27, 51 and 68) in setup.f to the directory name in which you put the data files.

```
open(10,file='/home/for/Data/mass.tbl',status='old')
open(13,file='/home/for/Data/level.tbl',status='old')
open(11,file='/home/for/Data/GEM/shell.tbl',status='old')
```

3. Execute 'make' at the directory in which user puts the source files to make a executable file 'gem'.
   Note: Since GEM is made for Linux, users who want to install GEM on other computer might need to change the subroutine getime.f and Makefile. Comment FFLAG in Makefile, comment all the 'call getime' line in the subroutines, and try again, when a user has any trouble with compiling on the computer other than Linux with g77 compiler.

4.4 Files

4.4.1 Input File

Prepare two input files for execution of the GEM code. One is for control parameters in GEM ('in' file). The other is named 'nucl.in' which contains the information about excited nuclei produced after initial non-equilibrium stage.

1. Control file (**in** file)

   User can chose the following parameters used in GEM. The details of the parameters are described in refs. [1, 5]. The contents of **in** file are as follows:

   - 1st record (MUL): the number of multiple simulations.

     MUL > 1 means that GEM performs MUL simulations for each excited nucleus written in the **nucl.in** file. Default MUL=1.

   - 2nd record (ALEV): the level density parameter a.

     0 (Default)→ The GCCI level density parameter
     1.0 → $a = A/8$
     >1.0 → $a = A/ALEV$

   - 3rd record (RCAL): the parameters for cross sections for inverse reactions .

     RCAL=0 (Default) → The precise parameter set
     (The Dostrovsky's parameter & Matsuse's parameter)
     RCAL> 0 → The simple parameter set with r_0 =RCAL.

   - 4th record (IFIS): the parameters in the RAL fission model.

     IFIS=0 (Default)→ The reevaluated parameter set.
     IFIS≠ 0 → The original parameter set in the RAL model.

   - 5th record (IRED): option for CPU time saving (see section 2.1.6).

     IRED=0 (default)→ Normal execution of GEM
     IRED≠ 0 → Use CPU time saving method

   - 6th record (IZMIN): the minimum Z which is written in the output file (default=0).
   - 7th record (IZMAX): the maximum Z which is written in the output file (default=100).
   - 8th record (IAMIN): the minimum A which is written in the output file (default=1).
   - 9th record (IAMAX): the maximum A which is written in the output file (default=300).
   - 10th record (ISEED): seed for random number (default=0).

The sample of the file is as follows:

```
1,   ! MUL
0.0,! ALEV
0.0,! RCAL
0,   ! IFIS
1,   ! IRED
1,   ! IZMIN
100,! IZMAX
2,   ! IAMIN
300,! IAMAX
100000,   !ISEED
```

2. The **nucl.in** file

User needs to prepare **nucl.in** which contains the following data for each excited nuclei. The file has to have 9 columns.

- 1st column : the mass number of the parent nucleus A_i
- 2nd column : the charge number of the parent nucleus Z_i
- 3rd column : the excitation energy E per mass number [MeV/A] of the parent nucleus
- 4th column : the recoil energy E_r [MeV] of the parent nucleus
- 5th to 7th column : the unit vector of the direction of motion $\boldsymbol{u}$ of the parent nuclei.
- 8th column : dummy variables
- 9th column : ID number of the nucleus

GEM reads **nucl.in** from the unit 66 with free format. The file should consist less than 1000000000 records.

The sample of the file is as follows:

```
 25  12  9.9634E-01  2.7227E+00 -9.2209E-01 -4.2556E-02 -3.8463E-01 1.0      3
 23   9  6.9504E+00  1.3242E+01 -3.7167E-01 -5.6194E-01  7.3898E-01 1.0      4
 25  12  2.6554E+00  2.6090E+00 -3.6274E-01  9.2190E-01  1.3605E-01 1.0      6
 26  12  8.6574E-01  2.2835E+00 -2.4526E-01  9.0220E-01 -3.5479E-01 1.0      7
 25  12  7.7239E+00  1.5559E+01 -5.2776E-01  4.6437E-01  7.1121E-01 1.0      8
 26  13  5.8512E-01  3.1267E-01 -6.5835E-01  6.8878E-01 -3.0358E-01 1.0      9
 23  12  5.6576E+00  8.2903E+00 -2.2042E-01  6.8172E-01  6.9762E-01 1.0     12
 26  12  0.0000E+00  3.5003E-01  9.4315E-01 -3.1941E-01  9.1844E-02 1.0     15
 25  13  8.3891E-01  1.6081E+00  7.4636E-01 -6.5825E-01  9.8301E-02 1.0     17
```

4.4.2 Output File

The GEM code produces only one output file whose name is **gem.out**. Each record have 8 columns of data as follows:

- 1st column : the charge number of the nucleus

- 2nd column : the mass number of the nucleus
- 3rd column : the kinetic energy of the nucleus [MeV]
- 4th to 6th column : the unit vector of the direction of motion of the nucleus
- 7th column : ID number of the parent nucleus
- 8th column : the origin of the nucleus: 'A' means the ejectile emitted from a fission fragment; 'B' means the fission fragment; 'C' means the ejectile emitted from a non-fissioned nucleus; 'D' means the non-fissioned residual nucleus.

GEM produces the file through the unit 70. The sample of the file is as follows:

```
12  24  3.42149E+00 -7.83797E-01 -9.86938E-02 -6.13125E-01     3 D
 2   4  4.42691E+00 -9.67199E-01  1.14025E-01 -2.26990E-01     4 C
 5  11  9.10349E+00  9.43127E-02 -6.74379E-01  7.32337E-01     4 D
10  20  2.96245E+00 -1.42428E-01  9.85870E-01 -8.81763E-02     6 D
 2   4  6.79151E+00  3.87006E-01 -7.99916E-01 -4.58650E-01     7 C
10  22  6.32966E+00 -3.31326E-01  9.43069E-01 -2.90370E-02     7 D
 1   2  1.27893E+01 -6.19001E-01  2.30555E-01  7.50787E-01     8 C
 2   4  1.50738E+01  5.90221E-01  2.25328E-01  7.75156E-01     8 C
 2   4  2.47649E+01 -7.86099E-01  5.60263E-01  2.61063E-01     8 C
 2   4  1.03814E+01  3.27841E-01 -8.95786E-01  3.00146E-01     8 C
 2   4  1.99565E+01 -5.37305E-01  8.26107E-01 -1.69855E-01     8 C
 2   4  7.37794E+00 -6.01539E-01  1.27111E-01 -7.88666E-01     8 D
12  25  5.62555E-02 -6.99022E-01  7.07365E-01  1.04893E-01     9 D
 2   4  2.54090E+01 -1.18718E-01  9.81072E-01  1.52984E-01    12 C
 2   4  8.70952E+00 -6.91556E-01  5.13647E-01  5.07856E-01    12 C
 2   4  2.29945E+00 -3.14501E-01 -9.41002E-01 -1.24916E-01    12 C
 2   4  7.59030E+00  4.84984E-01 -9.35248E-02  8.69508E-01    12 C
 2   4  1.46536E+01 -3.00091E-01  1.64825E-01  9.39563E-01    12 D
12  26  3.50030E-01  9.43150E-01 -3.19410E-01  9.18440E-02    15 D
 2   4  2.90745E+00 -9.65850E-01  5.94348E-02  2.52191E-01    17 C
10  20  3.54478E+00  8.58270E-01 -4.56647E-01 -2.34191E-01    17 D
```

4.4.3 Data Files

1. mass.tbl

   The mass.tbl file consists of the excess masses $M(Z, A)$[MeV] for each nuclei. The data are extracted from: (1) Audi-Wapstra's mass table [7]; (2) theoretical masses calculated by Moller *et al.* [8]; (3) theoretical masses calculated Comay *et al.* [9]. The file has three columns.

   - 1st column : Z
   - 2nd column : A
   - 3rd column : Excess mass [MeV]

The data are read from the unit 10 in subroutine SETUP.

2. level.tbl

   The level.tbl file includes the data for the excited state of the ejectiles, i.e., the level width ($= \hbar \ln 2/T_{1/2}$) [MeV], the spin S_j^*, and the excitation energy E_j^* [MeV]. The excited state of n, p, d, t, ^{3}He, and α are not included. The data are read with free format from the unit 13 in subroutine SETUP.

3. shell.tbl

   The shell.tbl file consists of the shell effect for the fission barrier calculation. The data are extracted from the penultimate column of the table in ref. [37] where the ground-state mass is known. For other nuclei, the calculated shell effect (column 7 in the table) is extracted. The file has three columns.

   - 1st column : Z
   - 2nd column : A
   - 3rd column : Shell effect [MeV]

   The shell.tbl file is read from the unit 11 in subroutine SETUP with free format.

4.5 Execution of GEM

The executable file name is **gem**. Type **gem** at the directory which holds **in** and **nucl.in**. GEM produces **gem.out** and standard output which contains the information about the parameters you choose. To obtain a production rate or a cross section, you need to edit **gem.out** file.

4.6 Important Notice

- When you publish any results calculated using GEM, Please refer [1] for a reaction on a light target, and also refer [5] for a reaction on a heavy target with $Z > 70$.
- Please send an e-mail to furihata@mri.co.jp when you find any bug in GEM.

Acknowledgements

The authors would thank to Dr. L. Moritz and Dr. Yoshizawa for valuable discussion on this study, and also appreciate Dr. R. E. Prael for the LAHET code.

References

[1] Furihata S. : Nucl. Inst. Meth. in Phys. Res. B, 171, 251 (2000).

[2] Weisskopf V. F. and Ewing P. H. : Phys. Rev., 57, 472 (1940).

[3] Dostrovsky I., Fraenkel Z., and Friedlander G. : Phys. Rev., 116, 683 (1959).

[4] Dresner L. : ORNL-TM-196, "EVAP - A Fortran Program for Calculating the Evaporation of Various Particles form Excited Compound Nuclei", Oak Ridge National Laboratory (1962).

[5] Furihata S. : " Proceedings of International Conference on Advanced Monte Carlo for Radiation Physics, Particle Transport Simulation and Applications, 23-26 October 2000, Lisbon, Portugal" (to be published by Springer Verlag).

[6] Prael R. E. and Lichtenstein H. : LA-UR-89-3014, "User Guide to LCS: The LAHET Code System" (1989).

[7] Audi G. and Wapstra A. H. : Nucl. Phys. A, 595, 409 (1995).

[8] Moller P., Nix J. R., Myers W. D., and Swiatecki W. J. : Atomic Data and Nuclear Data Tables, 59, 185 (1995).

[9] Haustein P. E. : Atomic Data and Nuclear Data Tables, 39, 185 (1988).

[10] Gilbert A. and Cameron A. G. W. : Can. J. Phys., 43, 1446 (1965).

[11] Cook J. L., Ferguson H., and Musgrove A. R. D. Aust. J. : Phys., 20, 477 (1967).

[12] Data extracted using the National Nuclear Data Center (NNDC) On-Line Data Service from the ENSDF database, file revised as of August 5 (1998).

[13] Matsuse T., Arima A., and Lee S. M. : Phys. Rev. C, 26, 2338 (1982).

[14] Shapiro M. M. : Phys, Rev., 90, 171 (1953).

[15] Blatt J. and Weisskopf F. : "Theoretical Nuclear Physics", Jonh Wiley & Sons, Inc., New York (1952).

[16] Prael R. E. and Bozoian M. : LA-UR-88-3238, "Adaptation of the Multistage Preequilibrium Model for the Monte Carlo Method (I)" (1988).

[17] Atchison F.: Jül-conf-34, "Proc. of Mtg. on Targets for Neutron Beam Spallation Source", KFA-Jülich, Germany, June 1979, 17 (1980).

[18] Vandenbosch R. and Huizenga J. R.: "Nuclear Fission", Academic Press, New York (1973).

[19] Neuzil E. F. and Fairhall A. W. : Phys. Rev., 129, 2705 (1963).

[20] Rusanov A. Y., Itkis M. G., and Okolovich V. N. : Phys. Atom. Nucl., 60, 683 (1997).

[21] Itkis M. G., Muzychka Y. A., Oganessan Y. T., Okolovich V. N., Oashkevich V. V., Rusanov A. Y., Salamation V. S., Smirenkin G. N., and Chubarian G. G. : Phys. Atom. Nucl., 58, 2026 (1995).

[22] Myers W. D. and Swiatecki W. J. : Phys, Rev. C., 60, 014606 (1999).

[23] Furihata S. and Moritz L.: TRI-DN-I7-3-14, "Benchmark calculations of cross sections for the production of nuclei by the bombardment of uranium with protons" , TRIUMF (1998).

[24] Itkis M. G., Lykyanov S. M., Okolovich V. N., Penionzhkevich Y. E., Rusanov A. Y., Salamatin V. S., Smirenkin G. N., and Chubaryan G. G. : Sov. J. Nuc. Phys., 52, 15 (1990).

[25] Prael R. E.: LA-UR-89-3347, "LAHET benchmark calculations of differential neutron production cross sections for 113 MeV and 256 MeV protons" (1989).

[26] Bertini H. W. : Phys. Rev., 188, 1711 (1969).

[27] Fermi E. : Prog. Theo. Phys., 5, 570 (1950).

[28] Amian W. B., Byrd R. C., Goulding C. A., Meier M. M., Morgan G. L., Moss C. E., and Clark D. A. : Nucl. Sci. Eng., 112, 78 (1992).

[29] Meier M. M., Clark D. A., Goulding C. A., Morgan J. B. M. G. L., Moss C. E., and Amian W. B. : Nucl. Sci. Eng., 102, 310 (1989).

[30] Green R. E. L., Korteling R. G., and Jackson K. P. : Phys. Rev. C, 29, 1806 (1984).

[31] Wlazlo W., Enqvist T., Benlliure J., Farget F., Schmidt K.-H., Armbruster P., Bernas M., Boudard A., Czajkowski S., Legrain R., Mustapha B., Pravikoff M., Stephan C., Taieb J., Tassan-Got L., and Volant C. : Phys. Rev. Lett, 84, 5736 (2000).

[32] The National Nuclear Data Center On-Line Data Service : http://www.nndc.bnl.gov/.

[33] Schopper H. (ed.): "LANDOLT-BÖRNSTEIN: Numerical Data and Functional Relationship in Science and Technology, Group I: Production of Radionuclides at Intermediate Energies, subvolme a, b, c, d : Interactions of Protons with Nuclei",Springer-Verlag, Berlin Heidelberg (1994).

[34] Michel R. and Nagel P. : NSC/DOC(97)-1, "International Codes and Model Intercomparison for Intermediate Energy Activation Yields" (1997)

[35] Benlliure J., Armbruster P., Bernas M., Boudard A., Dufour J. P., Enqvist T., Legrain R., Leray S., Mustapha B., Rejmund F., Schmidt K.-H., Stephan C., Tassan-Got L., and Volant C. : to be published in Nucl. Phys. A .

[36] Mashnik S. G., Sierk A. J., Bersillon O., and Gabriel T.: LA-UR-97-2905, "Cascade-Exciton Model Detailed Analysis of Proton Spallation at Energies From 10 MeV to 5 GeV" (1997).

[37] Myers W. D. and Swiatecki W. J.: LBL-36803, "Table of Nuclear Masses according to the 1994 Thomas-Fermi model" , Lawrence Berkeley Laboratory (1994).

Table 1 Paring energy and shell corrections [10, 11]

N or Z	$P(Z)$ [MeV]	$P(N)$ [MeV]	$S(Z)$ [MeV]	$S(N)$ [MeV]	N or Z	$P(Z)$ [MeV]	$P(N)$ [MeV]	$S(Z)$ [MeV]	$S(N)$ [MeV]
1					51		0.01	−19.14	13.23
2	5.44	5.98			52	1.05	0.62	−18.26	13.81
3					53		−0.50	−17.40	14.90
4	2.76	2.77			54	1.00	1.42	−16.42	14.86
5					55	0.09	0.13	−15.77	15.76
6	3.34	3.16			56	1.20	1.52	−14.37	16.20
7					57	0.20	−0.65	−13.91	17.62
8	2.70	3.01			58	1.40	0.80	−13.10	17.73
9			−0.11	10.30	59	0.93	−0.08	−13.11	18.16
10	2.50	2.50	−0.81	5.66	60	1.00	1.29	−11.43	18.67
11			−2.91	6.80	61	−0.20	−0.47	−10.89	19.69
12	2.46	2.67	−4.17	7.53	62	1.19	1.25	−10.75	19.51
13			−5.72	7.55	63	0.09	−0.44	−10.62	20.17
14	2.09	1.80	−7.80	7.21	64	0.97	0.97	−10.41	19.48
15			−8.97	7.44	65		0.08	−10.21	19.98
16	1.62	1.67	−9.70	8.07	66	0.92	1.65	−9.85	19.83
17			−10.10	8.94	67	0.11	−0.11	−9.47	20.20
18	1.62	1.86	−10.70	9.81	68	0.68	1.26	−9.03	19.72
19			−11.38	10.60	69	0.05	−0.46	−8.61	19.87
20	1.83	2.04	−12.07	11.39	70	0.68	1.06	−8.13	19.24
21			−12.55	12.54	71	−0.22	0.22	−7.46	18.44
22	1.73	1.64	−13.24	13.68	72	0.79	1.55	−7.48	17.61
23			−13.93	14.34	73	0.09	−0.07	−7.20	17.10
24	1.35	1.44	−14.71	14.19	74	0.69	1.37	−7.13	16.16
25			−15.53	13.83	75	0.01	0.10	−7.06	15.90
26	1.54	1.54	−16.37	13.50	76	0.72	1.20	−6.78	15.33
27			−17.36	13.00	77		−0.27	−6.64	14.76
28	1.28	1.30	−18.60	12.13	78	0.40	0.92	−6.64	13.54
29	0.26		−18.70	12.60	79	0.16	−0.35	−7.68	12.63
30	0.88	1.27	−18.01	13.26	80	0.73	1.19	−7.89	10.65
31	0.19		−17.87	14.13	81			−8.41	10.10
32	1.35	1.29	−17.08	14.92	82	0.46	1.05	−8.49	8.89
33	−0.05	0.08	−16.60	15.52	83	0.17	−0.25	−7.88	10.25
34	1.52	1.41	−16.75	16.38	84	0.89	1.61	−6.30	9.79
35	−0.09	−0.08	−16.50	17.16	85		−0.21	−5.47	11.39
36	1.17	1.50	−16.35	17.55	86	0.79	0.90	−4.78	11.72
37	0.04	−0.05	−16.22	18.03	87		−0.21	−4.37	12.43
38	1.24	2.24	−16.41	17.59	88	0.89	0.74	−4.17	12.96
39	0.29	−0.47	−16.89	19.03	89		−0.38	−4.13	13.43
40	1.09	1.43	−16.43	18.71	90	0.81	0.72	−4.32	13.37
41	0.26	−0.15	−16.68	18.80	91	−0.06	−0.34	−4.55	12.96
42	1.17	1.44	−16.73	18.99	92	0.69	0.92	−5.04	12.11
43	0.23	0.06	−17.45	18.46	93	−0.20	−0.26	−5.28	11.92
44	1.15	1.56	−17.29	18.25	94	0.71	0.94	−6.06	11.00
45	−0.08	0.25	−17.44	17.76	95	−0.12	0.01	−6.28	10.80
46	1.35	1.57	−17.82	17.38	96	0.72	0.65	−6.87	10.42
47	0.34	−0.16	−18.62	16.72	97		−0.36	−7.20	10.39
48	1.05	1.46	−18.27	15.62	98	0.77	0.83	−7.74	9.69
49	0.28		−19.39	14.38	99		0.11		9.27
50	1.27	0.93	−19.91	12.88	100		0.67		8.93

Table 1 (Concluded)

N or Z	$P(Z)$ [MeV]	$P(N)$ [MeV]	$S(Z)$ [MeV]	$S(N)$ [MeV]	N or Z	$P(Z)$ [MeV]	$P(N)$ [MeV]	$S(Z)$ [MeV]	$S(N)$ [MeV]
101		0.05		8.57	126		0.38		−3.16
102		1.00		8.02	127		0.15		−1.87
103		0.51		7.59	128		0.67		−0.41
104		1.04		7.33	129				0.71
105		0.33		7.23	130		0.61		1.66
106		0.68		7.05	131				2.62
107		−0.27		7.42	132		0.78		3.22
108		0.81		6.75	133				3.76
109		0.09		6.60	134		0.67		4.10
110		0.75		6.38	135				4.46
111		0.17		6.36	136		0.67		4.83
112		0.86		6.49	137				5.09
113		0.14		6.25	138		0.79		5.18
114		1.10		5.85	139				5.17
115		−0.22		5.48	140		0.60		5.10
116		0.84		4.53	141		0.04		5.01
117		−0.47		4.30	142		0.64		4.97
118		0.48		3.39	143		−0.06		5.09
119		0.02		2.35	144		0.45		5.03
120		0.88		1.66	145		0.05		4.93
121		0.24		0.81	146		0.26		5.28
122		0.52		0.46	147		−0.22		5.49
123		0.27		−0.96	148		0.39		5.50
124		0.41		−1.69	149				5.37
125		−0.05		−2.53	150		0.39		5.30

Table 2 Ejectiles

ID	nuclide	Z	A	spin	ID	nuclide	Z	A	spin
1	n	0	1	1/2	36	^{14}O	8	14	0
2	p	1	1	1/2	37	^{15}O	8	15	1/2
3	d	1	2	1	38	^{16}O	8	16	0
4	t	1	3	1/2	39	^{17}O	8	17	5/2
5	^{3}He	2	3	1/2	40	^{18}O	8	18	0
6	α	2	4	0	41	^{19}O	8	19	5/2
7	^{6}He	2	6	0	42	^{20}O	8	20	0
8	^{8}He	2	8	0	43	^{17}F	9	17	5/2
9	^{6}Li	3	6	1	44	^{18}F	9	18	1
10	^{7}Li	3	7	3/2	45	^{19}F	9	19	1/2
11	^{8}Li	3	8	2	46	^{20}F	9	20	2
12	^{9}Li	3	9	3/2	47	^{21}F	9	21	5/2
13	^{7}Be	4	7	3/2	48	^{18}Ne	10	18	0
14	^{9}Be	4	9	3/2	49	^{19}Ne	10	19	1/2
15	^{10}Be	4	10	0	50	^{20}Ne	10	20	0
16	^{11}Be	4	11	1/2	51	^{21}Ne	10	21	3/2
17	^{12}Be	4	12	0	52	^{22}Ne	10	22	0
18	^{8}B	5	8	2	53	^{23}Ne	10	23	5/2
19	^{10}B	5	10	3	54	^{24}Ne	10	24	0
20	^{11}B	5	11	3/2	55	^{21}Na	11	21	3/2
21	^{12}B	5	12	1	56	^{22}Na	11	22	3
22	^{13}B	5	13	3/2	57	^{23}Na	11	23	3/2
23	^{10}C	6	10	0	58	^{24}Na	11	24	4
24	^{11}C	6	11	3/2	59	^{25}Na	11	25	5/2
25	^{12}C	6	12	0	60	^{22}Mg	12	22	0
26	^{13}C	6	13	1/2	61	^{23}Mg	12	23	3/2
27	^{14}C	6	14	0	62	^{24}Mg	12	24	0
28	^{15}C	6	15	1/2	63	^{25}Mg	12	25	5/2
29	^{16}C	6	16	0	64	^{26}Mg	12	26	0
30	^{12}N	7	12	1	65	^{27}Mg	12	27	1/2
31	^{13}N	7	13	1/2	66	^{28}Mg	12	28	0
32	^{14}N	7	14	1					
33	^{15}N	7	15	1/2					
34	^{16}N	7	16	2					
35	^{17}N	7	17	1/2					

Table 3 The Dostrovsky's parameters for inverse cross sections c, k, and k_α.

Z_d	k	k_α	c
$\leq$20	0.51	0.81	0.0
30	0.60	0.85	-0.06
40	0.66	0.89	-0.10
$\geq$50	0.68	0.93	-0.10

Table 4 Fission parameter Φ and Ψ by Vandenbosch and Huizenga[18]

Z	Φ	Ψ
89	0.23	219.4
90	0.233	226.9
91	0.12225	229.75
92	0.14727	234.04
93	0.13559	238.88
94	0.15735	241.34
95	0.16597	243.04
96	0.17589	245.52
97	0.18018	246.84
98	0.19568	250.18
99	0.16313	254.
100	0.17123	257.8

Table 5 Models and parameters used in INC/GEM and LAHET

	INC/GEM	LAHET
INC	Bertini INC model	Bertini INC model
Preeq.	none	none
De-excitation	GEM	Fermi break-up model and EVAP
Level density parameter	GCCI parameter	GCCI parameter
Inverse reaction	Dostrovsky's parameter (n ∼ α) and Matuse's parameter (heavy fragments)	Dostrovsky's parameter
Fission	Atchison model with new parameter set	Atchison model with original parameter set

Table 6 Nuclides produced from proton induced reactions. Parentheses shows the charge of radioactive progenitors, whose mass number is the same as the nuclide, for calculations of cumulative cross sections.

Target	Nuclide
O	^{3}H, ^{3}He, ^{6}Li, ^{7}Li, ^{7}Be, ^{9}Be, ^{10}Be, ^{10}B, ^{11}B, ^{11}C, ^{14}C, ^{13}N
Al	^{3}H, ^{3}He, ^{4}He, ^{7}Be, ^{10}Be, ^{18}F, ^{20}Ne($Z < 10$), ^{21}Ne($Z > 10$), ^{22}Ne, ^{22}Na($Z > 11$), ^{24}Na($Z < 11$), ^{26}Al($Z > 13$)
Fe	^{3}H, ^{3}He, ^{4}He, ^{7}Be, ^{10}Be, ^{20}Ne($Z < 10$), ^{21}Ne($Z > 10$), ^{22}Ne, ^{22}Na($Z > 11$), ^{24}Na($Z < 11$), ^{28}Mg($Z < 12$), ^{26}Al, ^{32}P, ^{36}Cl, ^{39}Cl, ^{36}Ar, ^{42}K, ^{43}K($Z < 19$), ^{41}Ca($Z > 20$), ^{44}Sc, ^{46}Sc, ^{47}Sc($Z < 21$), ^{48}Sc, ^{44}Ti($Z > 22$), ^{48}V, ^{49}V, ^{48}Cr($Z > 24$), ^{51}Cr($Z > 24$), ^{52}Mn, ^{54}Mn, ^{52}Fe, ^{55}Fe, ^{55}Co, ^{56}Co, ^{57}Co, ^{58}Co
Nb	^{7}Be, ^{22}Na($Z > 11$), ^{46}Sc, ^{48}V($Z > 23$), ^{52}Mn($Z > 25$), ^{54}Mn, ^{59}Fe($Z < 26$), ^{56}Co($Z > 27$), ^{58}Co, ^{60}Co, ^{65}Zn($Z > 30$), ^{67}Ga($Z > 31$), ^{68}Ge($Z > 32$), ^{69}Ge($Z > 32$), ^{71}As($Z > 33$), ^{73}As($Z > 33$), ^{74}As, ^{72}Se($Z > 34$), ^{75}Se($Z > 34$), ^{77}Br($Z > 35$), ^{79}Kr($Z > 36$), ^{83}Rb($Z > 37$), ^{84}Rb, ^{82}Sr($Z > 38$), ^{83}Sr($Z > 38$), ^{85}Sr($Z > 38$), ^{86}Y($Z > 39$), ^{88}Y, ^{86}Zr($Z > 40$), ^{88}Zr($Z > 40$), ^{89}Zr($Z > 40$), ^{90}Nb($Z > 41$), ^{87}Y($Z > 39$)
Au	^{2}H, ^{3}H, ^{3}He, ^{4}He, ^{7}Be, ^{18}F($Z > 9$), ^{22}Na($Z > 11$), ^{24}Na($Z < 11$), ^{28}Mg($Z < 12$), ^{32}P, ^{46}Sc, ^{48}V($Z > 23$), ^{54}Mn, ^{59}Fe($Z < 26$), ^{58}Co, ^{60}Co, ^{65}Zn($Z > 30$), ^{74}As, ^{75}Se($Z > 34$), ^{82}Br, ^{83}Rb($Z > 37$), ^{84}Rb, ^{86}Rb, ^{85}Sr($Z > 38$), ^{87}Y($Z > 39$), ^{88}Y, ^{88}Zr($Z > 40$), ^{95}Zr($Z < 40$), ^{95}Nb, ^{96}Tc, ^{103}Ru($Z < 44$), ^{127}Xe($Z > 54$), ^{131}Ba($Z > 56$), ^{133}Ba($Z > 56$), ^{139}Ce($Z > 58$), ^{143}Pm($Z > 61$), ^{148}Eu, ^{155}Tb($Z > 65$), ^{160}Er($Z > 68$), ^{165}Tm($Z > 69$), ^{167}Tm($Z > 69$), ^{168}Tm, ^{166}Yb($Z > 70$), ^{169}Yb($Z > 70$), ^{169}Lu($Z > 71$), ^{170}Lu($Z > 71$), ^{171}Lu($Z > 71$), ^{173}Lu($Z > 71$), ^{170}Hf($Z > 72$), ^{173}Hf($Z > 72$), ^{175}Hf($Z > 72$), ^{178}W($Z > 74$), ^{181}Re($Z > 75$), ^{183}Re($Z > 75$), ^{182}Os($Z > 76$), ^{185}Os($Z > 76$), ^{191}Os($Z < 76$), ^{185}Ir($Z > 77$), ^{186}Ir($Z > 77$), ^{187}Ir($Z > 77$), ^{188}Ir, ^{190}Ir, ^{192}Ir, ^{188}Pt($Z > 78$), ^{189}Pt($Z > 78$), ^{191}Pt($Z > 78$), ^{193}Au($Z > 79$), ^{194}Au, ^{195}Au($Z > 79$), ^{196}Au, ^{193}Hg, ^{194}Hg
U	^{9}Li, ^{7}Be, ^{13}N, ^{16}C, ^{24}Na, ^{28}Mg, ^{45}Ca($Z < 20$), ^{47}Ca($Z < 20$), ^{43}Sc($Z > 21$), ^{46}Sc, ^{47}Sc, ^{48}Sc, ^{47}V($Z > 23$), ^{48}V, ^{49}V($Z > 23$), ^{49}Cr($Z > 24$), ^{51}Cr($Z > 24$), ^{66}Ni($Z < 28$), ^{67}Cu($Z < 29$), ^{72}Ga, ^{73}Ga($Z < 31$), ^{83}Rb($Z > 37$), ^{84}Rb, ^{86}Rb, ^{87}Rb($Z < 37$), ^{89}Rb, ^{90}Rb, ^{91}Rb, ^{92}Rb, ^{93}Rb, ^{94}Rb, ^{95}Rb, ^{96}Rb, ^{97}Rb, ^{82}Sr($Z > 38$), ^{83}Sr($Z > 38$), ^{89}Sr($Z < 38$), ^{91}Sr($Z < 38$), ^{90}Y, ^{91}Y($Z < 39$), ^{93}Y($Z < 39$), ^{97}Zr($Z < 40$), ^{99}Mo($Z < 42$), ^{103}Pd($Z > 46$), ^{111}Pd, ^{112}Pd($Z < 46$), ^{111}Ag($Z < 47$), ^{112}Ag, ^{113}Ag($Z < 47$), ^{115}Ag($Z < 47$), ^{115}Cd, ^{111}In($Z > 49$), ^{115}In, ^{117}In, ^{122}Sb, ^{124}Sb, ^{125}Sb($Z < 51$), ^{126}Sb, ^{127}Sb($Z < 51$), ^{132}Te($Z < 52$), ^{134}Te($Z < 52$), ^{123}I, ^{124}I, ^{125}I, ^{130}I, ^{131}I, ^{132}I, ^{134}I, ^{135}I, ^{125}Cs($Z > 55$), ^{127}Cs($Z > 55$), ^{129}Cs, ^{130}Cs, ^{131}Cs, ^{132}Cs, ^{134}Cs, ^{135}Cs($Z < 55$), ^{136}Cs, ^{137}Cs($Z < 55$), ^{128}Ba($Z > 56$), ^{129}Ba($Z > 56$), ^{131}Ba, ^{133}Ba, ^{135}Ba, ^{139}Ba($Z < 56$), ^{140}Ba($Z < 56$), ^{131}La($Z > 57$), ^{140}La, ^{131}Ce($Z > 58$), ^{141}Ce($Z < 58$), ^{143}Ce($Z < 58$), ^{144}Ce($Z < 58$), ^{143}Pr, ^{147}Nd($Z < 60$), ^{153}Sm($Z < 62$), ^{156}Eu($Z < 63$), ^{157}Eu($Z < 63$), ^{224}Ra, ^{224}Ac, ^{225}Ac, ^{226}Ac, ^{228}Ac, ^{226}Th, ^{227}Th, ^{228}Th, ^{231}Th, ^{234}Th, ^{227}Pa, ^{228}Pa, ^{229}Pa, ^{230}Pa, ^{232}Pa, ^{233}Pa, ^{234}Pa, ^{235}Pa, ^{237}Pa, ^{228}U, ^{229}U, ^{230}U, ^{236}Np, ^{238}Np

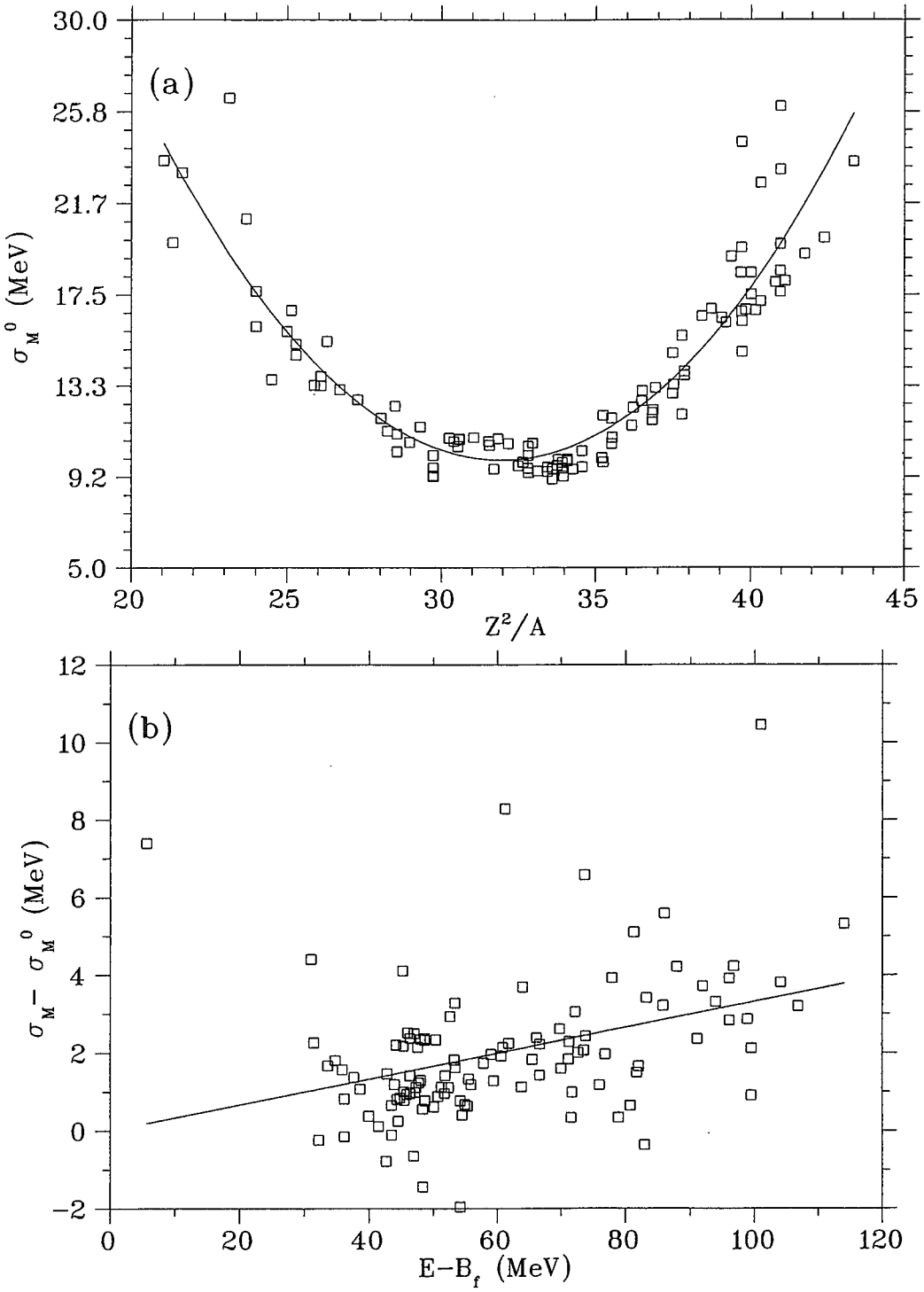

Fig. 1 The dependency of the dispersion of fission fragment mass distribution on Z^2/A and $E-B_f$: (a) σ_M adjusted to $E-B_f = 0(\equiv \sigma_M^0)$ versus Z^2/A; (b) $\sigma_M - \sigma_M^0$ versus $E-B_f$. The squares represent the experimental data collected in ref. [20] and ref. [21], and the solid lines show the values given by Eq. 21.

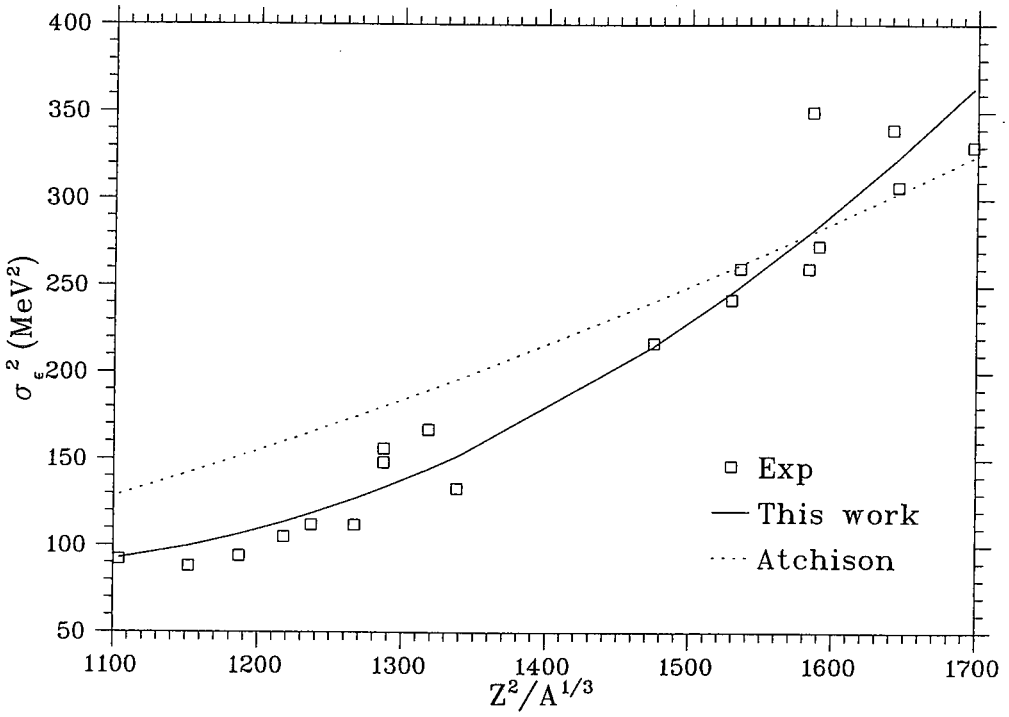

Fig. 2 The dispersion of kinetic energy $\sigma^2_{\epsilon_f}$ versus $Z_i^2/A_i^{1/3}$: The experimental values [24] are shown by open squares. The fitted values given by Eq. (25) are shown (the solid line) as well as those calculated by using the expression in the Atchison model (the dotted line).

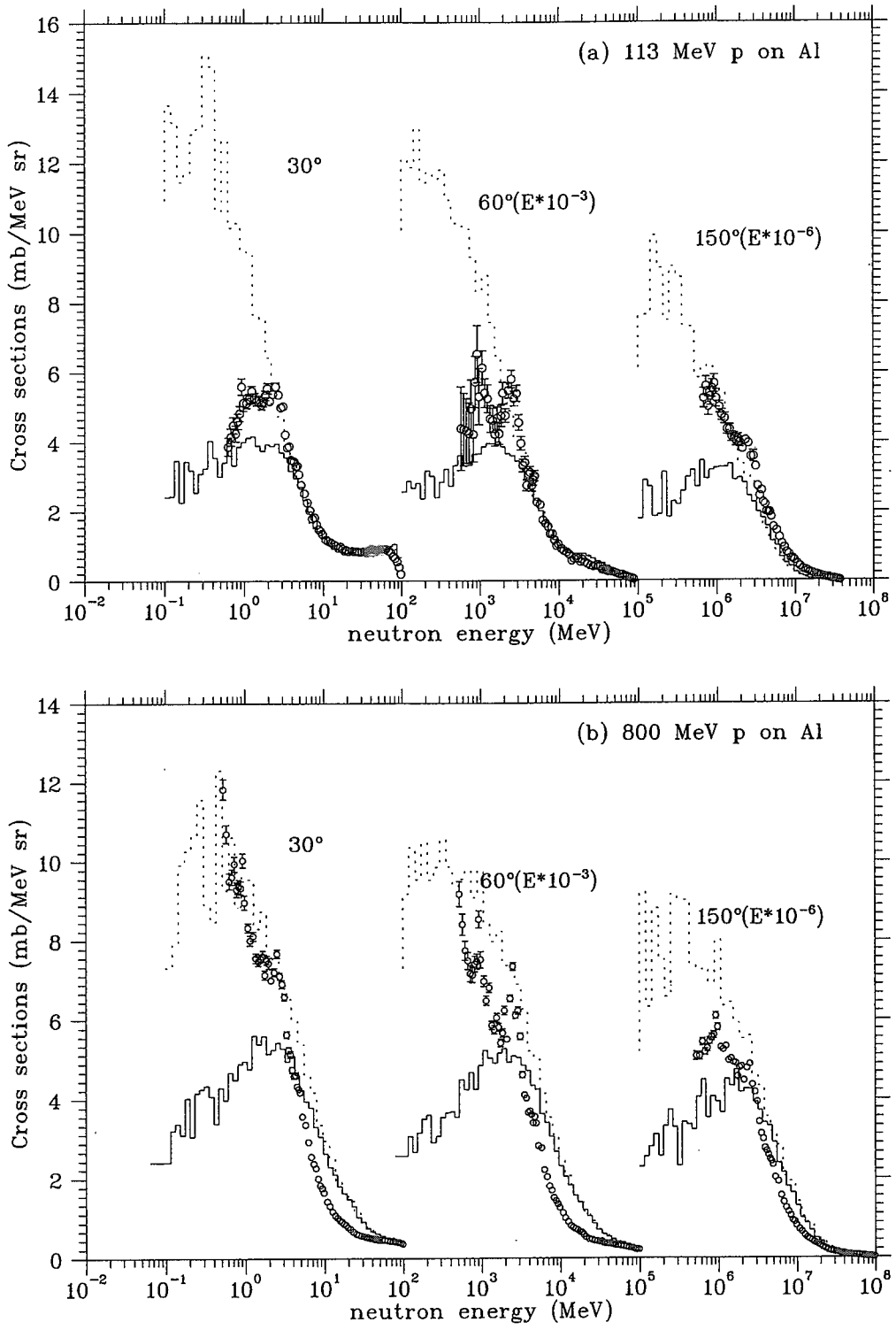

Fig. 3 Neutron energy spectra for the reactions on Al irradiated by: (a) 113 MeV protons; (b) 800 MeV protons. The solid lines are the INC/GEM estimates, and the open squares for 113 MeV are experimental data by Amian *et al.* [28], and those for 800 MeV are by Meier *et al.* [29].

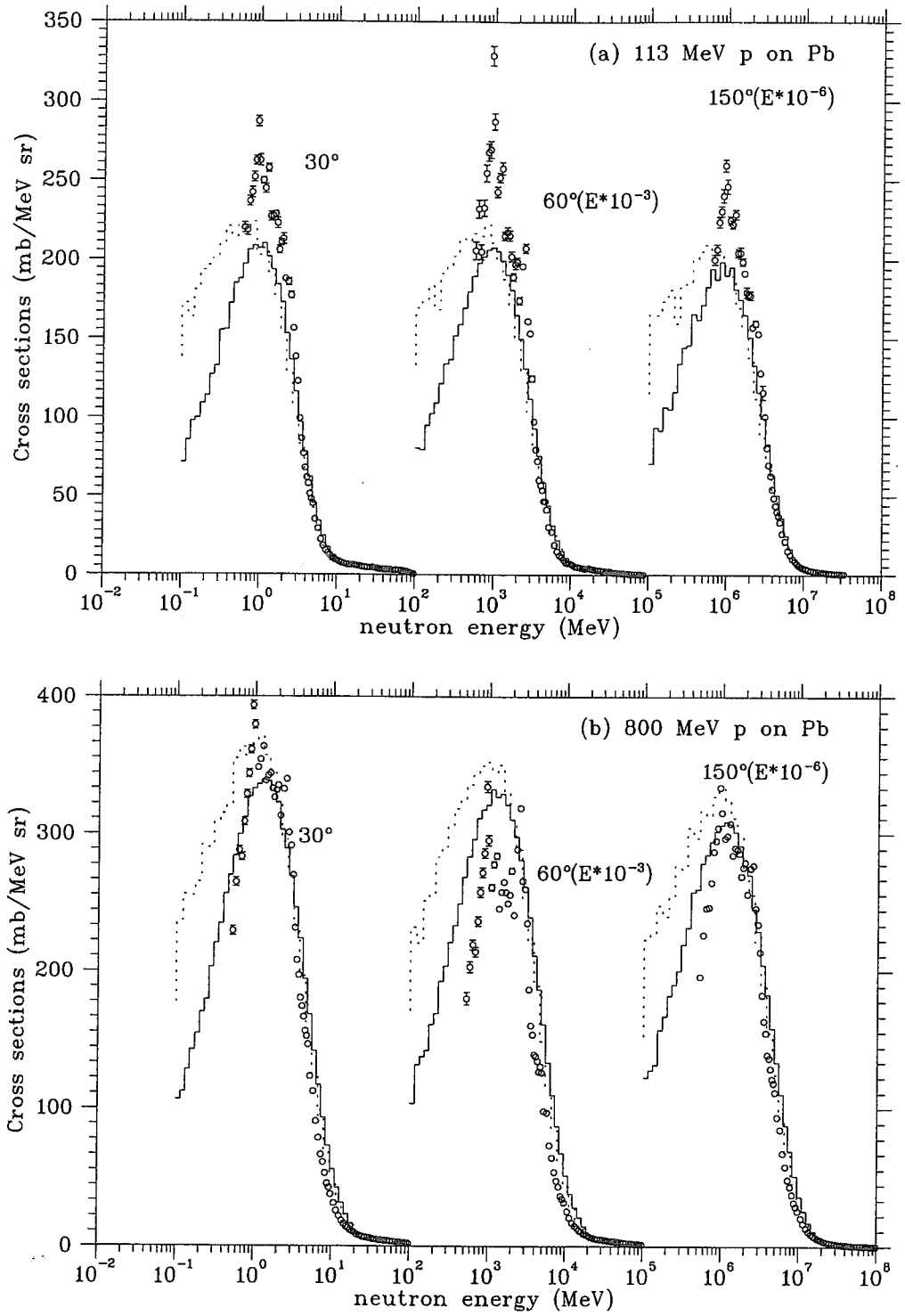

Fig. 4 Neutron energy spectra for the reactions on Pb irradiated by: (a) 113 MeV protons; (b) 800 MeV protons. The solid lines are the INC/GEM estimates, and the open squares for 113 MeV are experimental data by Amian *et al.* [28], and those for 800 MeV are by Meier *et al.* [29].

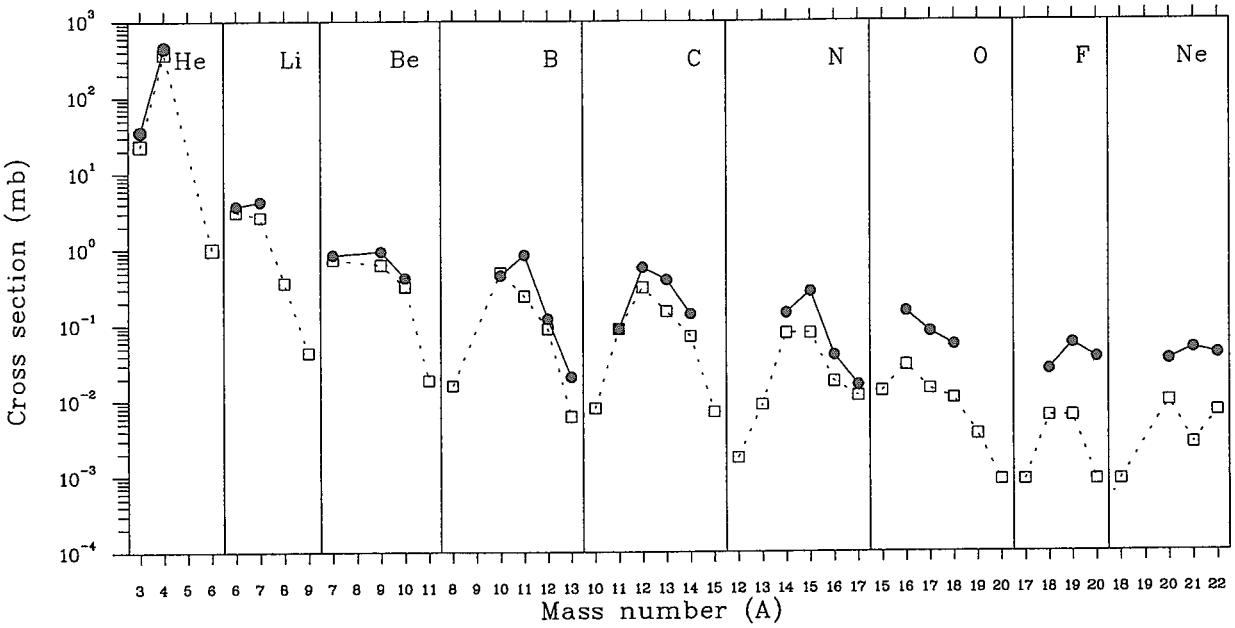

Fig. 5 Isotopic distributions of the nuclei produced from 480 MeV protons incident on ^{nat}Ag. The open squares with the solid lines denotes the results by calculated INC/GEM and the black circles with the dashed lines denotes experimental data [30]. The lines are drawn to guide to eyes.

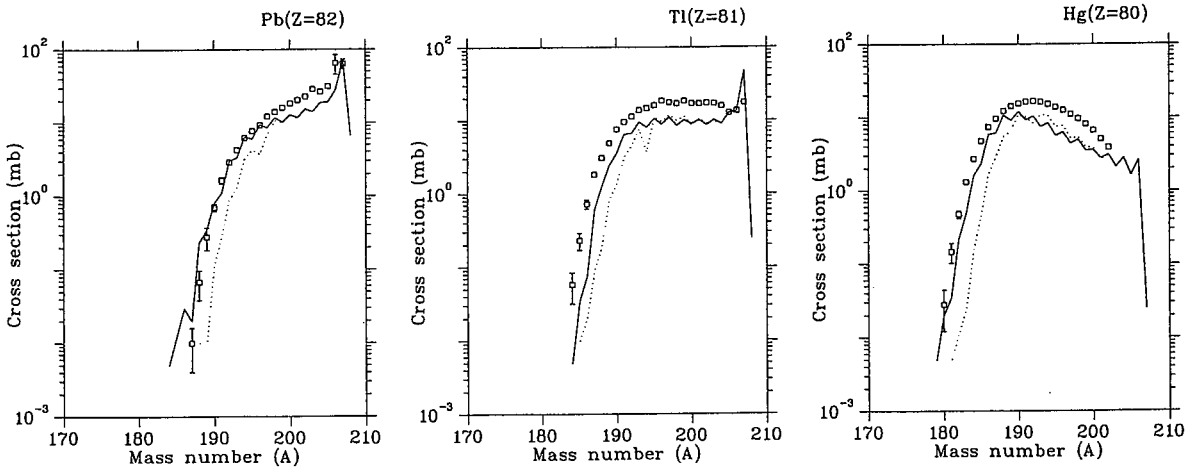

Fig. 6 Isotopic distributions of the residues with $82 \leq Z \leq 86$ produced from the bombardment of ^{208} Pb with protons at 1 GeV. The open squares are the experimental data measured by GSI [31], the solid lines are the estimates by using INC/GEM, and the dashed lines are those by LAHET

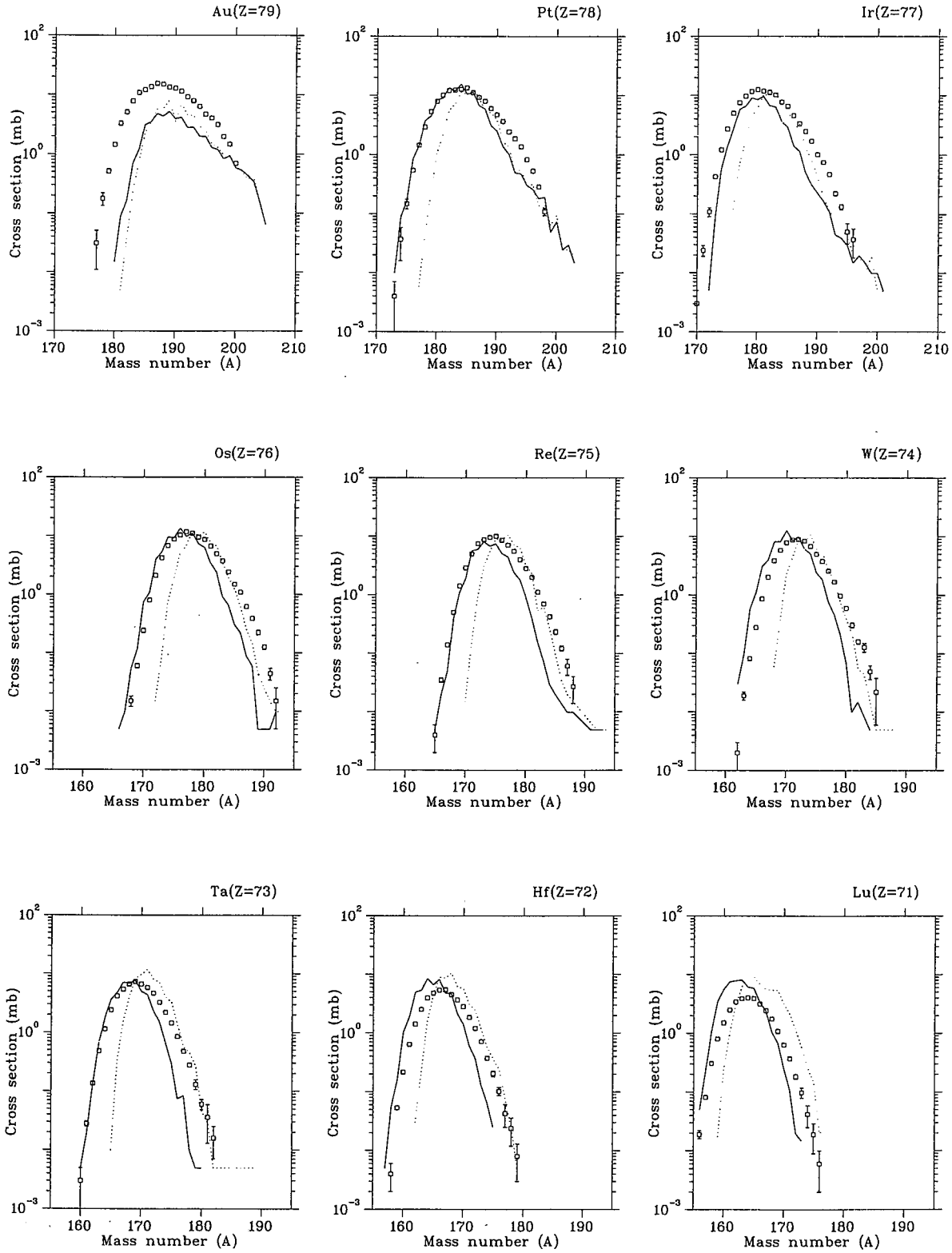

Fig. 7 Isotopic distributions of the residues with $71 \leq Z \leq 79$ produced from the bombardment of ^{208} Pb with protons at 1 GeV. The open squares are the experimental data measured by GSI [31], the solid lines are the estimates by using INC/GEM, and the dashed lines are those by LAHET

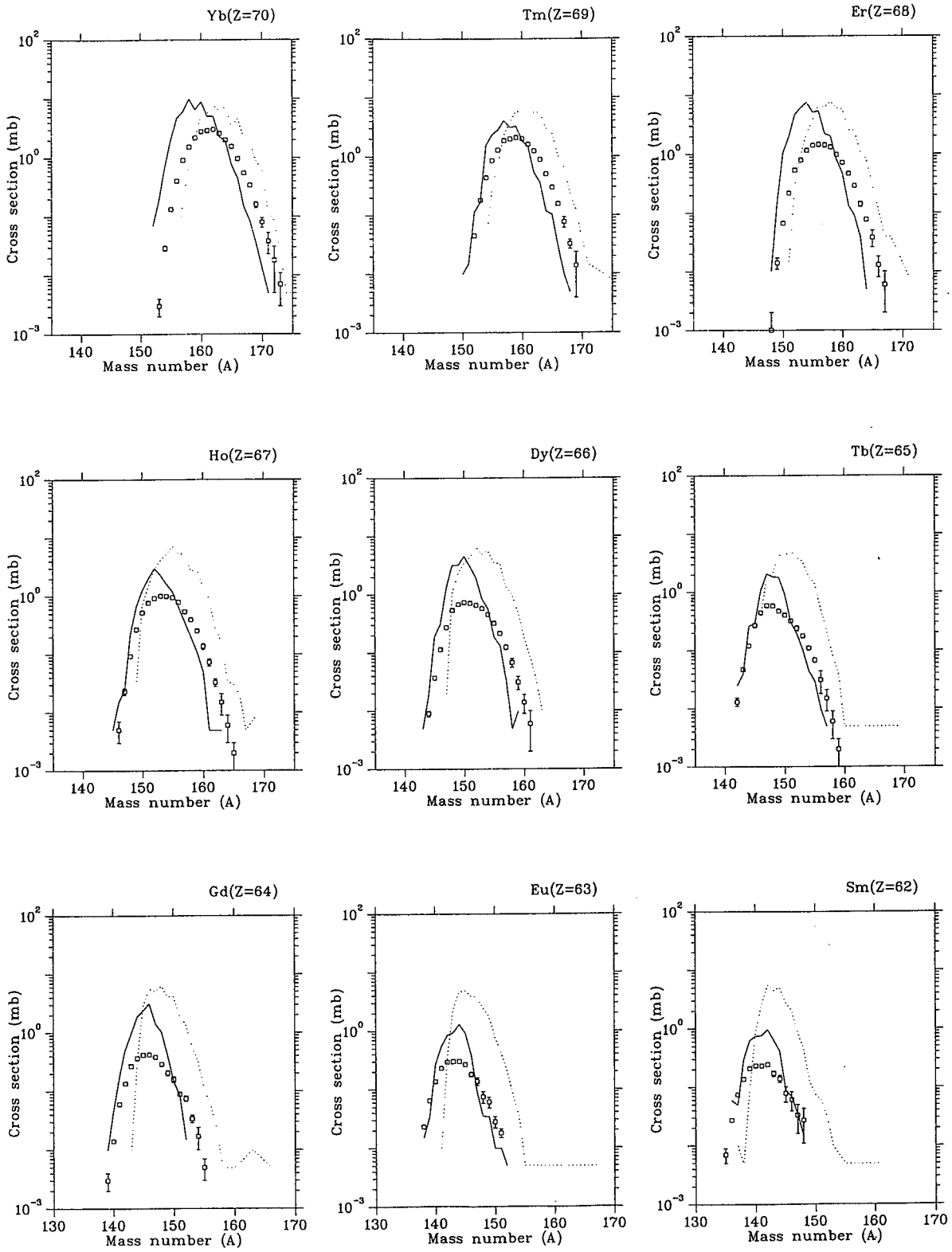

Fig. 8 Isotopic distributions of the residues with $62 \leq Z \leq 70$ produced from the bombardment of ^{208} Pb with protons at 1 GeV. The open squares are the experimental data measured by GSI [31], the solid lines are the estimates by using INC/GEM, and the dashed lines are those by LAHET

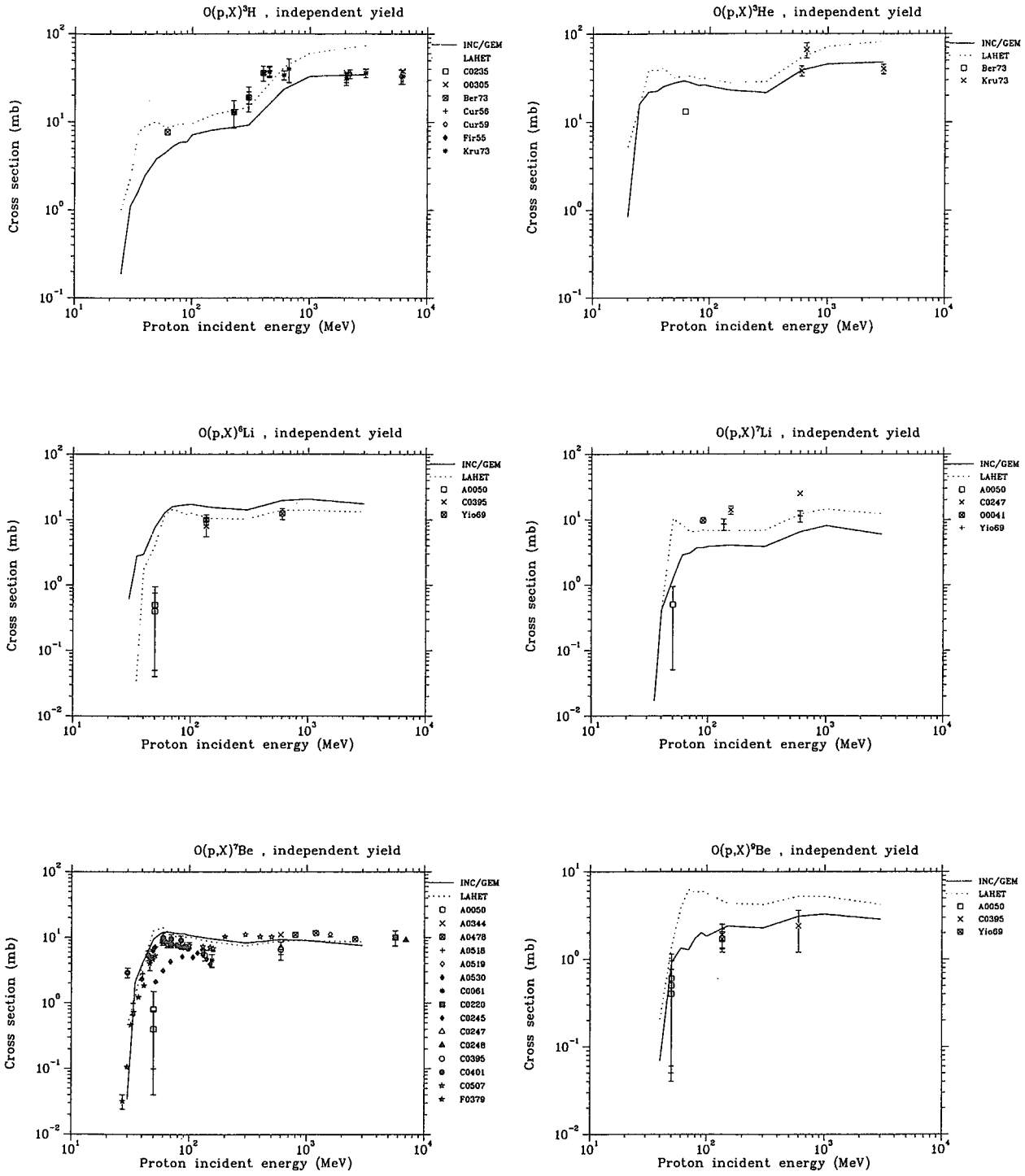

Fig. 9 Excitation functions for nuclide productions from the reactions on O irradiated by protons. See section 3.3 for explanatory notes of experimental data.

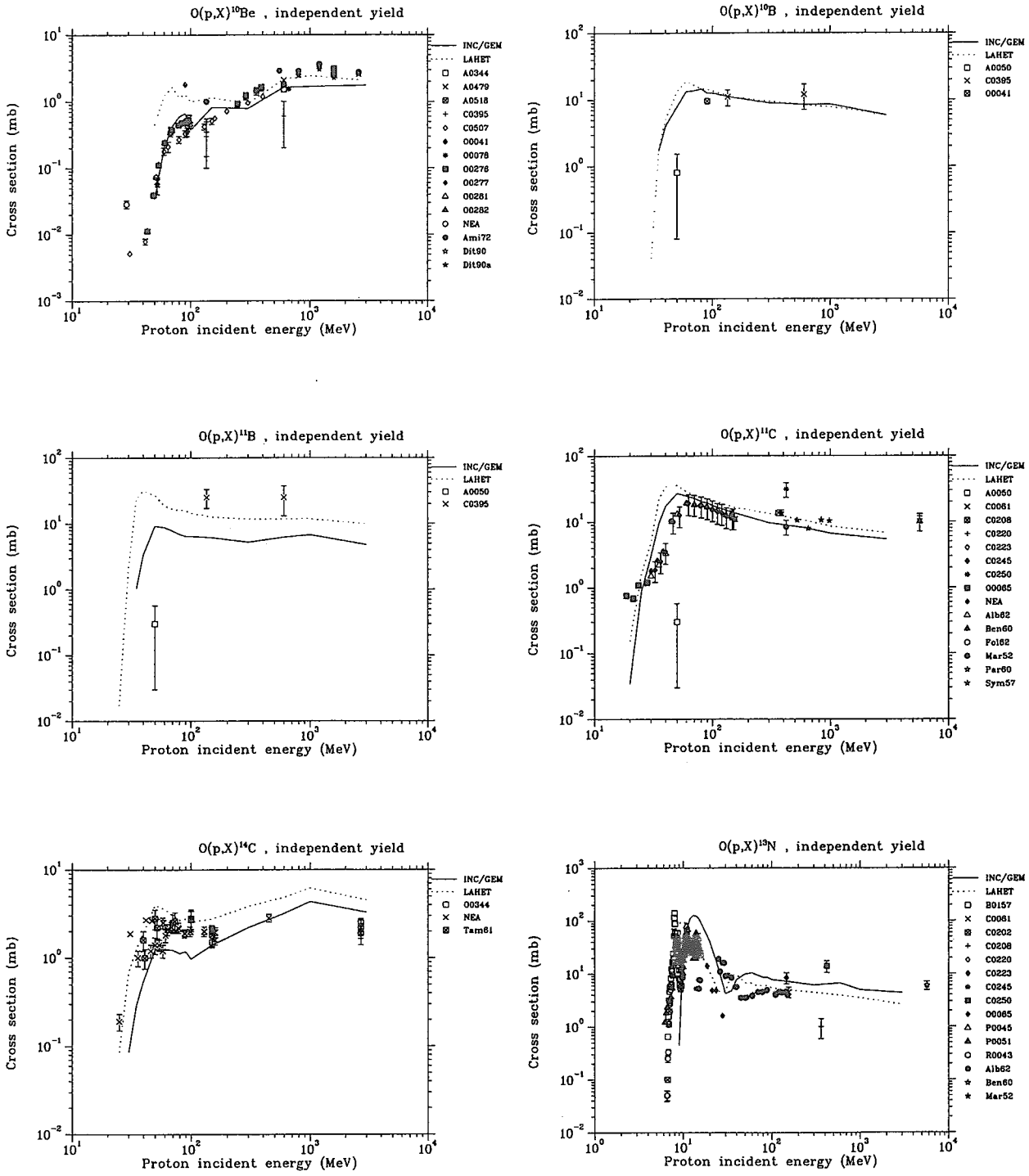

Fig. 10 Excitation functions for nuclide production from the reactions on O irradiated by protons. See section 3.3 for explanatory notes of experimental data.

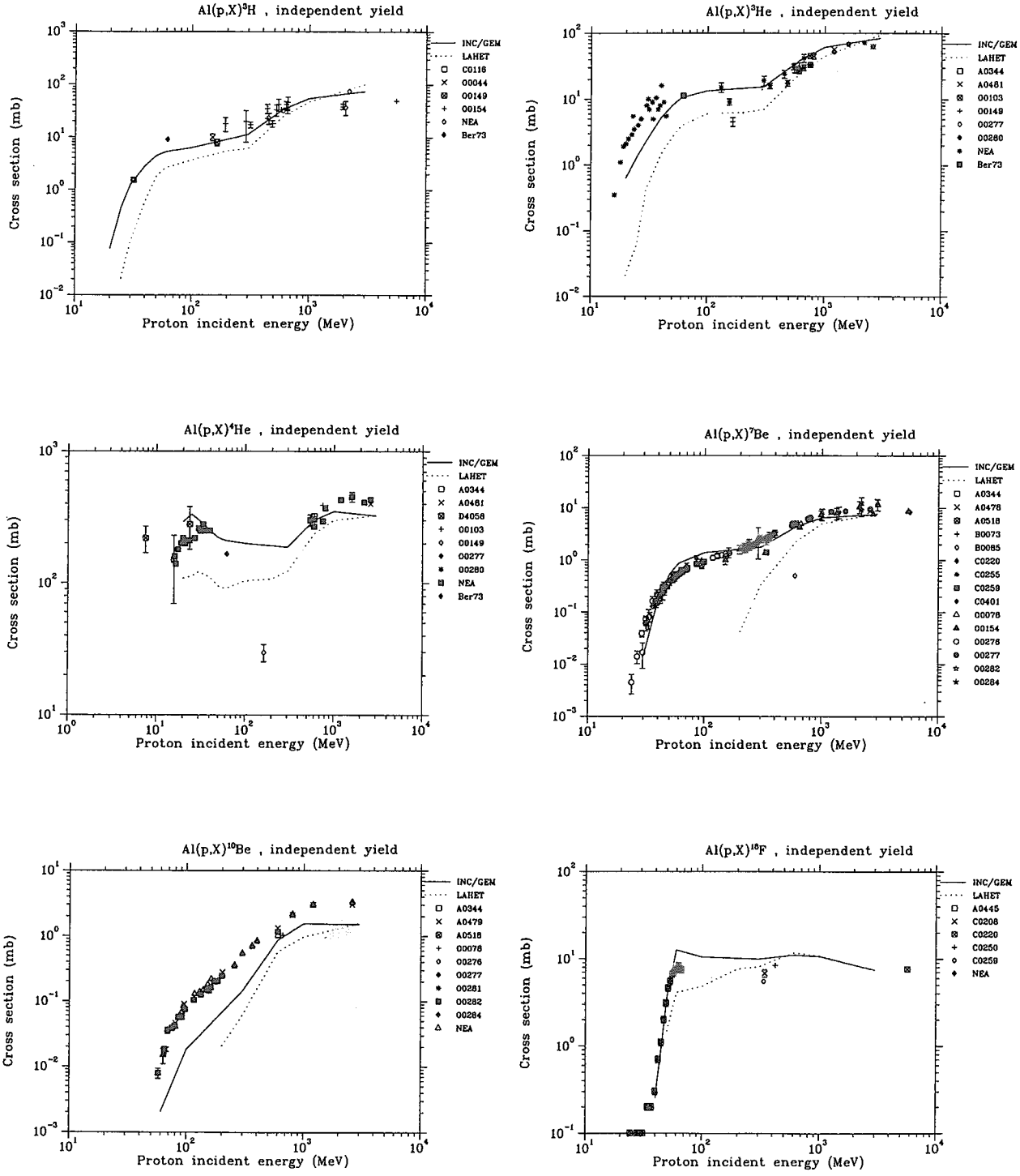

Fig. 11 Excitation functions for nuclide production from the reactions on Al irradiated by protons. See section 3.3 for explanatory notes of experimental data.

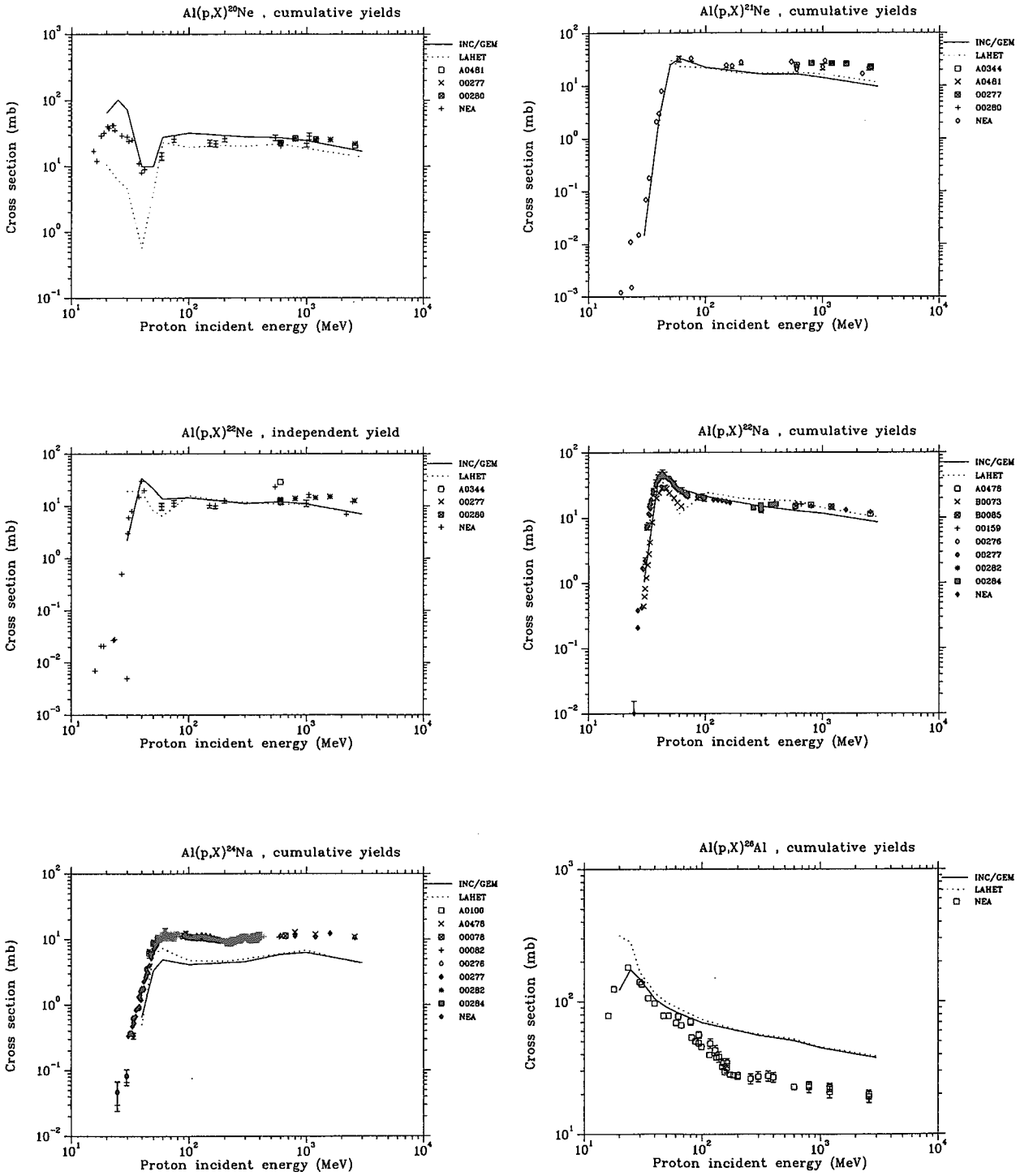

Fig. 12 Excitation functions for nuclide production from the reactions on Al irradiated by protons. See section 3.3 for explanatory notes of experimental data.

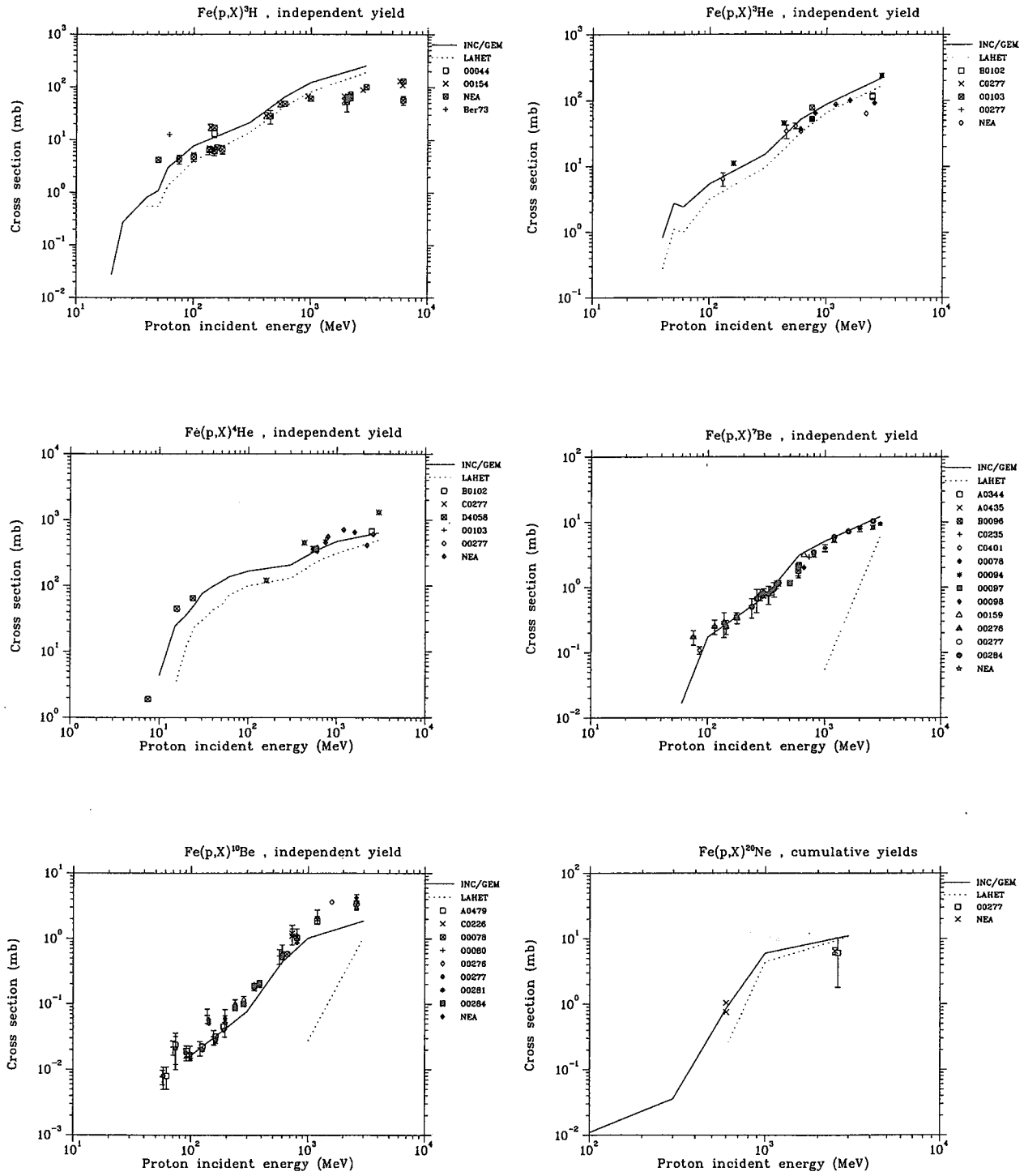

Fig. 13 Excitation functions for nuclide production from the reactions on Fe irradiated by protons. See section 3.3 for explanatory notes of experimental data.

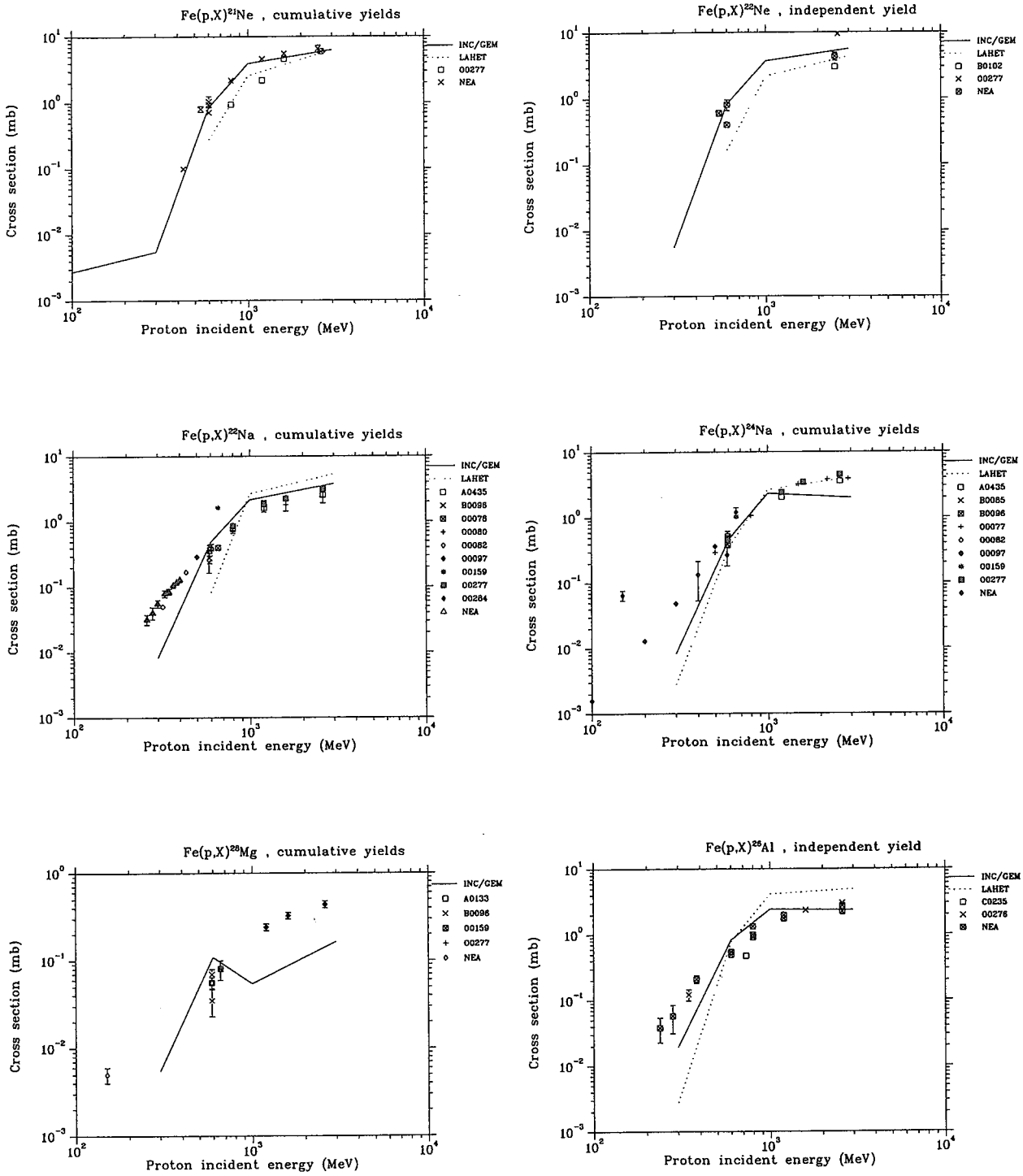

Fig. 14 Excitation functions for nuclide production from the reactions on Fe irradiated by protons. See section 3.3 for explanatory notes of experimental data.

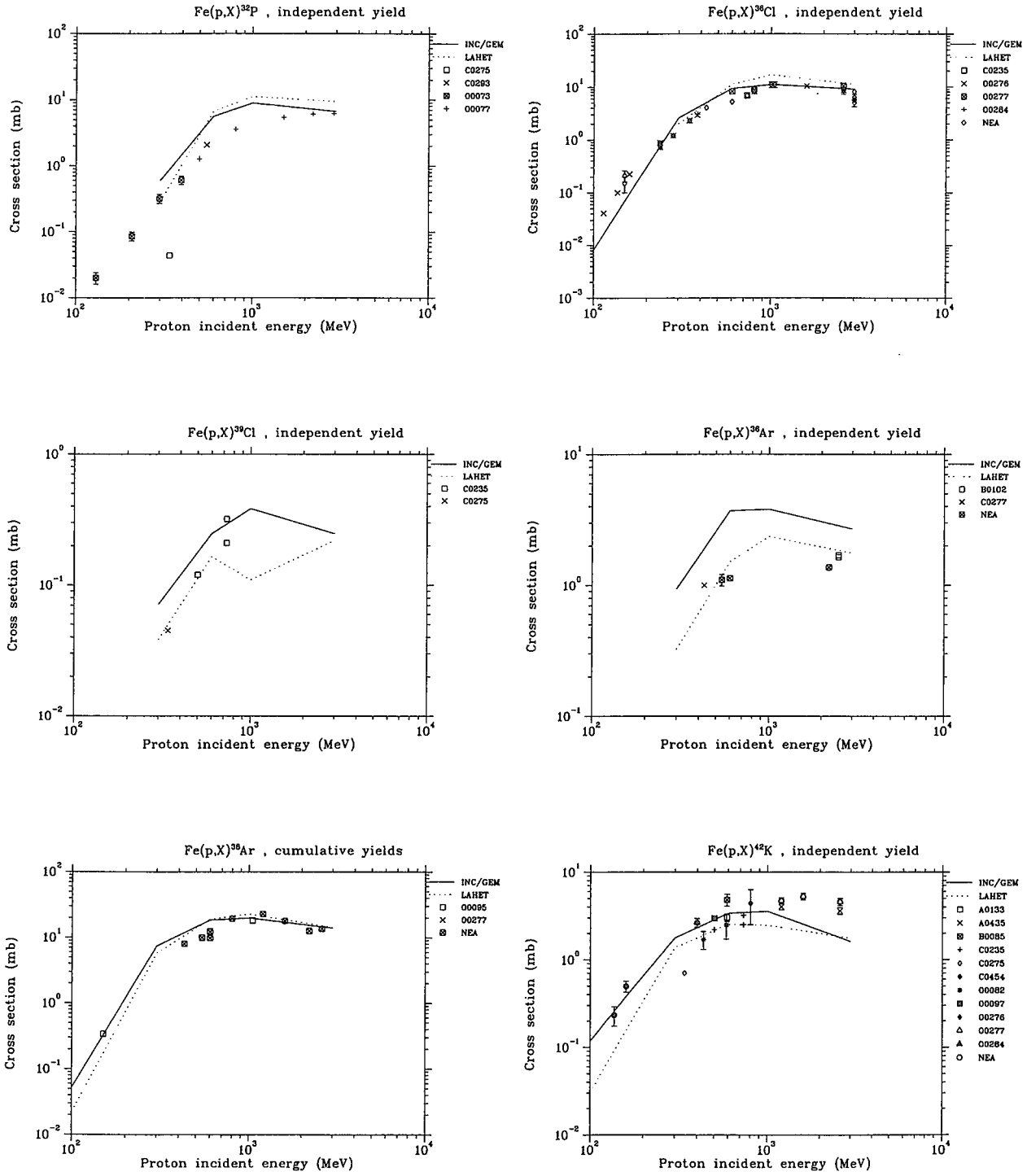

Fig. 15 Excitation functions for nuclide production from the reactions on Fe irradiated by protons. See section 3.3 for explanatory notes of experimental data.

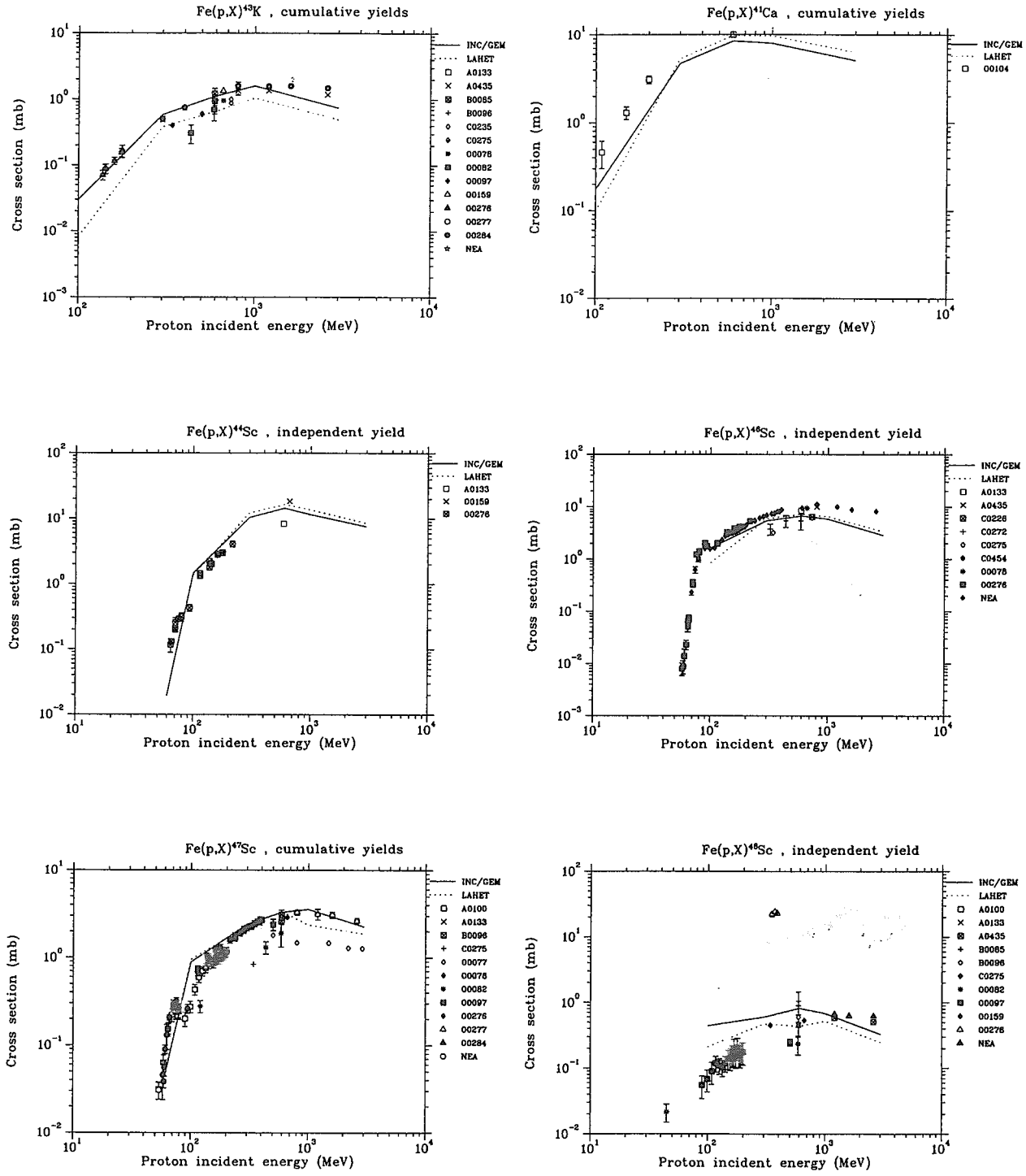

Fig. 16 Excitation functions for nuclide production from the reactions on Fe irradiated by protons. See section 3.3 for explanatory notes of experimental data.

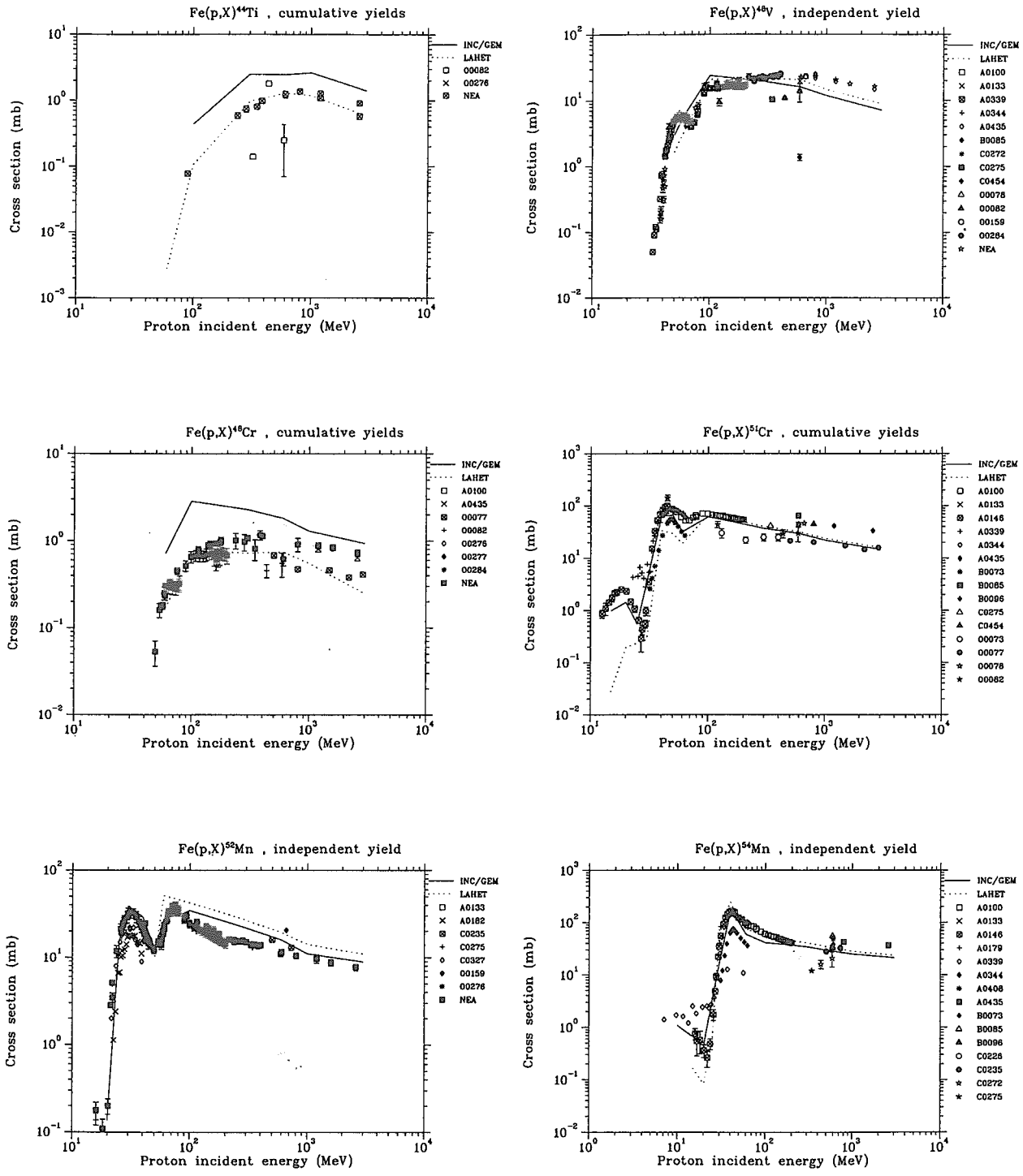

Fig. 17 Excitation functions for nuclide production from the reactions on Fe irradiated by protons. See section 3.3 for explanatory notes of experimental data.

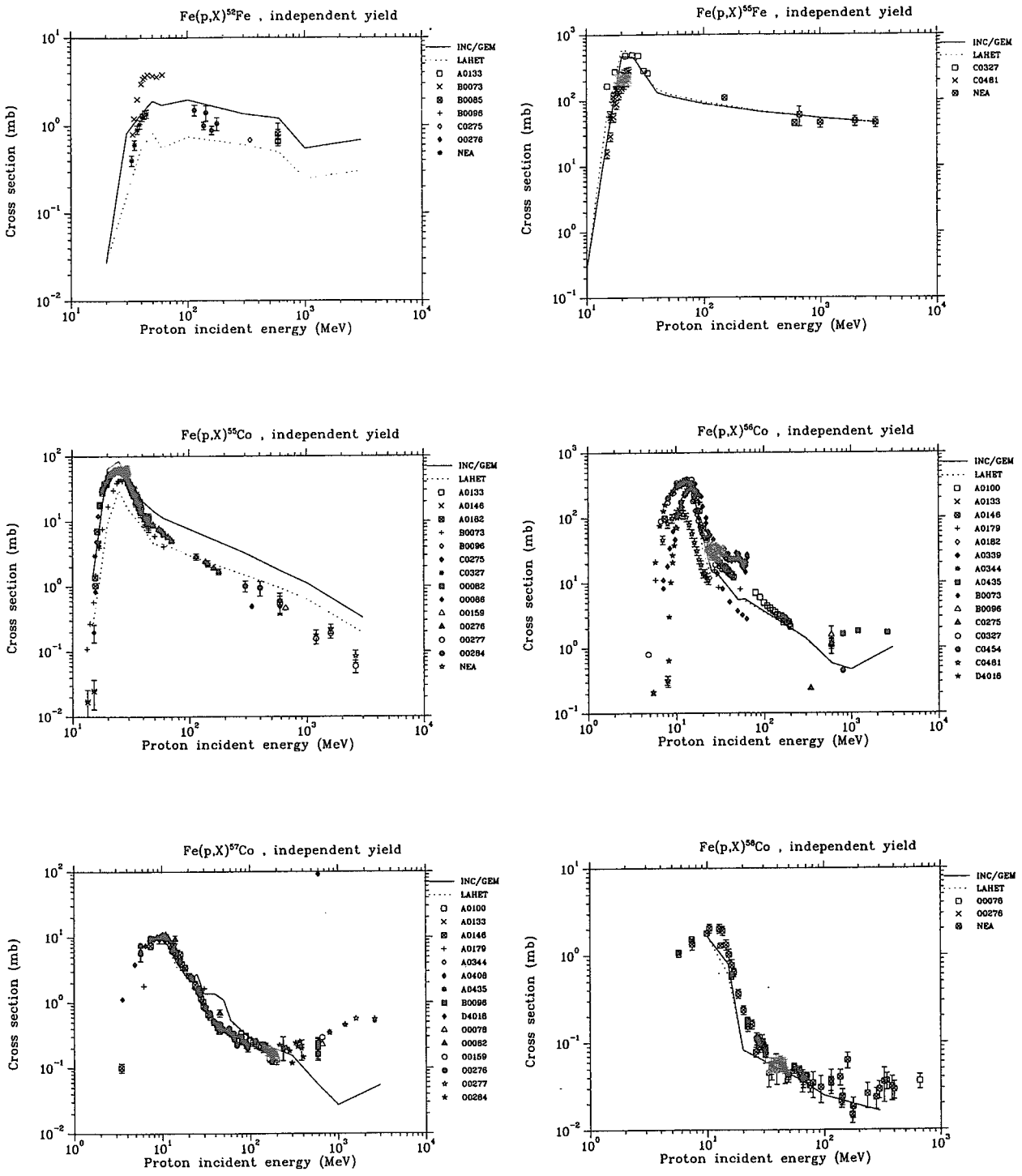

Fig. 18 Excitation functions for nuclide production from the reactions on Fe irradiated by protons. See section 3.3 for explanatory notes of experimental data.

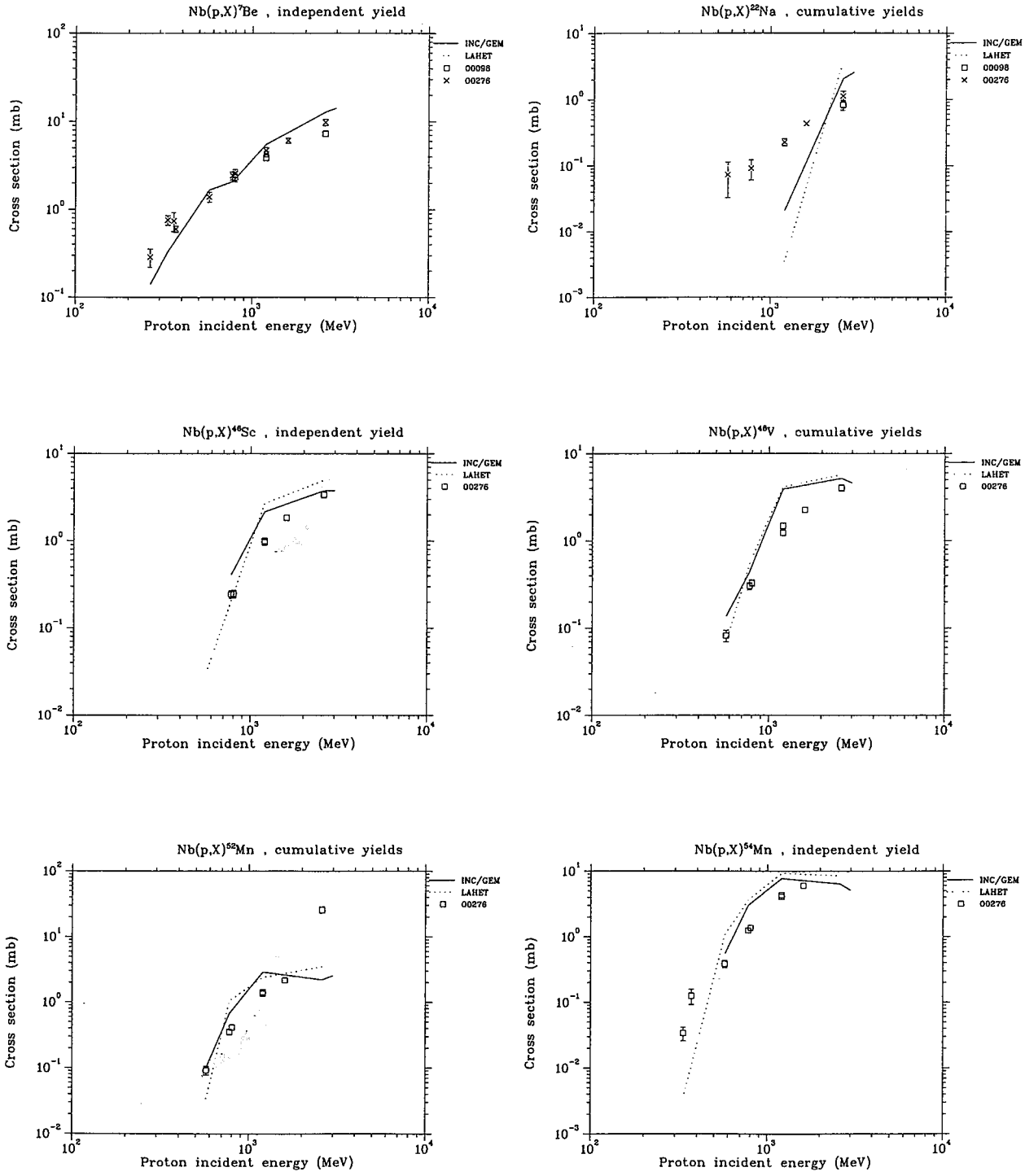

Fig. 19 Excitation functions for nuclide production from the reactions on Nb irradiated by protons. See section 3.3 for explanatory notes of experimental data.

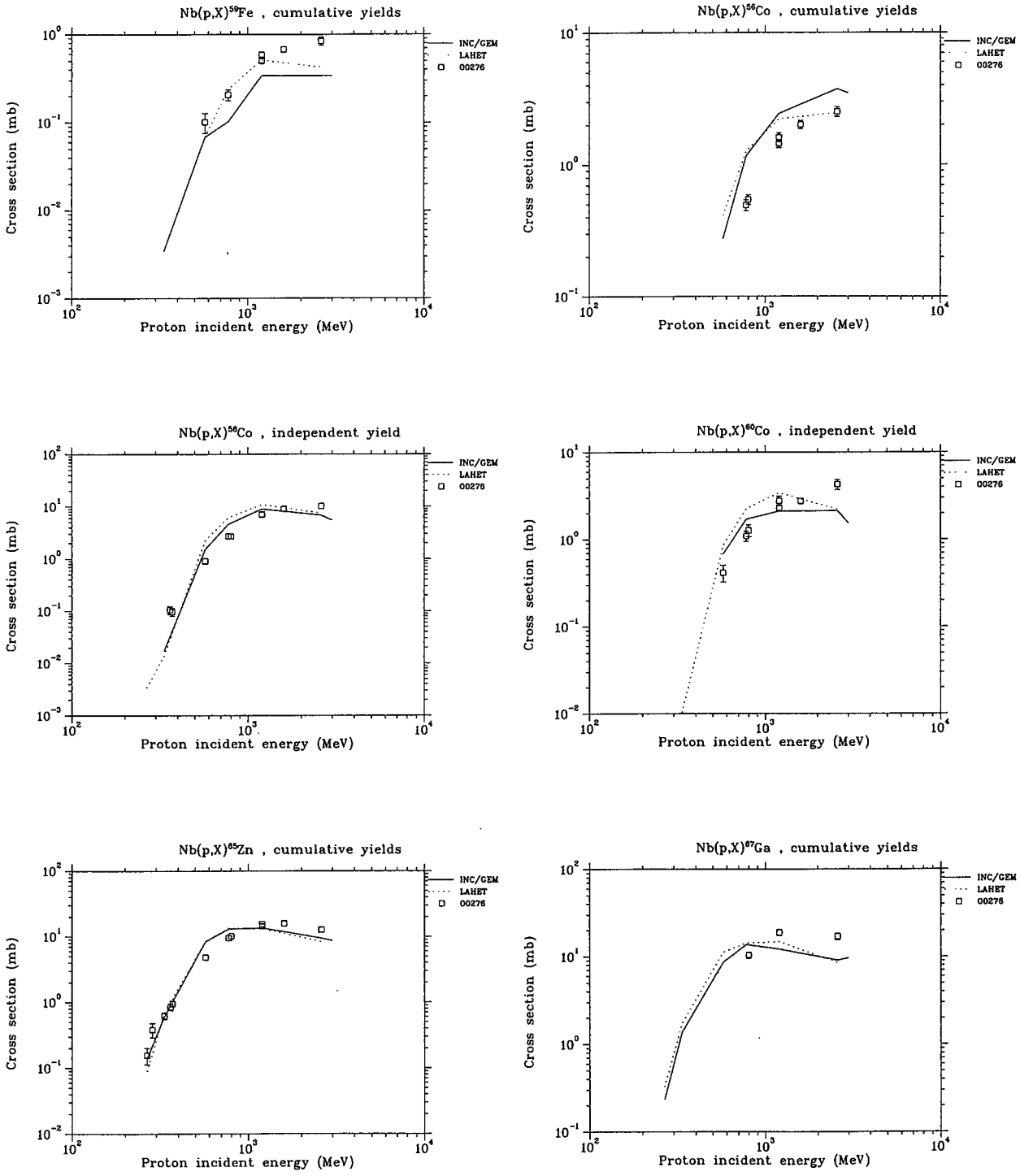

Fig. 20 Excitation functions for nuclide production from the reactions on Nb irradiated by protons. See section 3.3 for explanatory notes of experimental data.

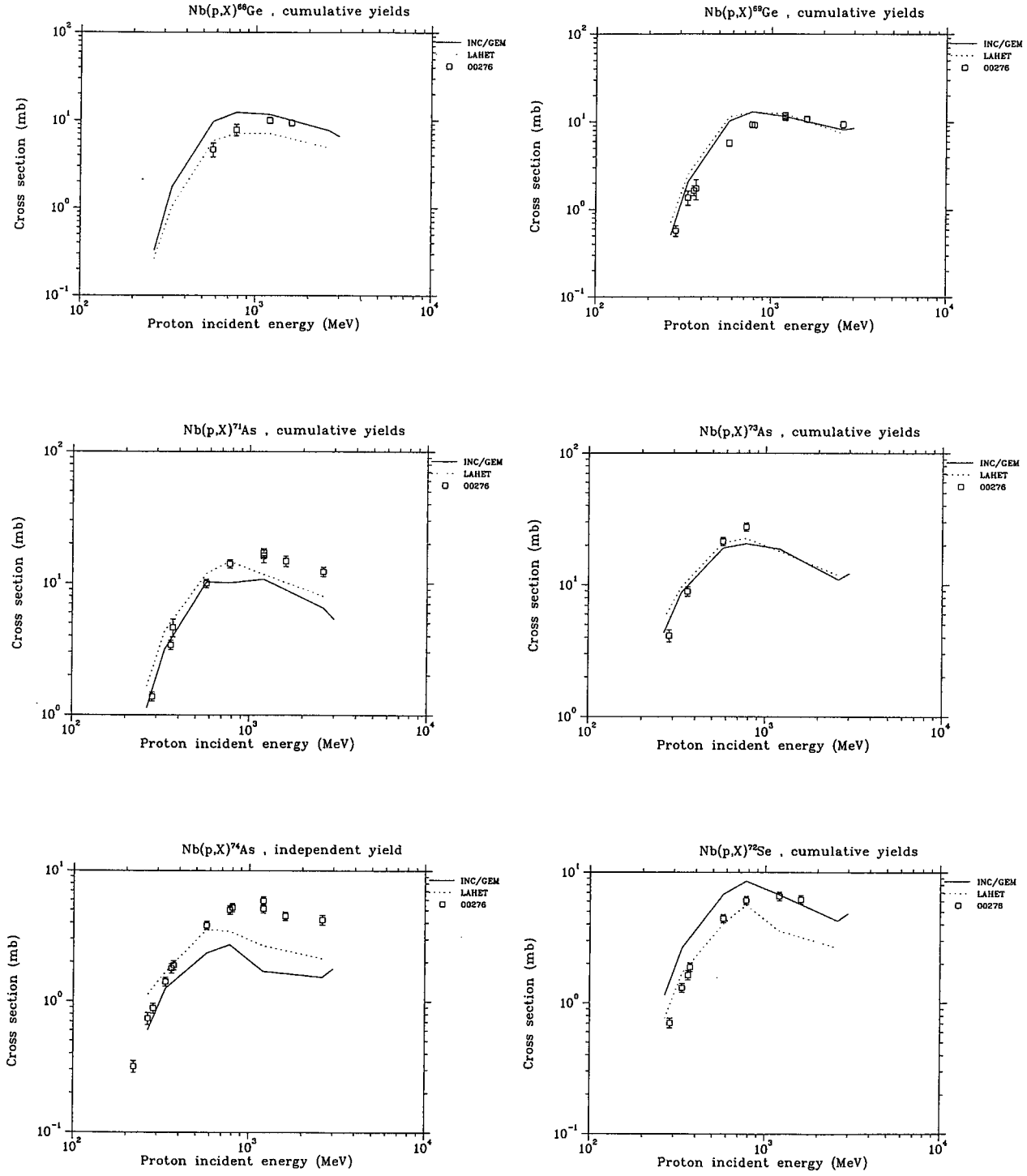

Fig. 21 Excitation functions for nuclide production from the reactions on Nb irradiated by protons. See section 3.3 for explanatory notes of experimental data.

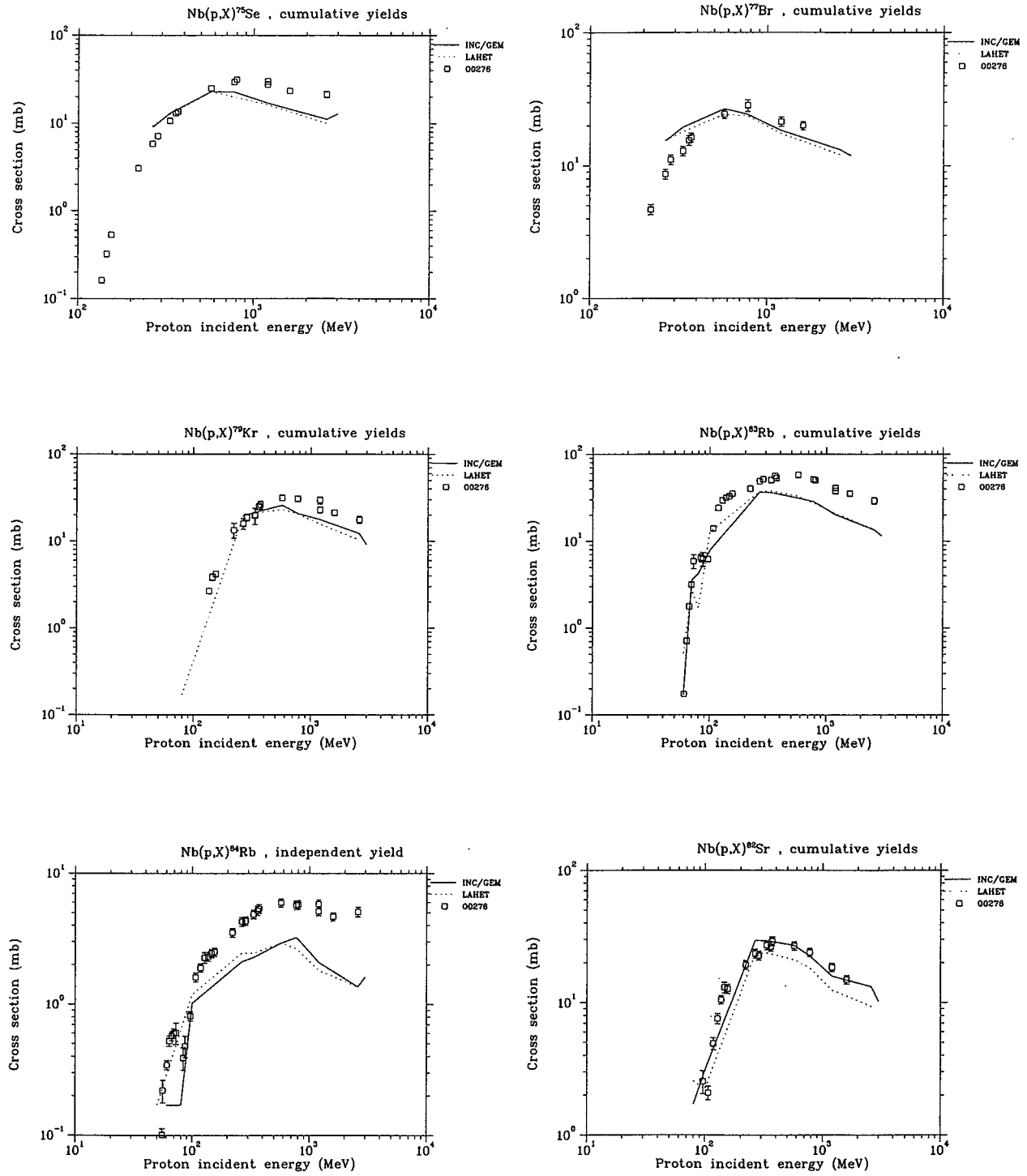

Fig. 22 Excitation functions for nuclide production from the reactions on Nb irradiated by protons. See section 3.3 for explanatory notes of experimental data.

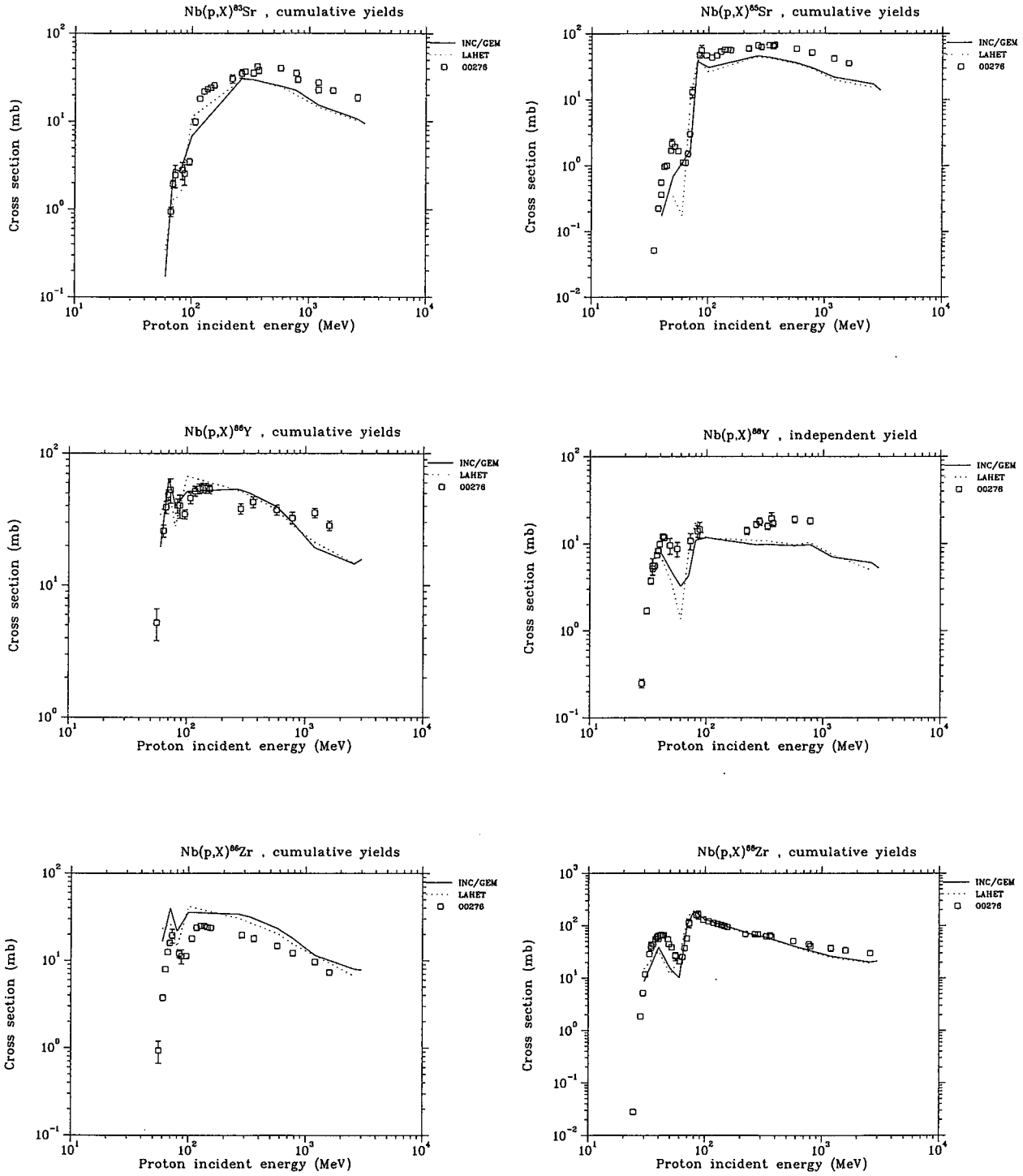

Fig. 23 Excitation functions for nuclide production from the reactions on Nb irradiated by protons. See section 3.3 for explanatory notes of experimental data.

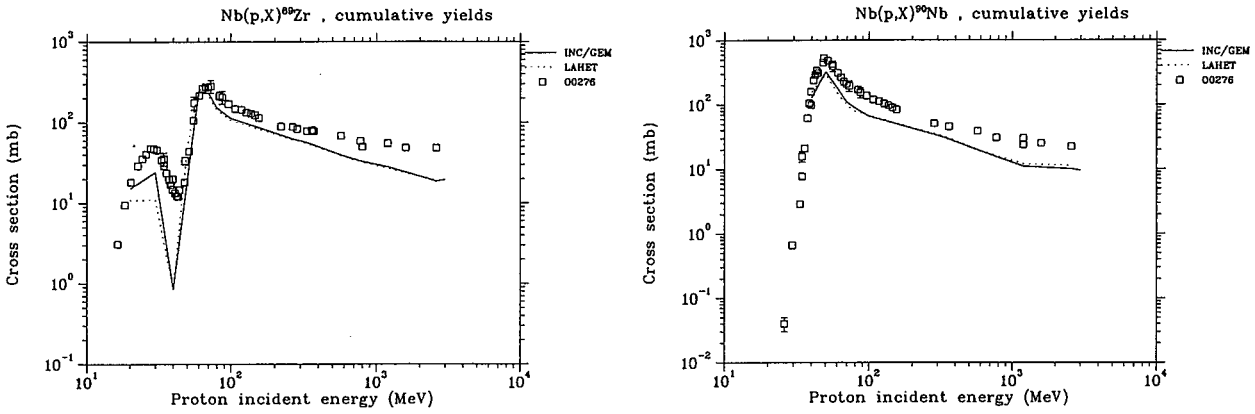

Fig. 24 Excitation functions for nuclide production from the reactions on Nb irradiated by protons. See section 3.3 for explanatory notes of experimental data.

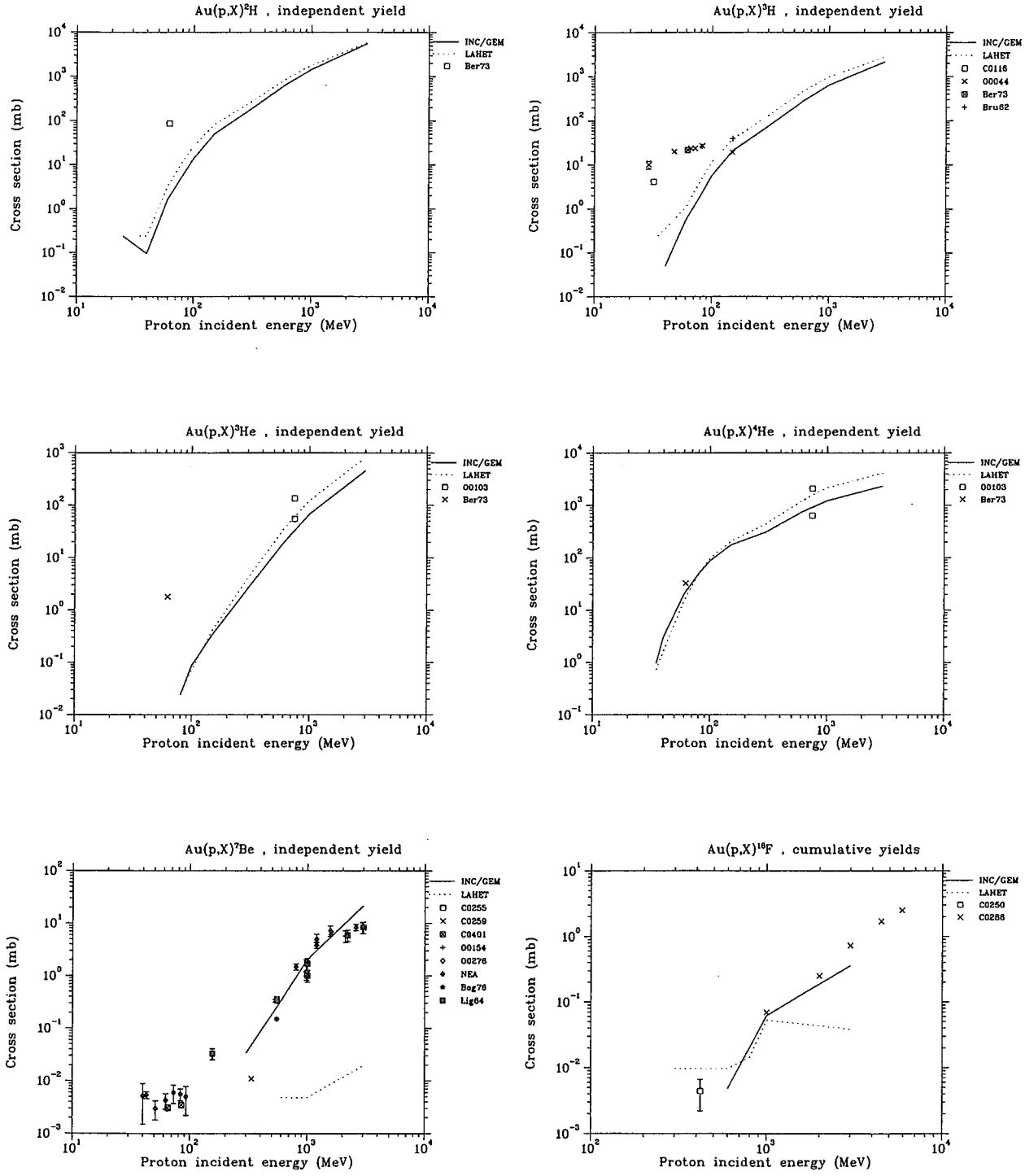

Fig. 25 Excitation functions for nuclide production from the reactions on Au irradiated by protons. See section 3.3 for explanatory notes of experimental data.

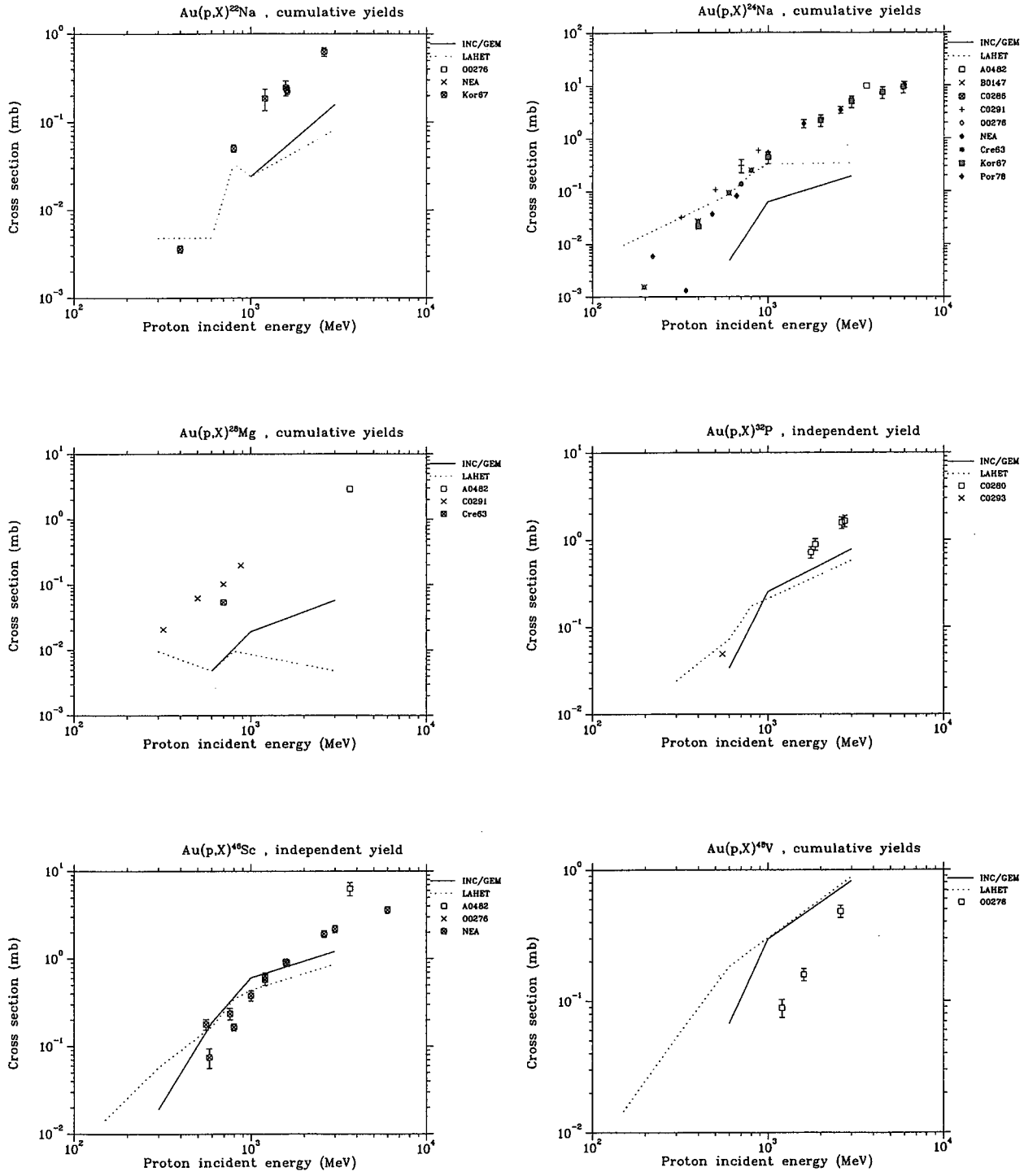

Fig. 26 Excitation functions for nuclide production from the reactions on Au irradiated by protons. See section 3.3 for explanatory notes of experimental data.

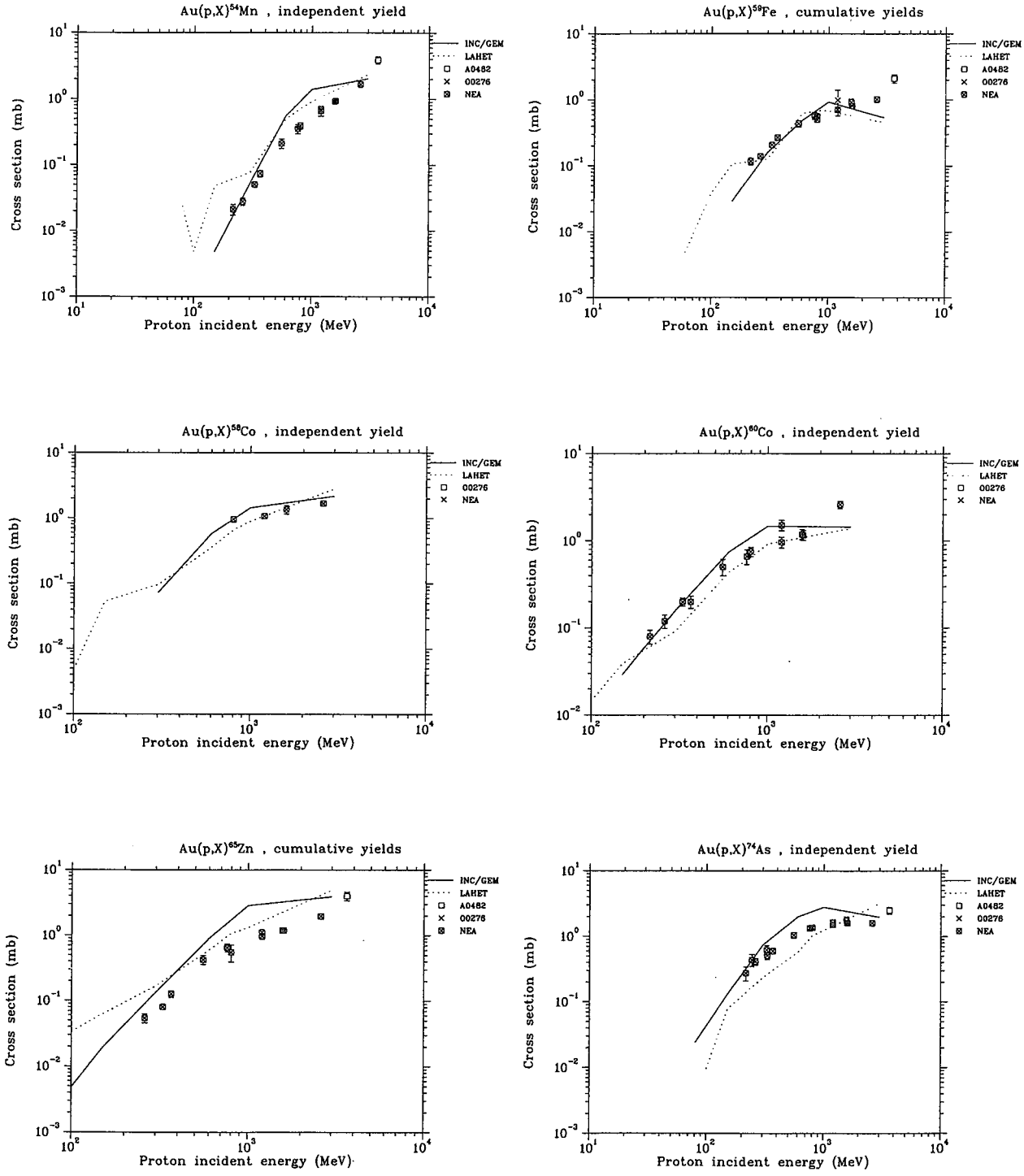

Fig. 27 Excitation functions for nuclide production from the reactions on Au irradiated by protons. See section 3.3 for explanatory notes of experimental data.

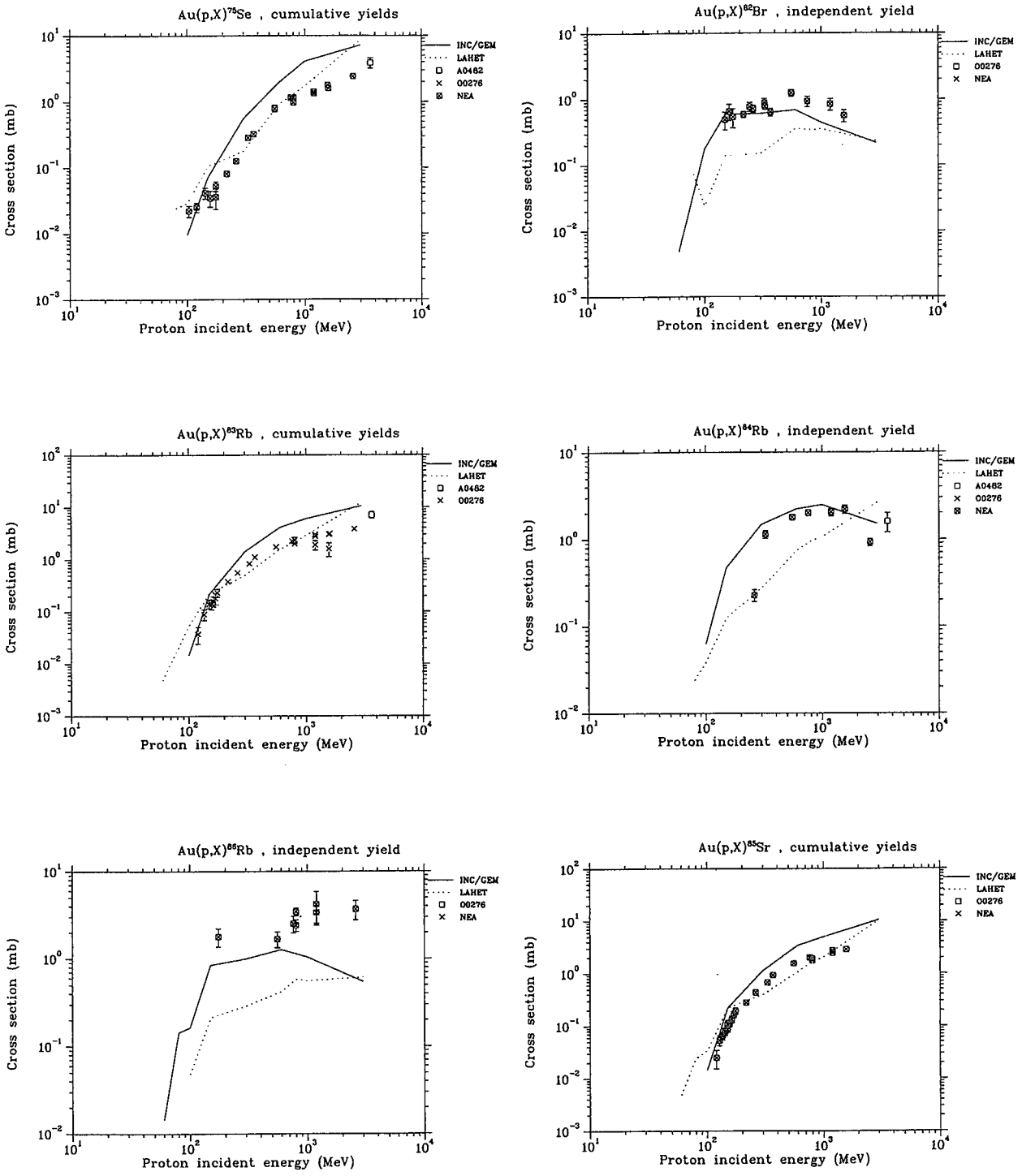

Fig. 28 Excitation functions for nuclide production from the reactions on Au irradiated by protons. See section 3.3 for explanatory notes of experimental data.

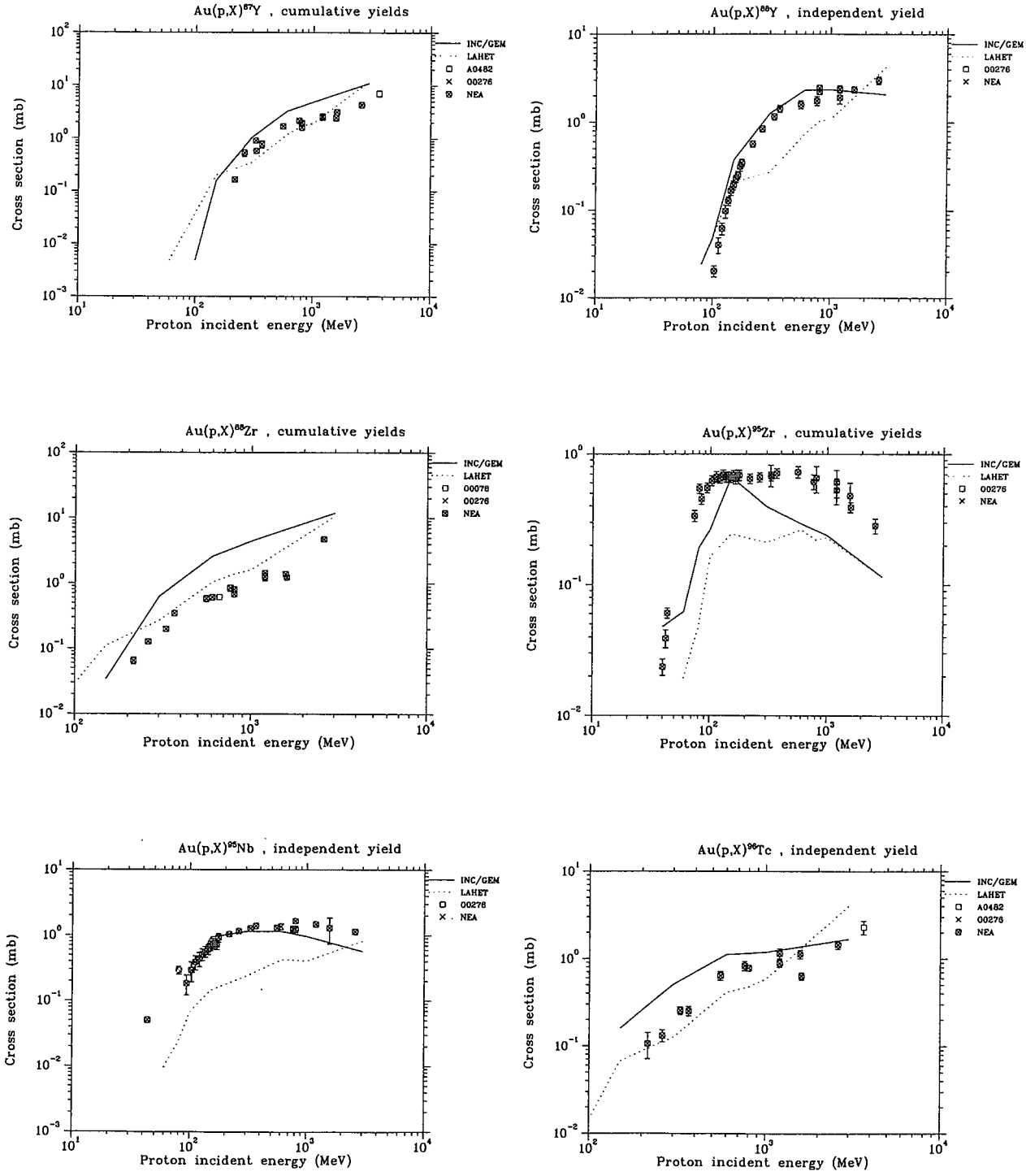

Fig. 29 Excitation functions for nuclide production from the reactions on Au irradiated by protons. See section 3.3 for explanatory notes of experimental data.

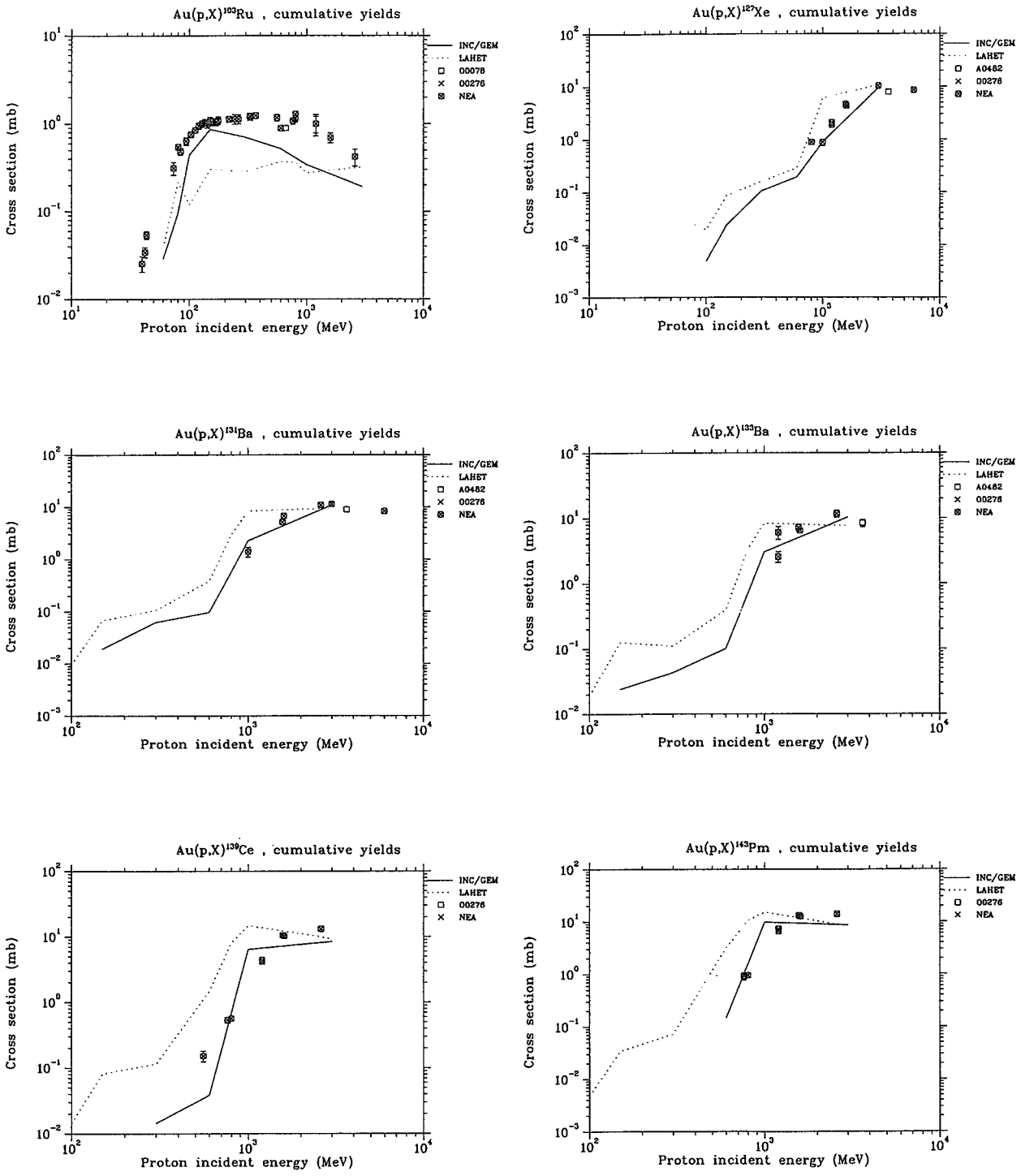

Fig. 30 Excitation functions for nuclide production from the reactions on Au irradiated by protons. See section 3.3 for explanatory notes of experimental data.

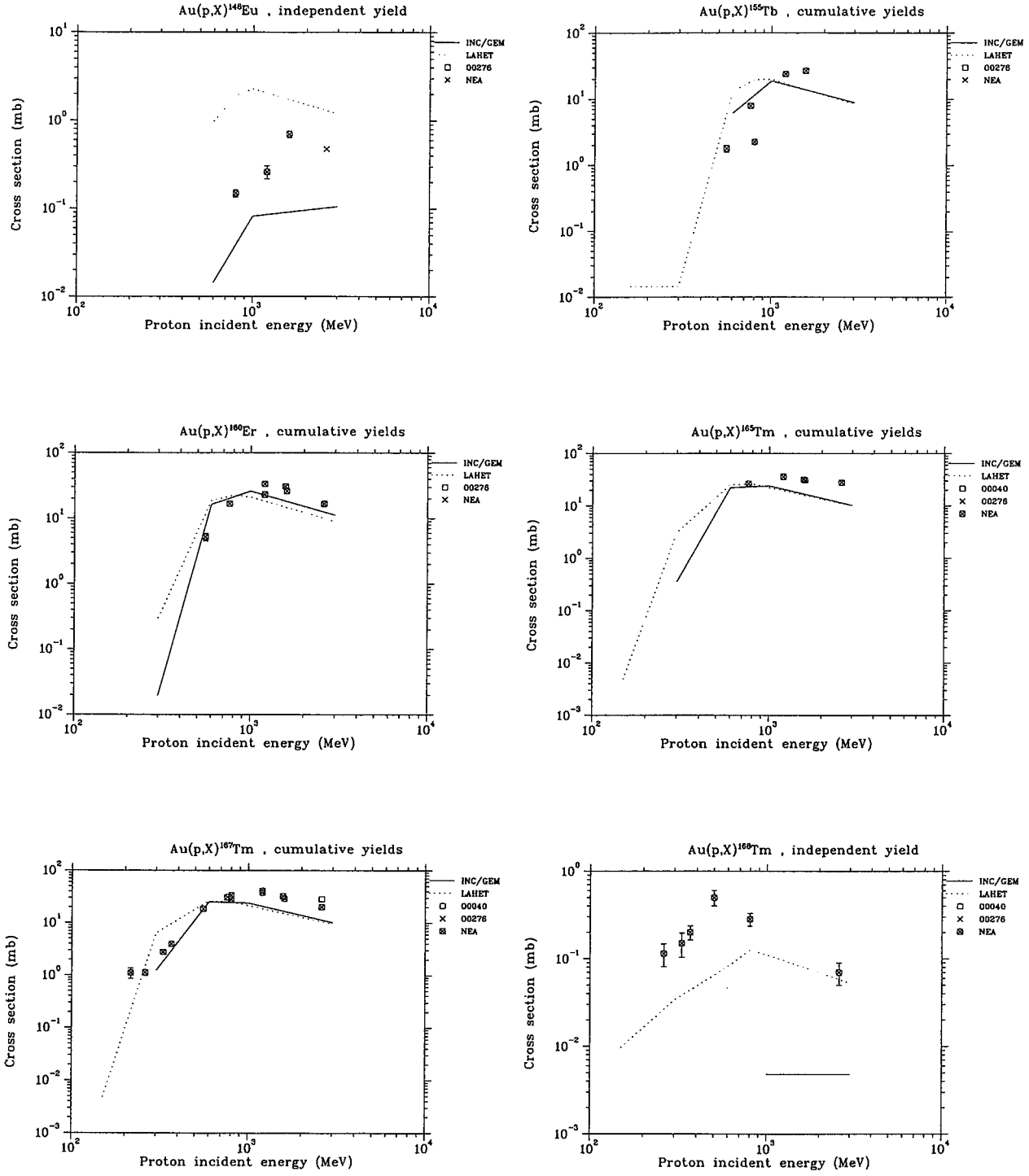

Fig. 31 Excitation functions for nuclide production from the reactions on Au irradiated by protons. See section 3.3 for explanatory notes of experimental data.

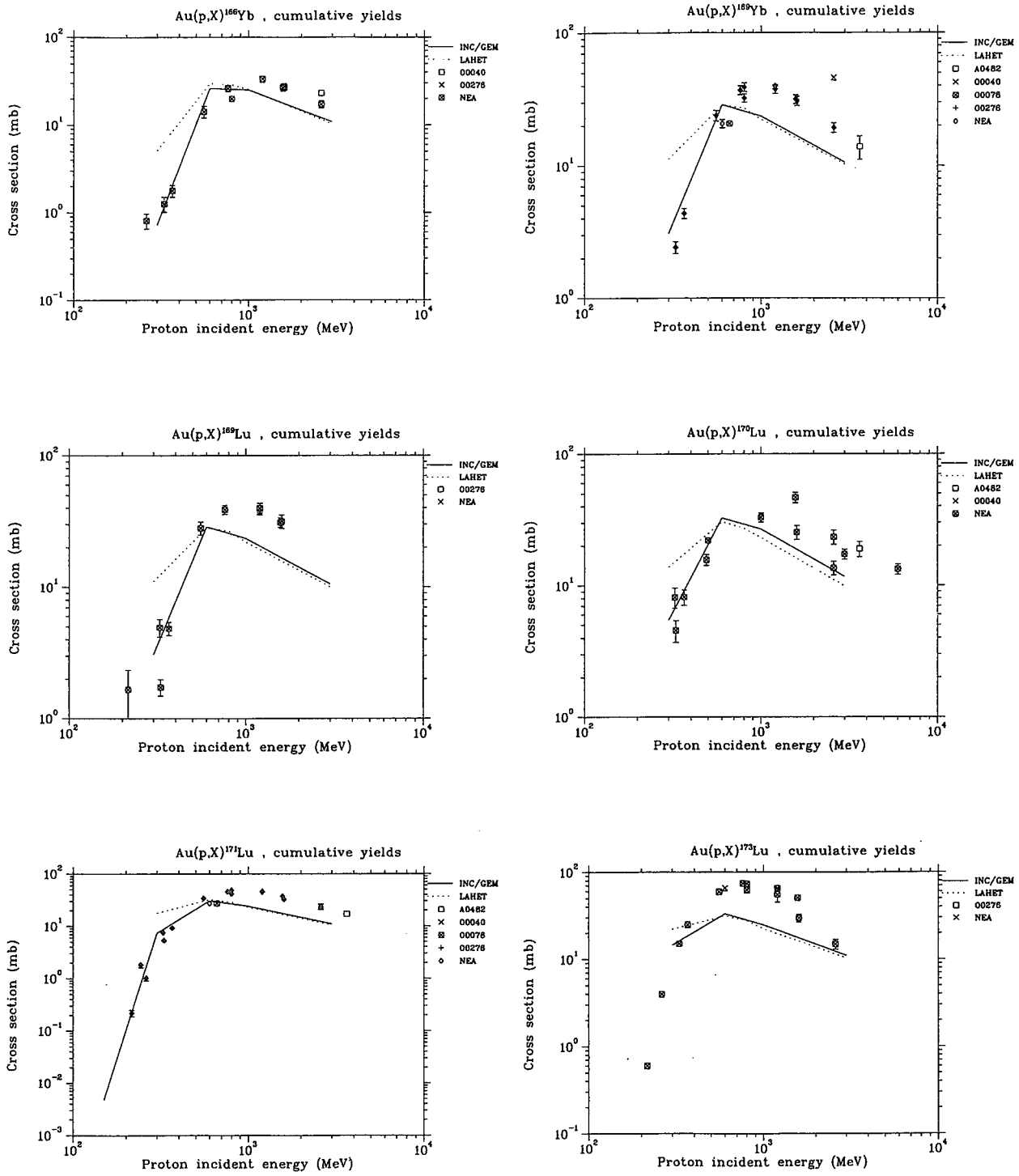

Fig. 32 Excitation functions for nuclide production from the reactions on Au irradiated by protons. See section 3.3 for explanatory notes of experimental data.

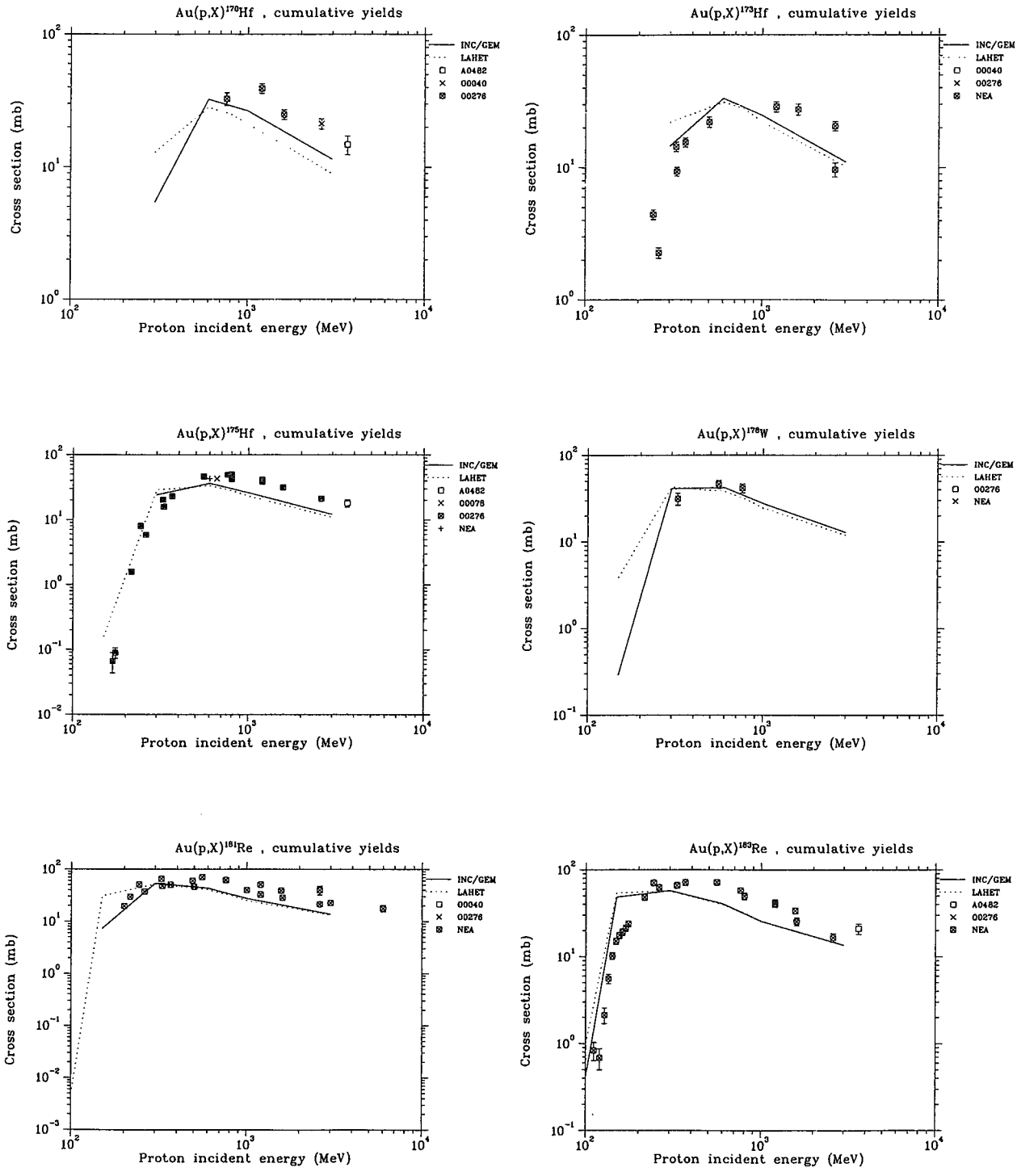

Fig. 33 Excitation functions for nuclide production from the reactions on Au irradiated by protons. See section 3.3 for explanatory notes of experimental data.

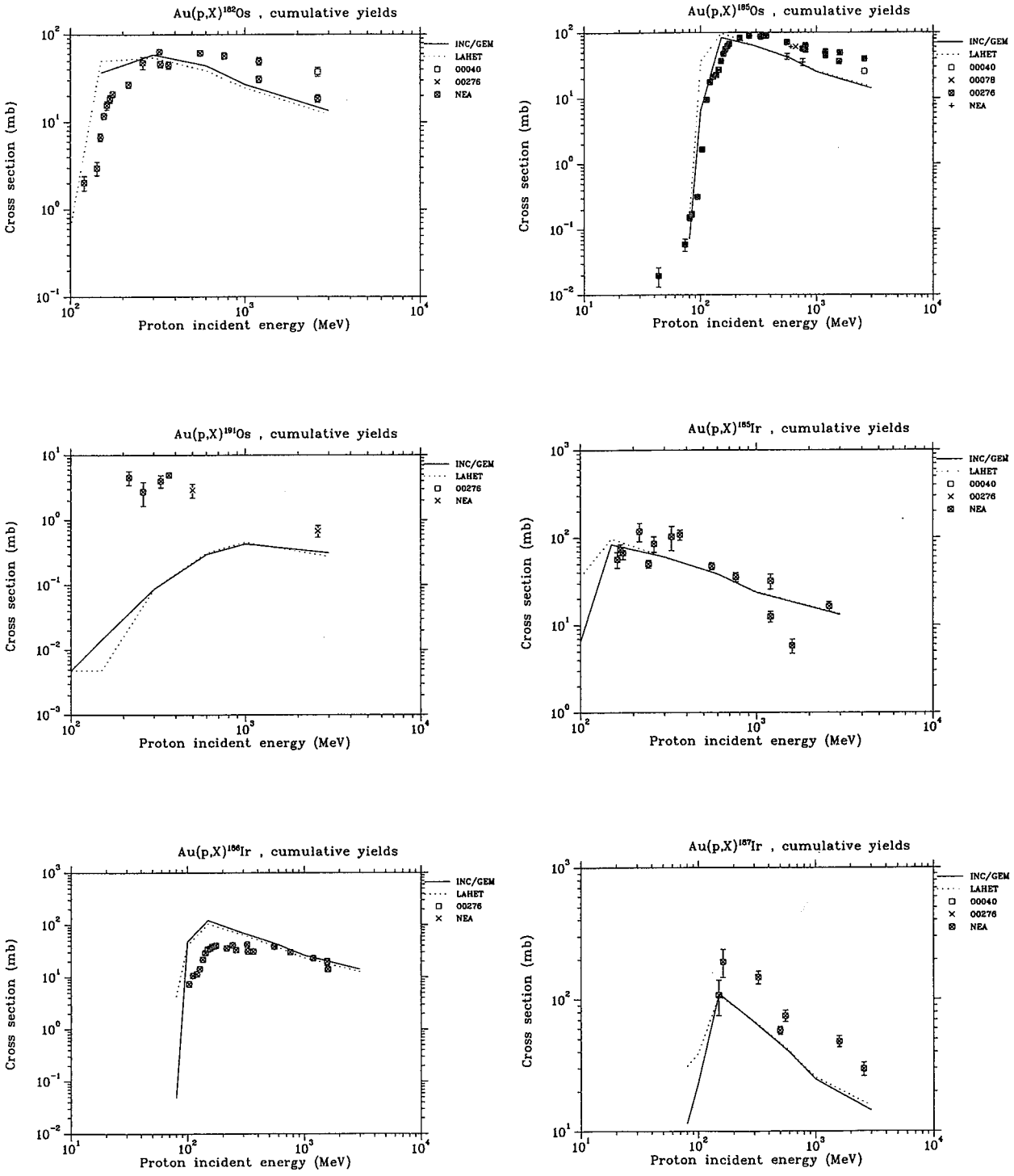

Fig. 34 Excitation functions for nuclide production from the reactions on Au irradiated by protons. See section 3.3 for explanatory notes of experimental data.

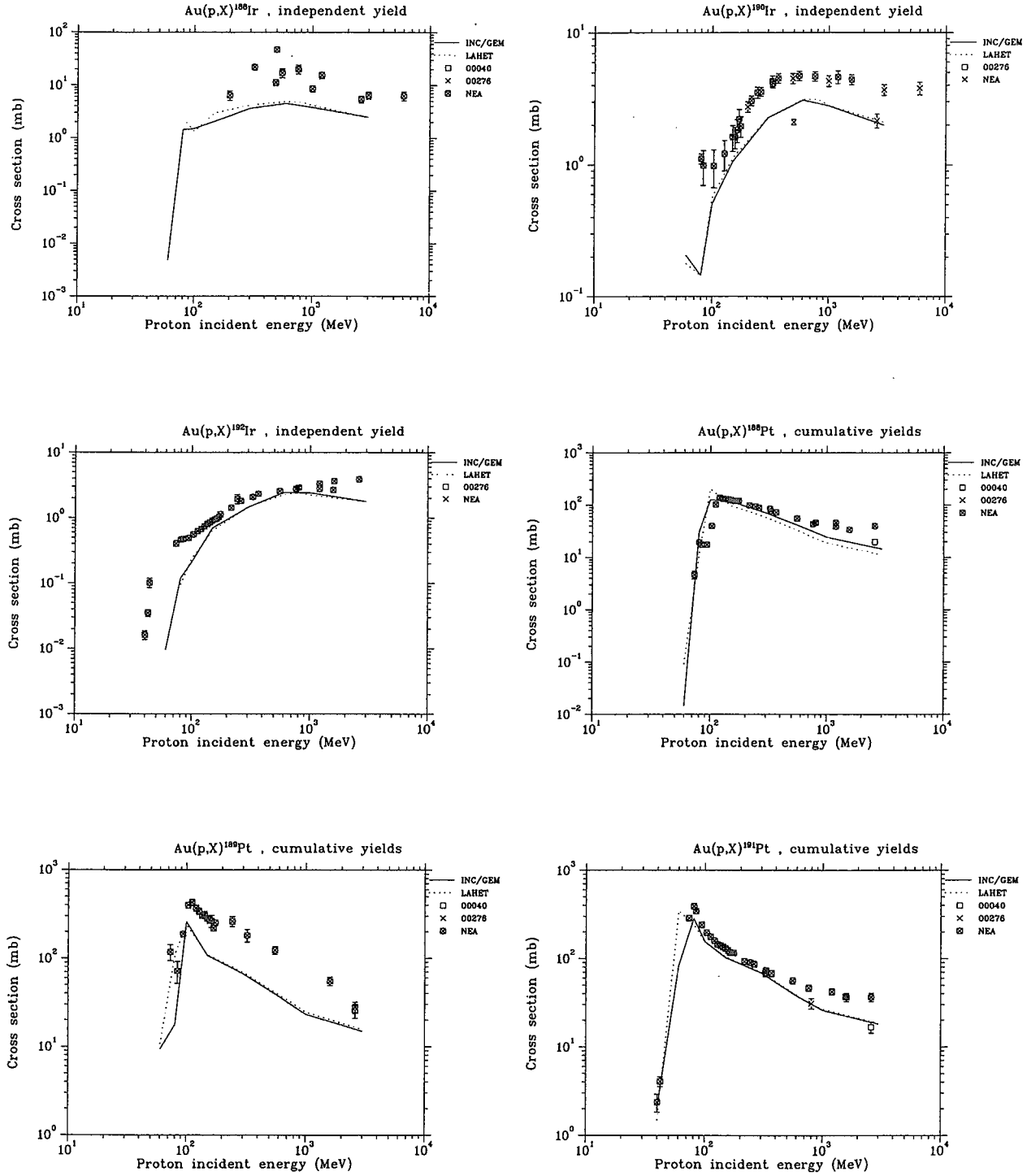

Fig. 35 Excitation functions for nuclide production from the reactions on Au irradiated by protons. See section 3.3 for explanatory notes of experimental data.

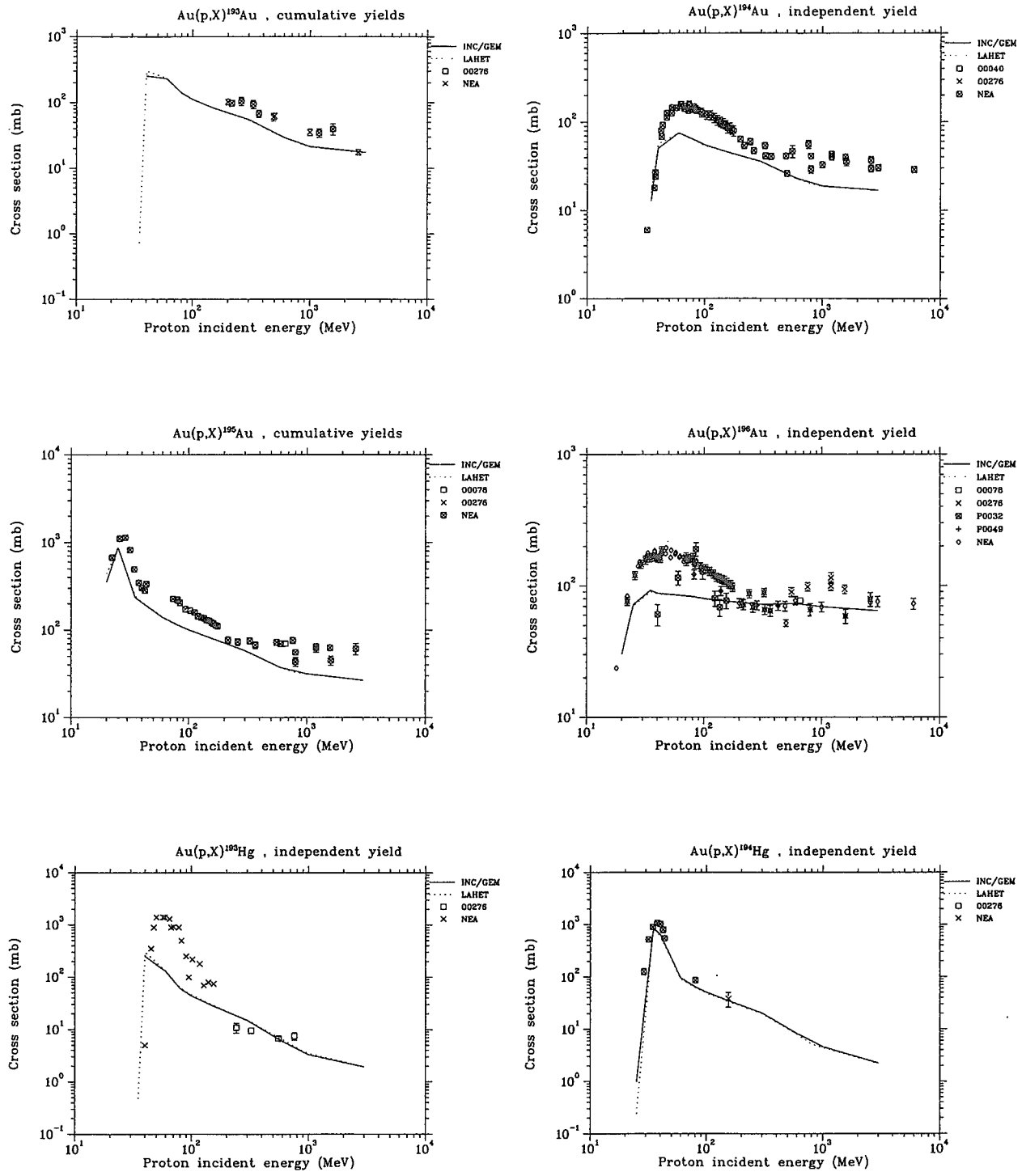

Fig. 36 Excitation functions for nuclide production from the reactions on Au irradiated by protons. See section 3.3 for explanatory notes of experimental data.

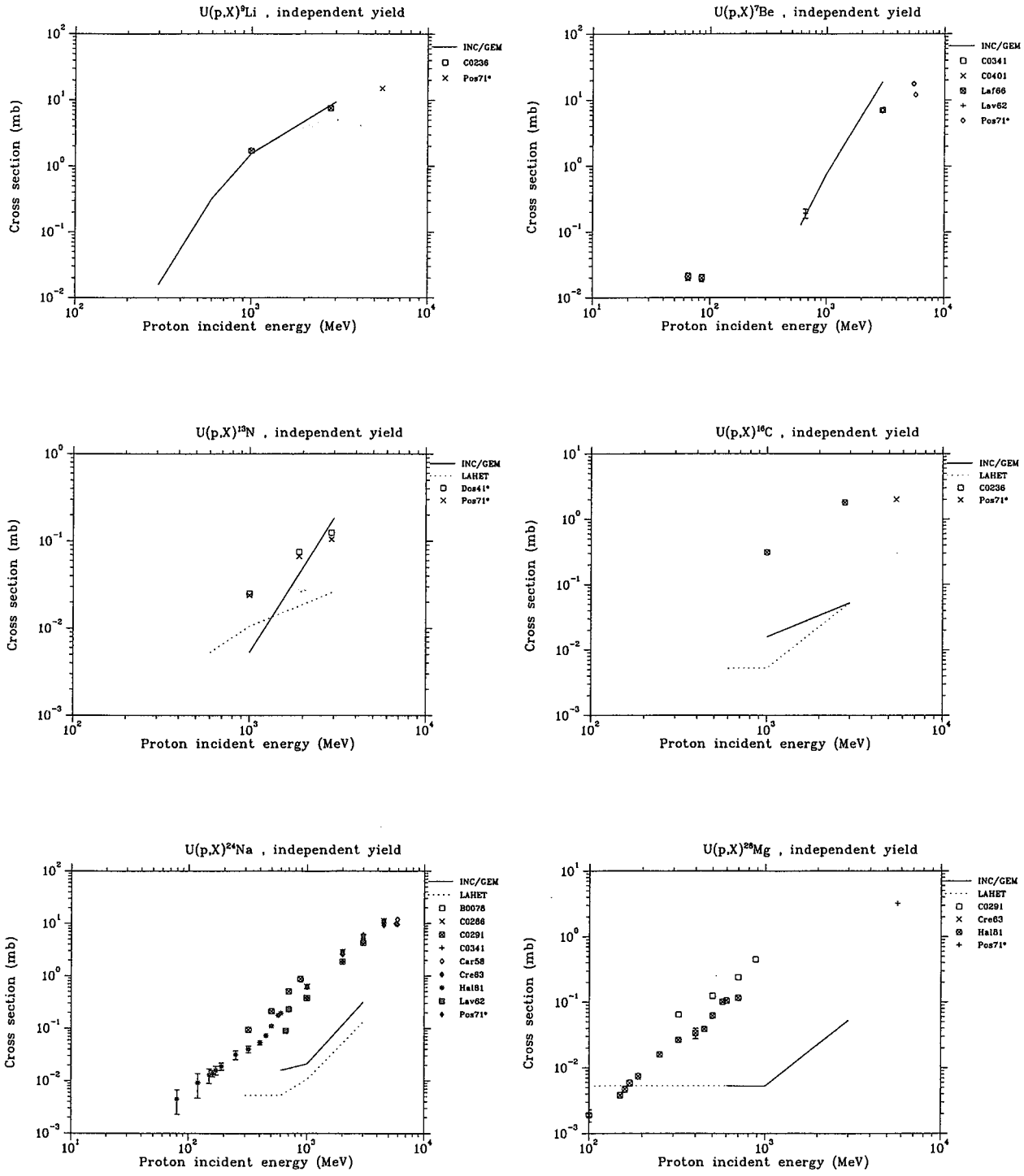

Fig. 37 Excitation functions for nuclide production from the reactions on U irradiated by protons. See section 3.3 for explanatory notes of experimental data.

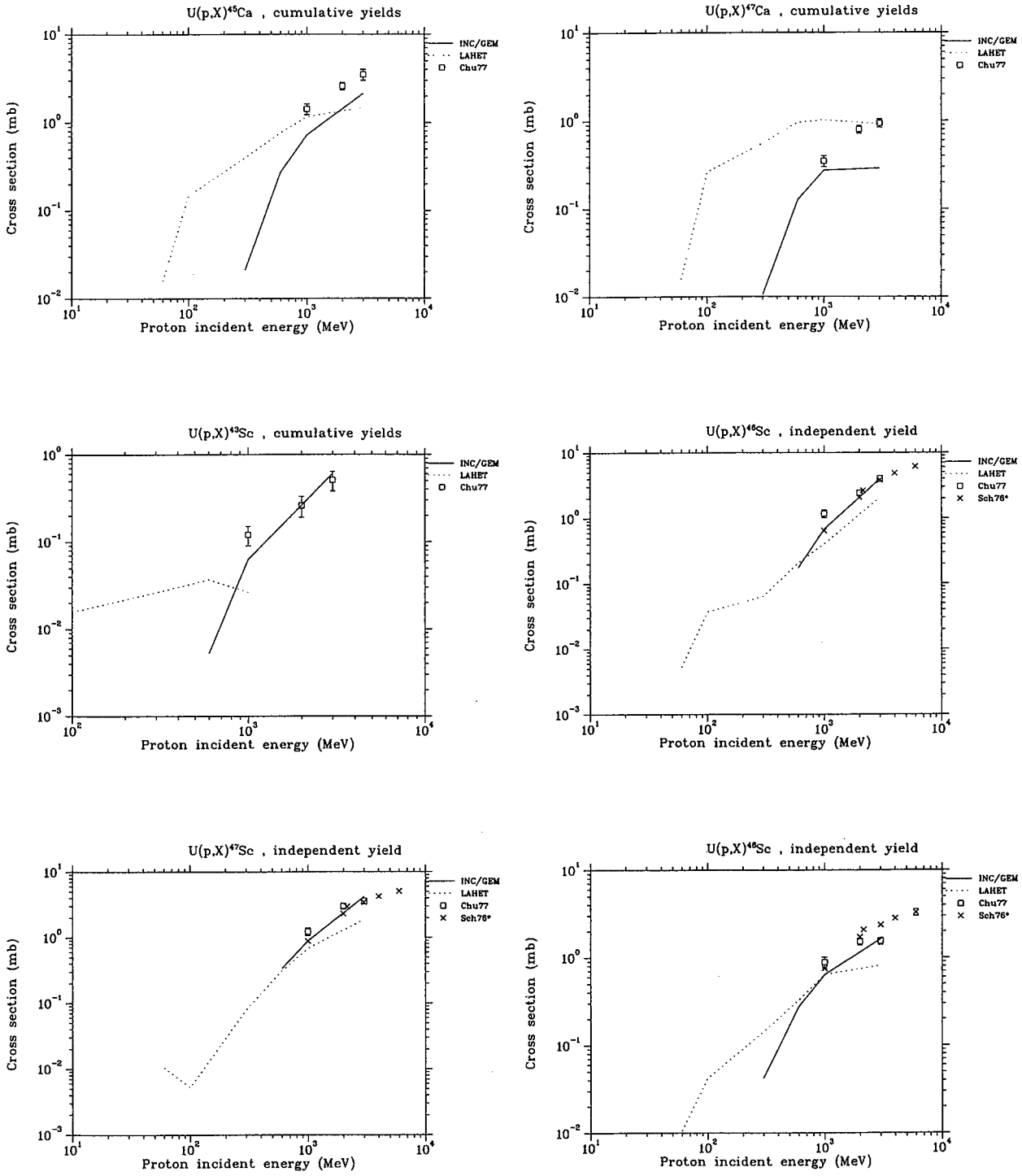

Fig. 38 Excitation functions for nuclide production from the reactions on U irradiated by protons. See section 3.3 for explanatory notes of experimental data.

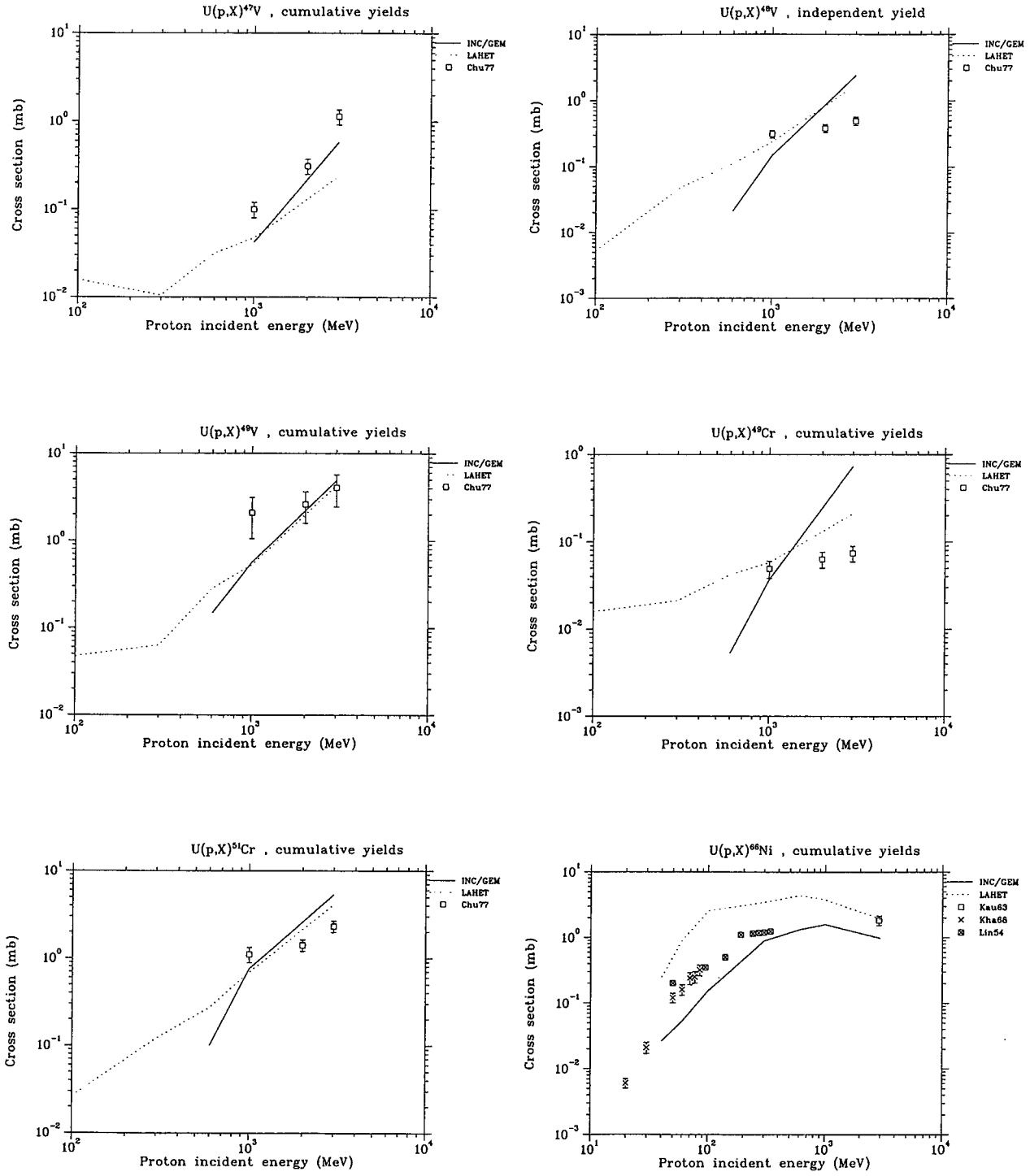

Fig. 39 Excitation functions for nuclide production from the reactions on U irradiated by protons. See section 3.3 for explanatory notes of experimental data.

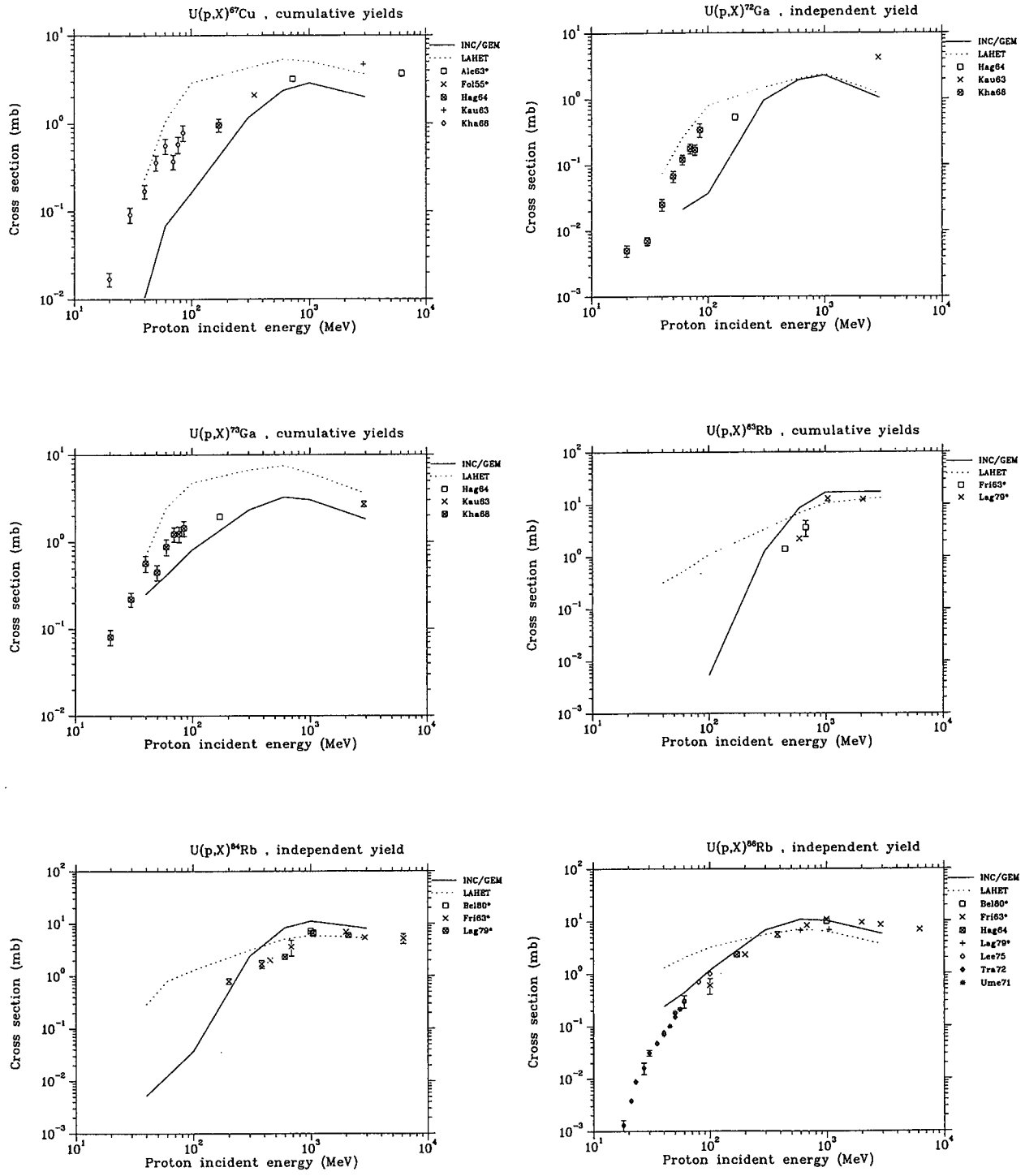

Fig. 40 Excitation functions for nuclide production from the reactions on U irradiated by protons. See section 3.3 for explanatory notes of experimental data.

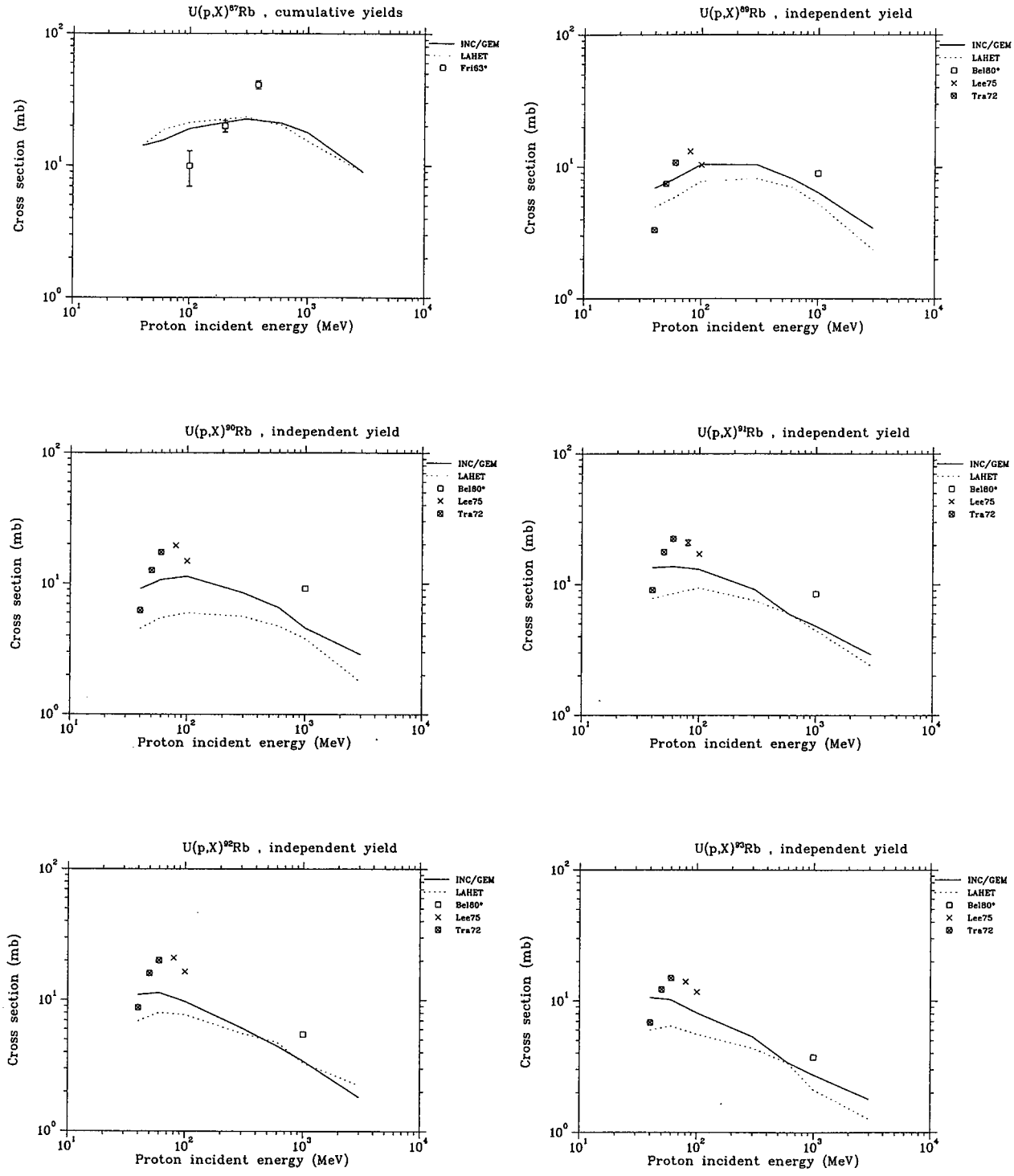

Fig. 41 Excitation functions for nuclide production from the reactions on U irradiated by protons. See section 3.3 for explanatory notes of experimental data.

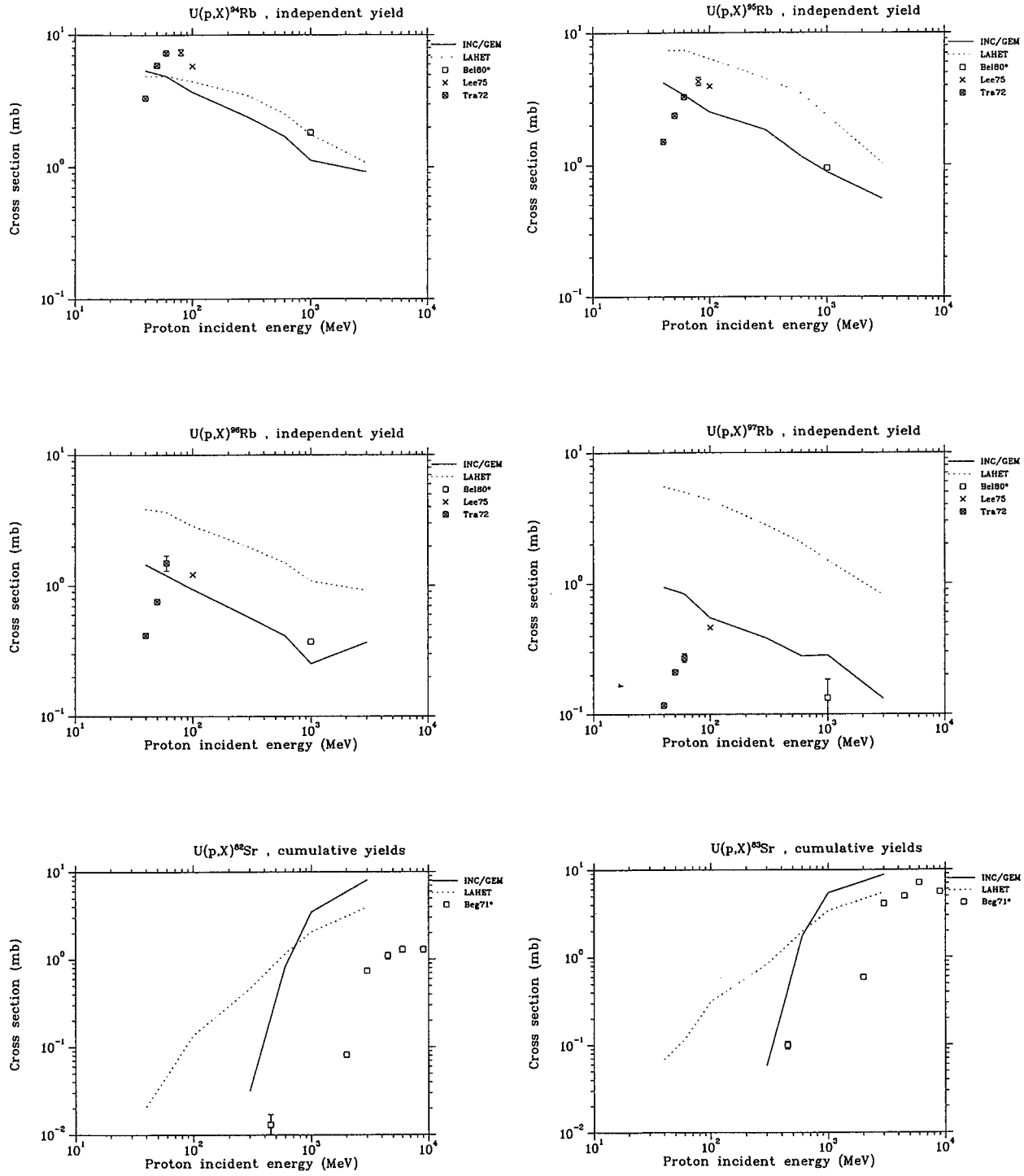

Fig. 42 Excitation functions for nuclide production from the reactions on U irradiated by protons. See section 3.3 for explanatory notes of experimental data.

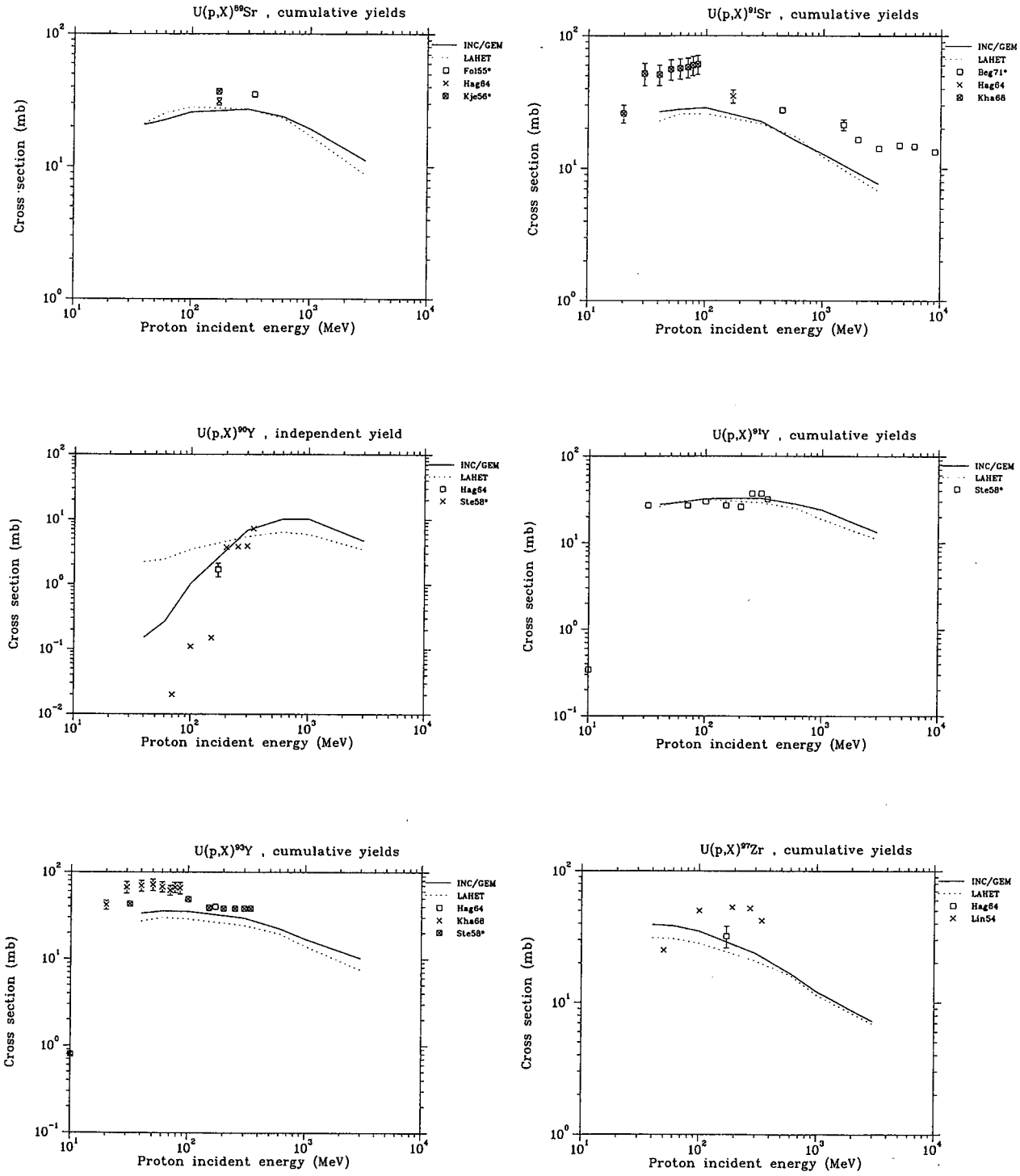

Fig. 43 Excitation functions for nuclide production from the reactions on U irradiated by protons. See section 3.3 for explanatory notes of experimental data.

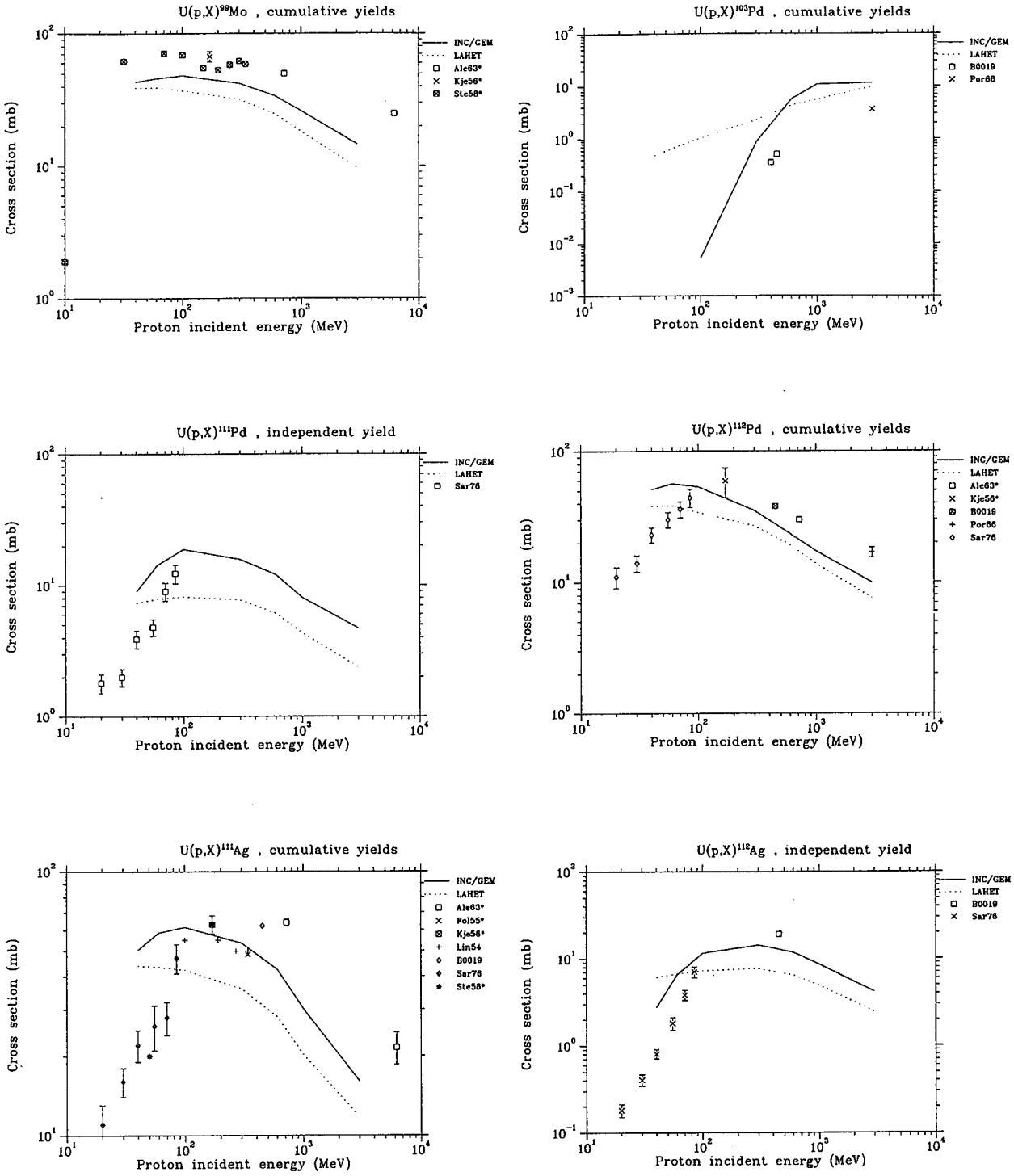

Fig. 44 Excitation functions for nuclide production from the reactions on U irradiated by protons. See section 3.3 for explanatory notes of experimental data.

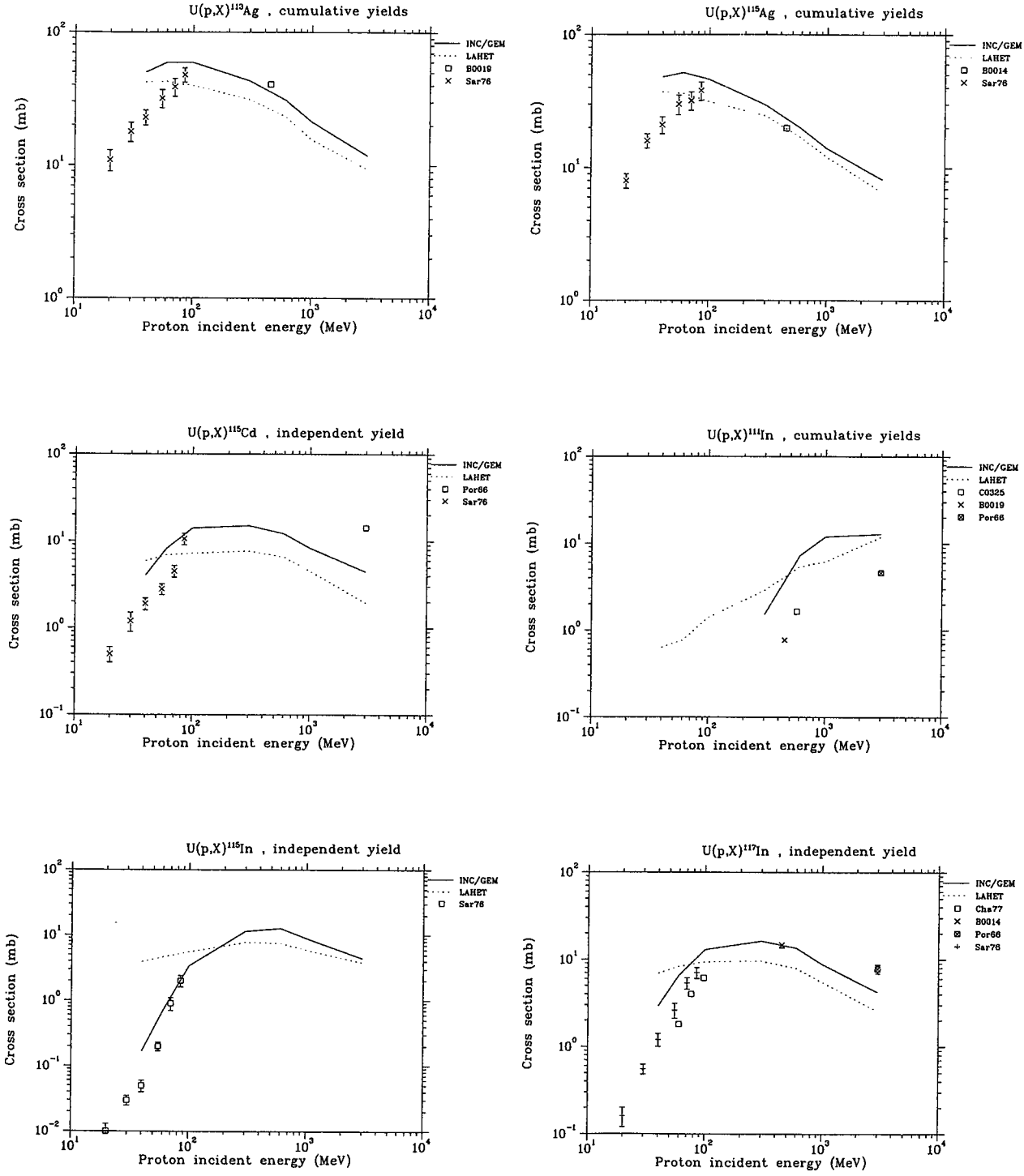

Fig. 45 Excitation functions for nuclide production from the reactions on U irradiated by protons. See section 3.3 for explanatory notes of experimental data.

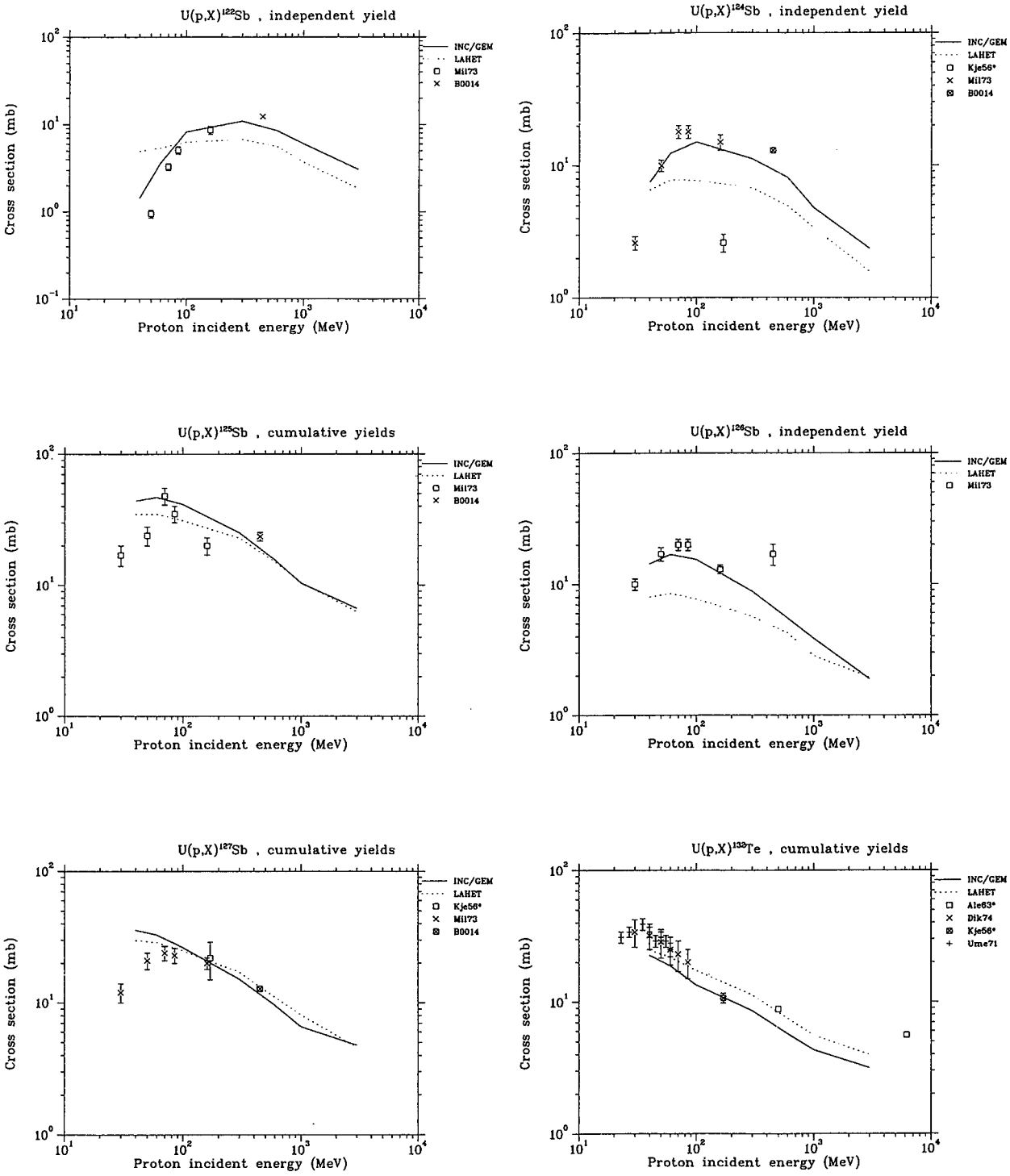

Fig. 46 Excitation functions for nuclide production from the reactions on U irradiated by protons. See section 3.3 for explanatory notes of experimental data.

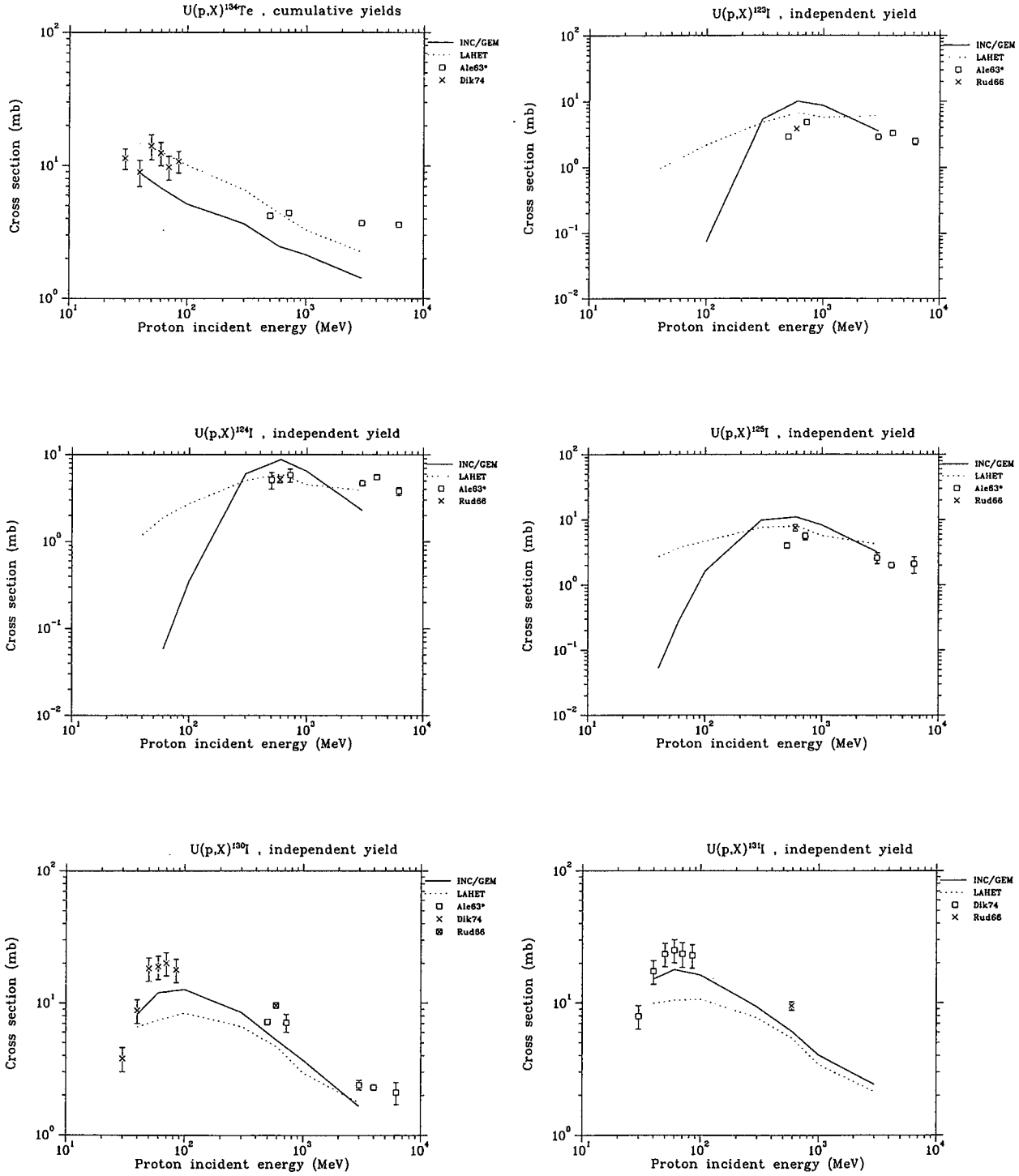

Fig. 47 Excitation functions for nuclide production from the reactions on U irradiated by protons. See section 3.3 for explanatory notes of experimental data.

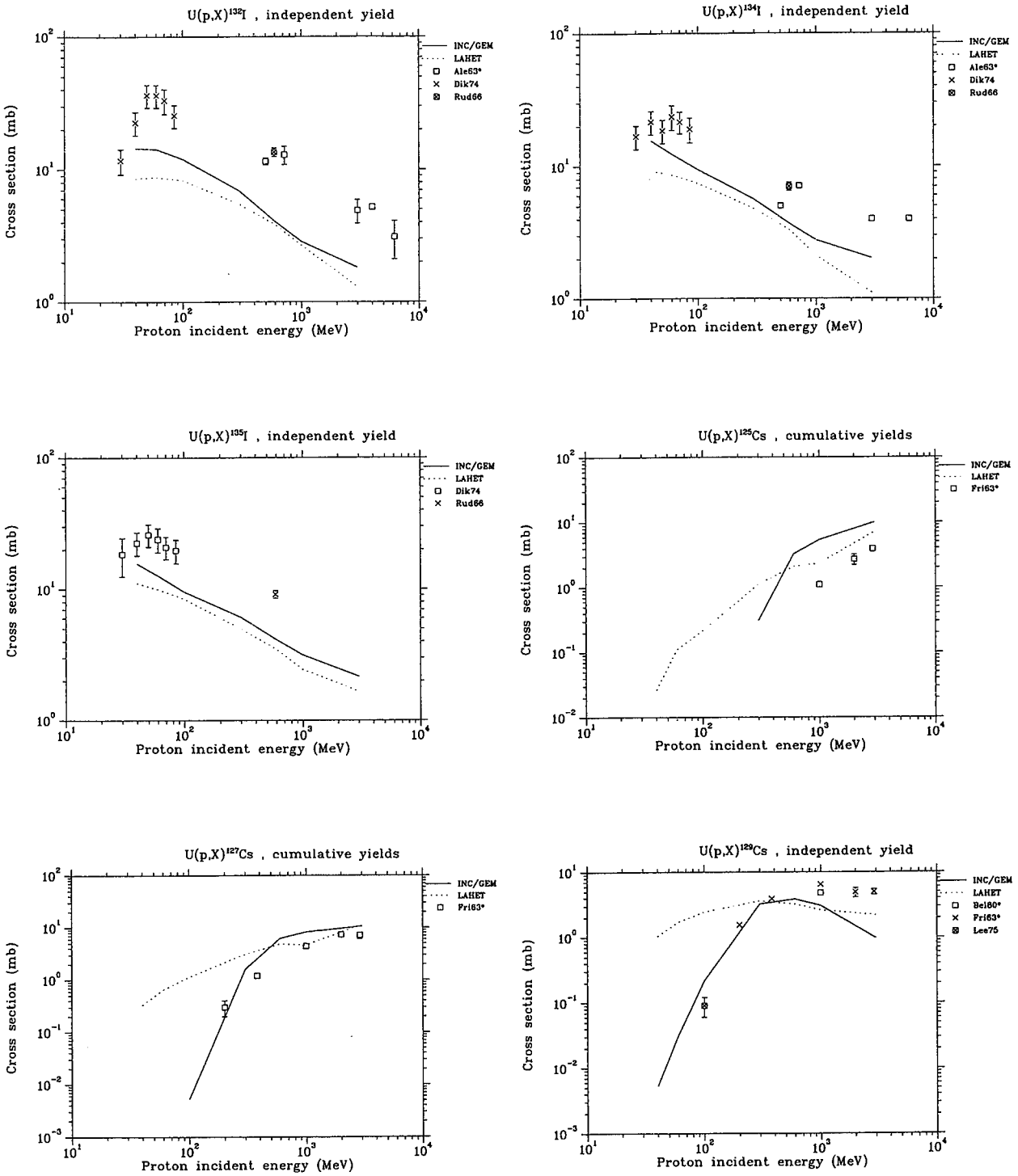

Fig. 48 Excitation functions for nuclide production from the reactions on U irradiated by protons. See section 3.3 for explanatory notes of experimental data.

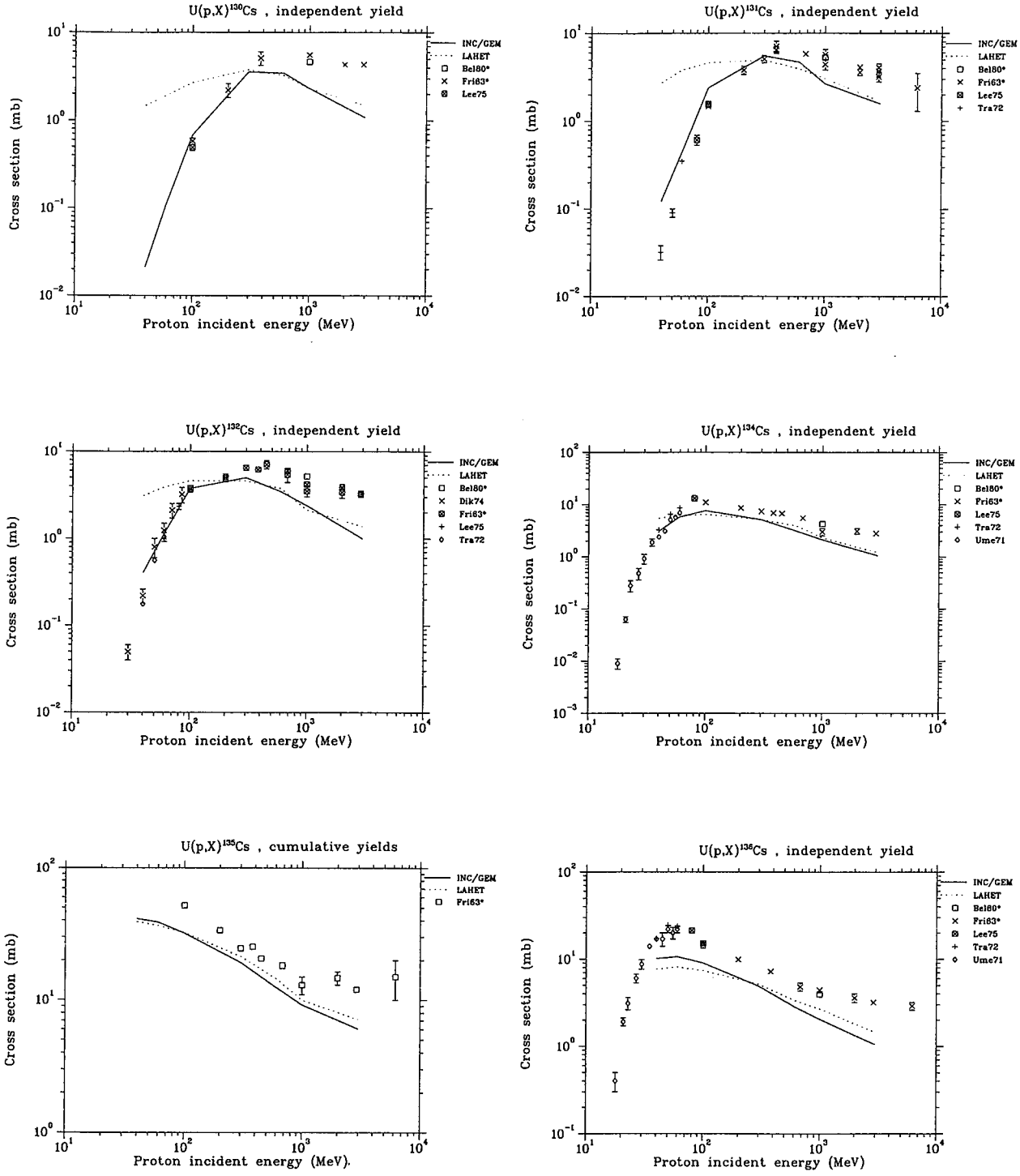

Fig. 49 Excitation functions for nuclide production from the reactions on U irradiated by protons. See section 3.3 for explanatory notes of experimental data.

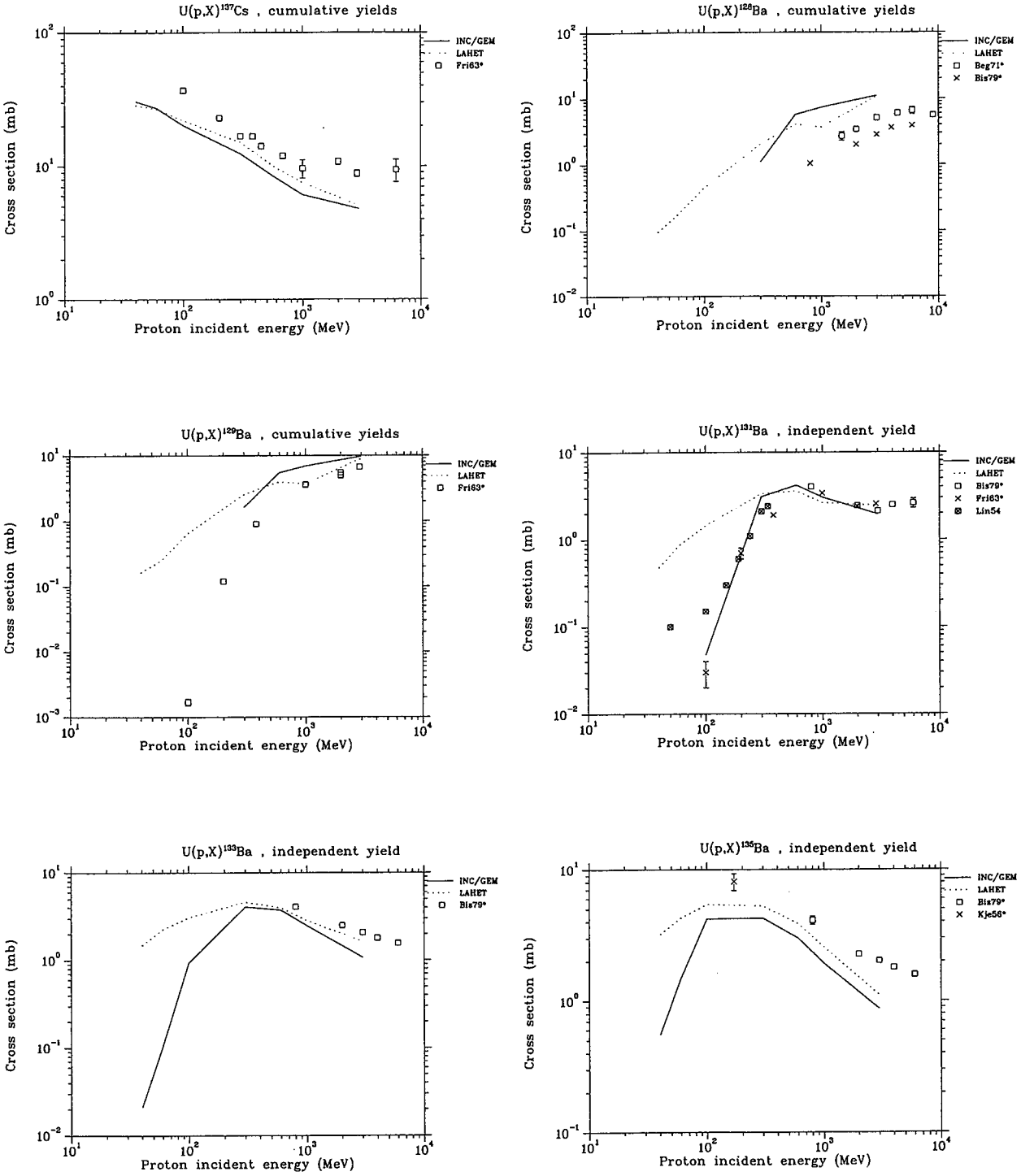

Fig. 50 Excitation functions for nuclide production from the reactions on U irradiated by protons. See section 3.3 for explanatory notes of experimental data.

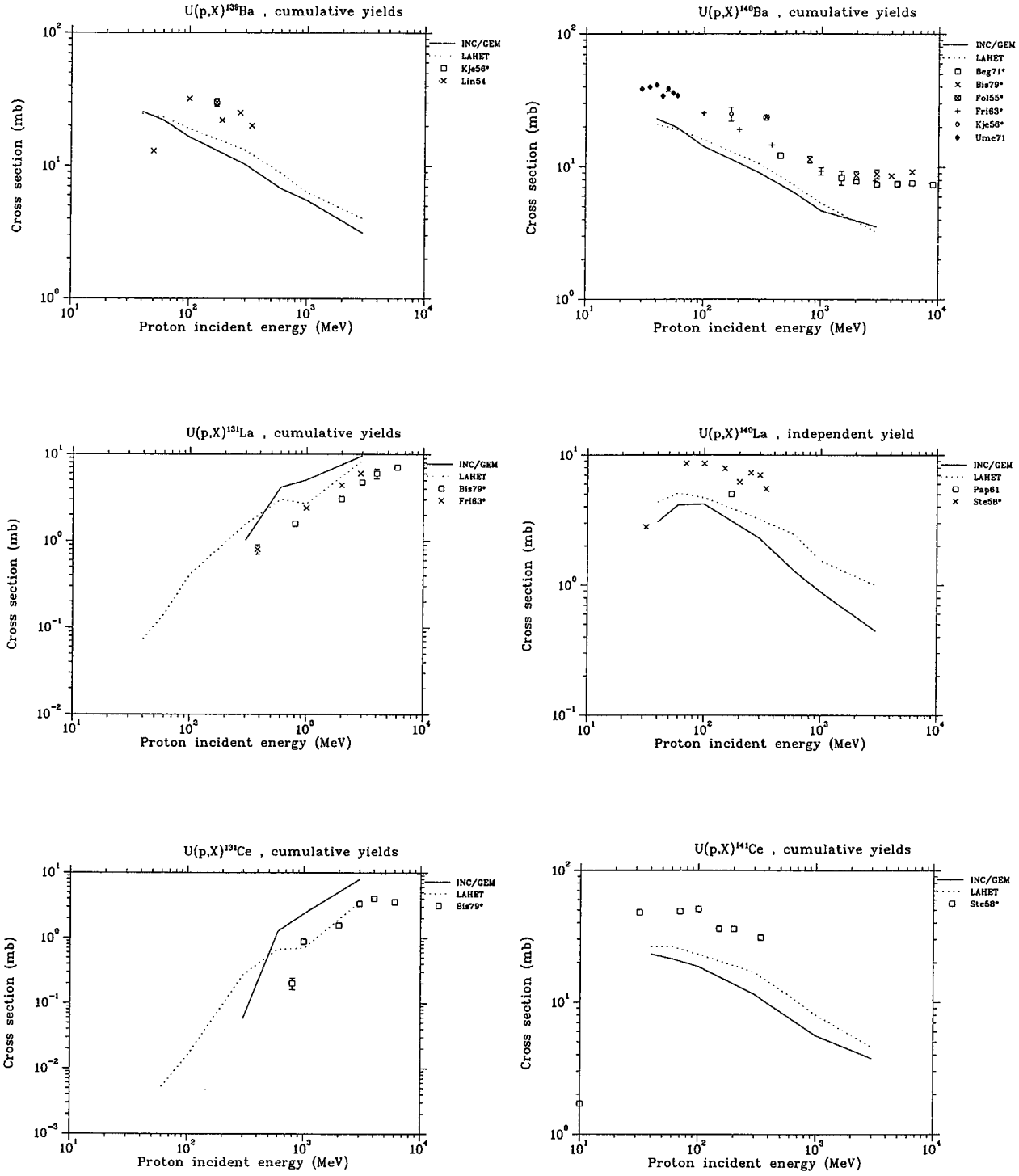

Fig. 51 Excitation functions for nuclide production from the reactions on U irradiated by protons. See section 3.3 for explanatory notes of experimental data.

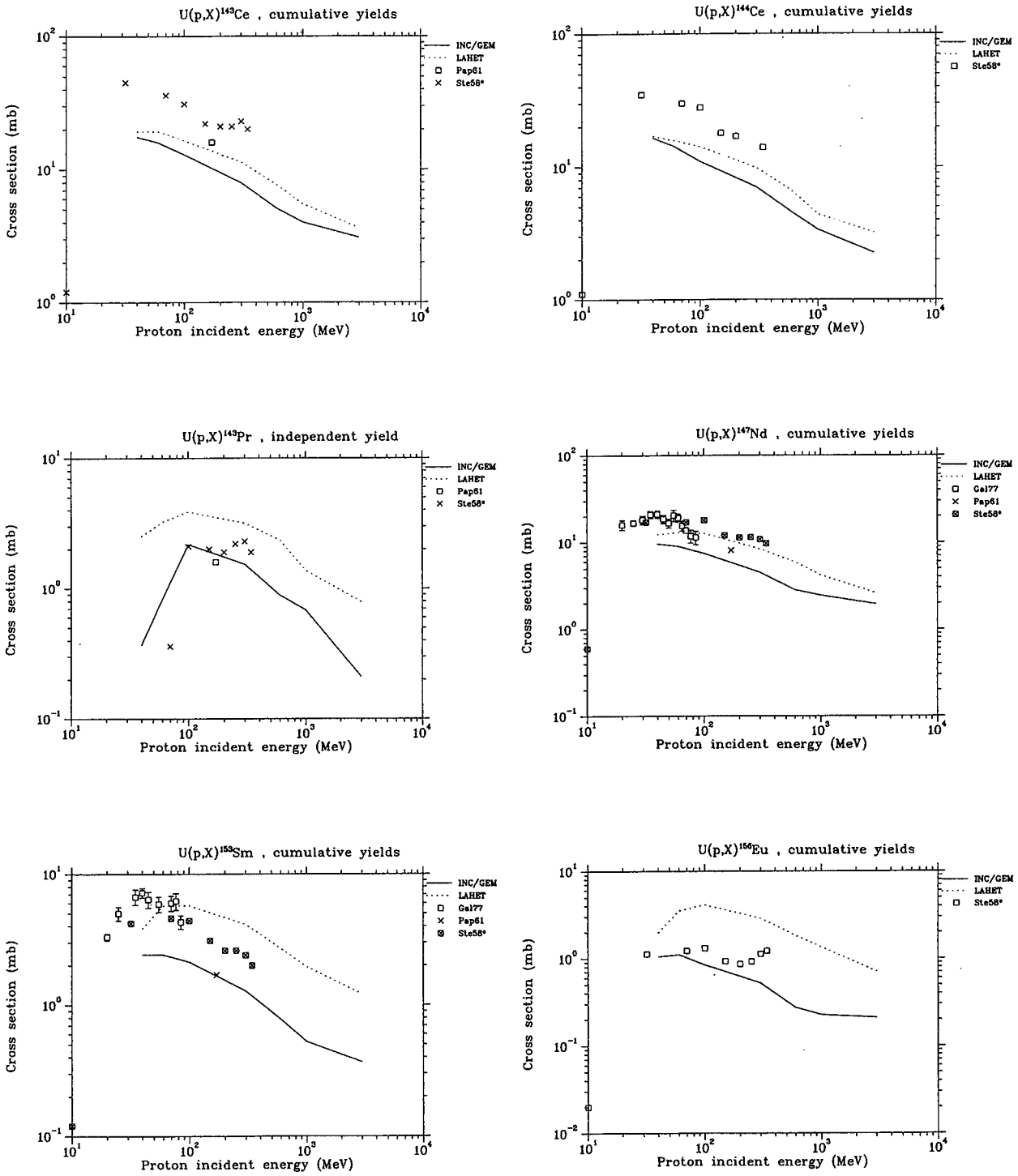

Fig. 52 Excitation functions for nuclide production from the reactions on U irradiated by protons. See section 3.3 for explanatory notes of experimental data.

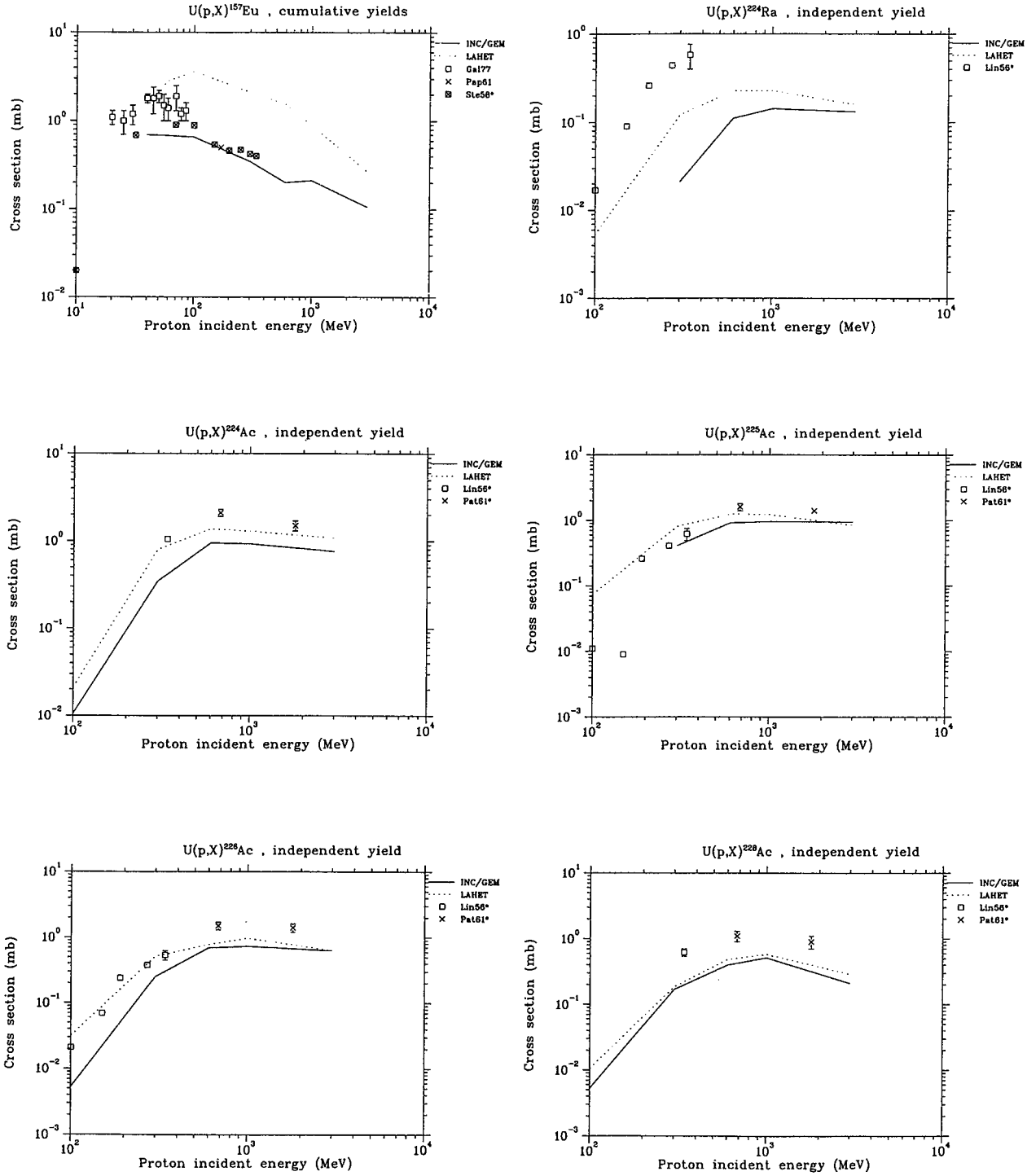

Fig. 53 Excitation functions for nuclide production from the reactions on U irradiated by protons. See section 3.3 for explanatory notes of experimental data.

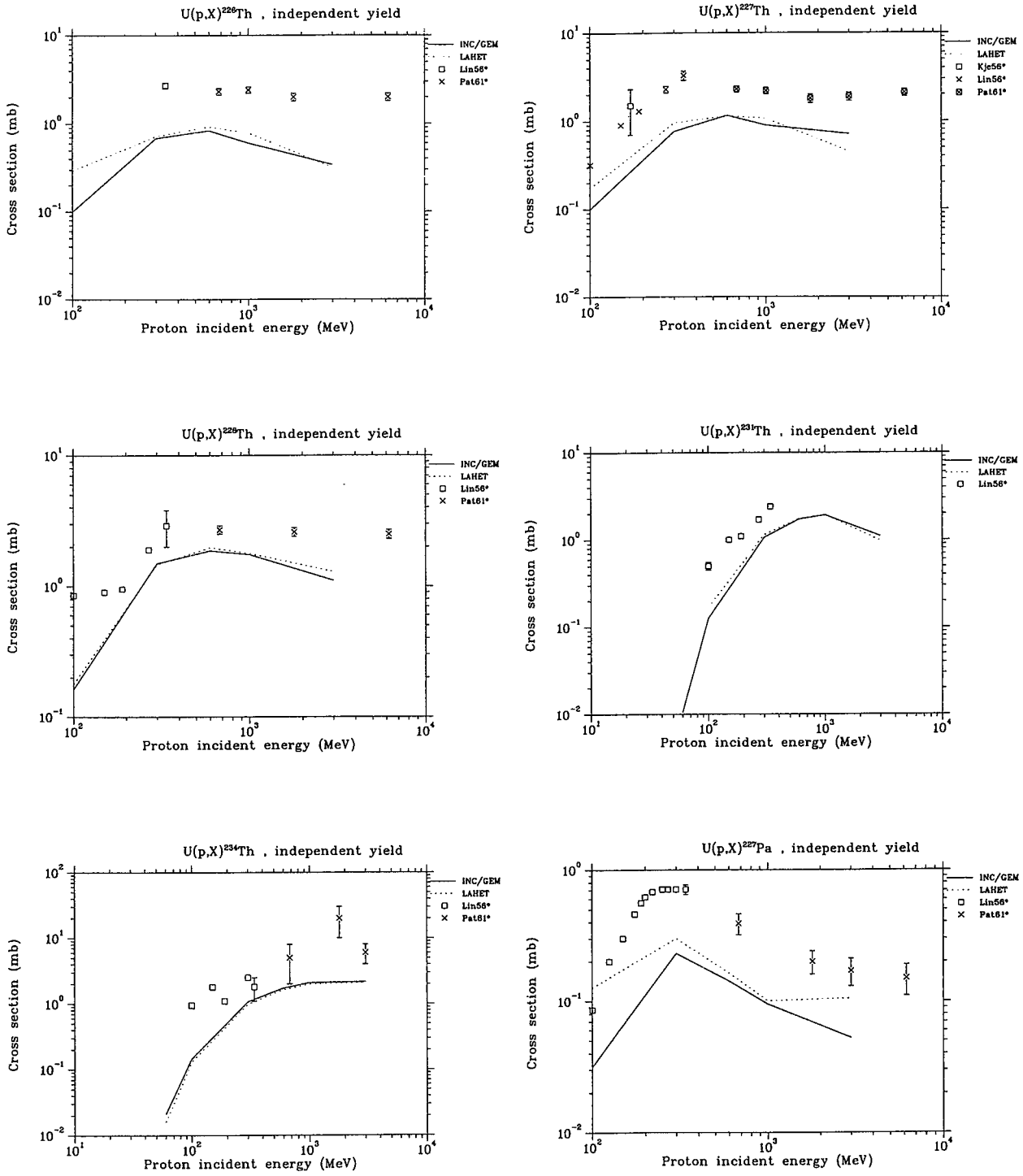

Fig. 54 Excitation functions for nuclide production from the reactions on U irradiated by protons. See section 3.3 for explanatory notes of experimental data.

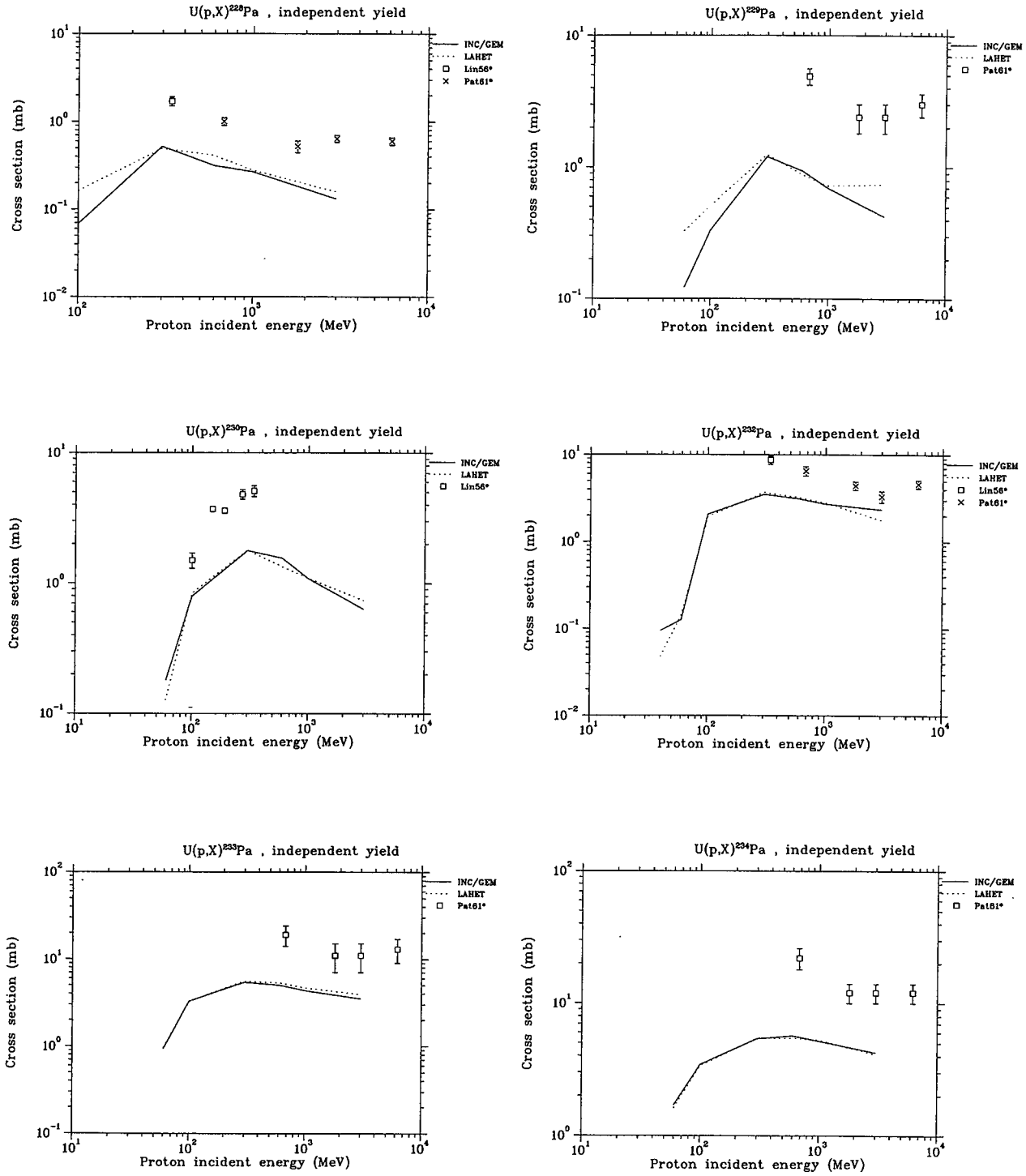

Fig. 55 Excitation functions for nuclide production from the reactions on U irradiated by protons. See section 3.3 for explanatory notes of experimental data.

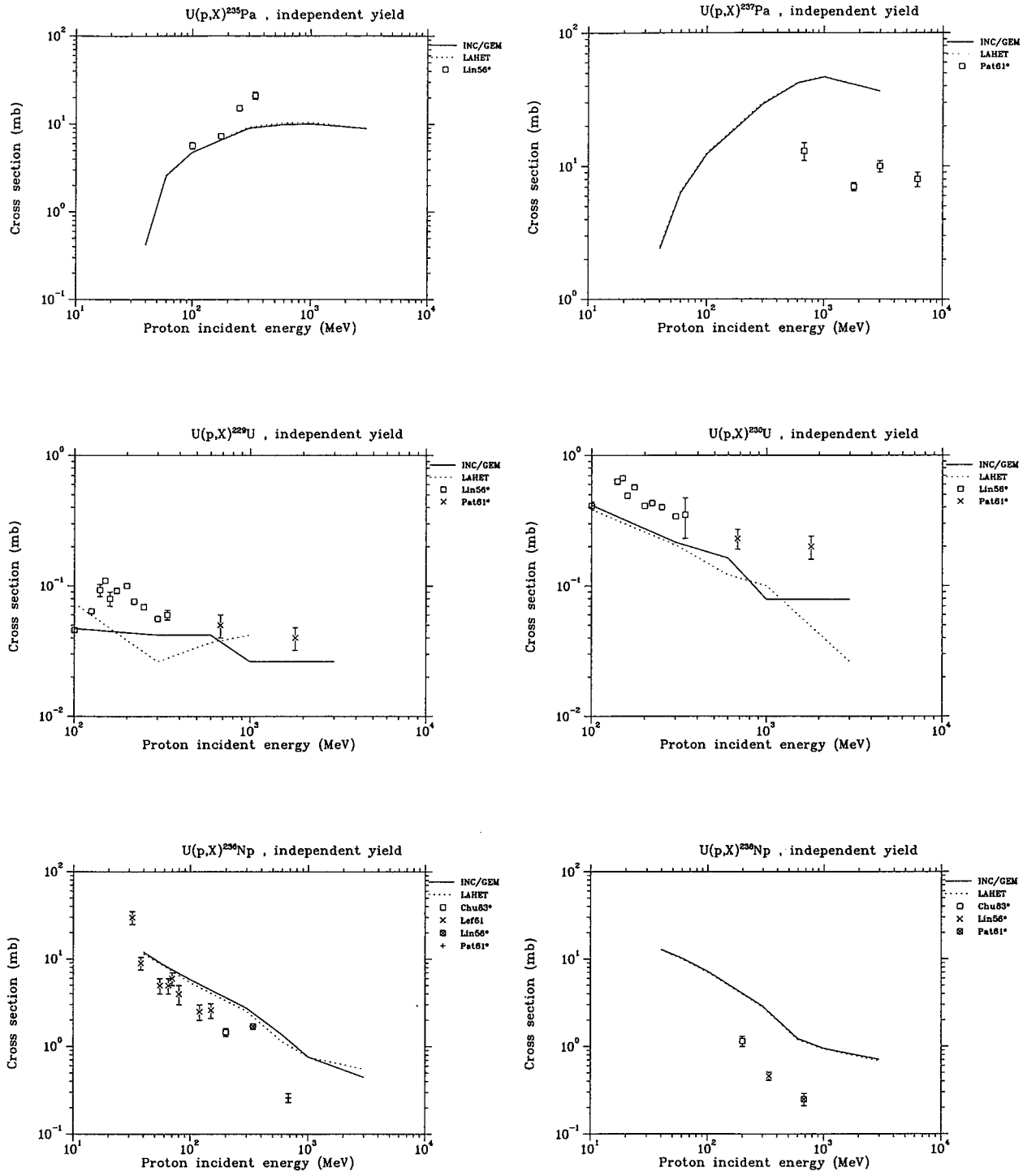

Fig. 56 Excitation functions for nuclide production from the reactions on U irradiated by protons. See section 3.3 for explanatory notes of experimental data.

This is a blank page.

Appendix A: The List of References for the Experimental Data

Ale63 J. M. Alexander, C. Baltzinger, and M. F. Gazdik. *"Cross section and Recoil Studies of Reactions of U^{238} with Protons of 0.5 to 6.2 GeV"*. Phys. Rev. **129** (1963) 1826–1834

Bee83 P. A. Beely and L. Yaffe. *"Isotopic and neutron yields of products from the asymmetric and near-symmetric proton-induced fission of ^{233}U and ^{235}U"*. Phys. Rev. C. **28** (1983) 1188–1205.

Beg71 K. Beg and N. T. Porile. *"Energy Dependence of the Recoil Properties of Products form the Interaction of U^{238} with 0.45-11.5-GeV Protons"*. Phys. Rev. C **3** (1971) 1631–1645

Bel80 B. N. Belyaev, V. D. Domkin, Y. G. Korobulin, L. N. Androneko, and G. E. Solyakin. *"Rb and Cs Isotopic Distributions from 1 GeV Proton Fission of ^{238}U"*. Nucl. Phys. A **348** (1980) 479–492

Bis79 S. Biswas and N. T. Porile. *"Formation of isobaric nuclides with A= 131 in the interaction of ^{238}U with 0.8-11.5 GeV protons"*. Phys. Rev. C **20** (1979) 1467–1478

Chu83 Y. Y. Chu and M. L. Zhou. *"Comparison of the (p,xn) cross sections from ^{238}U, ^{235}U and ^{232}Th targets irradiated with 200 MeV protons"*. IEEE. Trans. Nuc. Sci. **30** (1983) 1153–1155

Dos41 I. Dostrovsky, Z. Fraenkel, and J. Hudis. *"Formation of N^{13} in High-Energy Nuclear Reactions"*. Phys. Rev. **123** (1961) 1452–1458

Fol55 R. L. Folger, P. C. Stevenson, and G. T. Seaborg. *"High-Energy Proton Spallation-Fission of Uranium"*. Phys. Rev **98** (1955) 107–120

Fri63 G. Friedlander, K Friedman, B. Gordon, and L. Yaffe. *"Excitation Functions and Nuclear Charge Dispersion in the Fission of Uranium by 0.1- to 6.2-GeV Protons"*. Phys. Rev. **129** (1963) 1809–1825

Hud70 J. Hudis, T. Kirsten, R. W. Stoenner, and O. A. Schaeffer. *"Yields of Stable and Radioactive Rare-Gas Isotopes Formed by 3- and 29-GeV Proton Bombardment of Cu, Ag, Au, and U"*. Phys. Rev. C **1** (1970) 2019–2030

Kje56 A. Kjelberg and A. C. Pappas. *"Fission of uranium with 170 MeV protons"*. Nucl. Phys. **1** (1956) 322–325

Kor70 R. Korteling and R. Kiefer. *"Production of ^{32}P and ^{33}P from Various Targets with 550-MeV Protons"*. Phys. Rev. C **2** (1970) 957–963

Lag79 M. Lagarde-Simonoff and G. N. Simonoff. *"Cross sections and recoil properties of $^{83,84,86}Rb$ formed by 0.6-21 GeV ^{1}H reactions with targets of Y to U"*. Phys. Rev. C **20** (1979) 1498–1516

Lin56 M. Lindner and R. N. Osborne. *"Nonfission Inelastic Events in Uranium and Thorium Induced by High-Energy Protons"*. Phys. Rev. **103** (1956) 378–385

Nik80 L. Nikkinen, B. P. Pathak, L. Lessard, and I. S. Grant. *"Independent yields of Rb, In, and Cs isotopes in the proton-induced fission of ^{232}Th"*. Phys. Rev. C. **22** (1980) 617–626.

Pat61 B. D. Pate and A. M. Poskanzer. *"Spallation of Uranium and Thorium Nuclei with Bev-Energy Protons"*. Phys. Rev. **123** (1961) 647–654

Pos71 A. M. Poskanzer, G. W. Butler, and E. K. Hyde. *"Fragment Production in the Interaction of 5.5-GeV Protons with Uranium"*. Phys. Rev. C **3** (1971) 882–904

Sch76 O. Scheidemann and N. T. Porile. *"Production of Sc nuclides in the interaction of ^{238}U with 1-300 GeV protons"*. Phys. Rev. C **14** (1976) 1534–1544

Ste58 P. C. Stevenson, H. G. Hicks, W. E. Nervik, and D. R. Nethaway. *"Further Radiochemical Studies of the High-Energy Fission Products"*. Phys. Rev. **111** (1958) 886–891

Yu73a Y. W. Yu and N. T. Porile. *"Charge Dispersion and Recoil Properties at A=131 from the Interaction of ^{238}U with 11.5-GeV Protons"*. Phys. Rev. C **7** (1973) 1597–1610

Yu74 Y. W. Yu and N. T. Porile. *"Interaction of ^{238}U with 300- and 11.5-GeV protons: Cross sections and recoil properties in the $A \sim 130$ mass region"*. Phys. Rev. C **10** (1974) 167–172

Yu75 Y. W. Yu, S. Biswas, and N. T. Porile. *"Nuclear reactions of ^{238}U with 300- and 11.5-GeV protons: Formation of nuclides in the A = 110-140 mass region"*. Phys. Rev. C **11** (1975) 2111–2113

国際単位系 (SI) と換算表

表1　SI基本単位および補助単位

量	名称	記号
長さ	メートル	m
質量	キログラム	kg
時間	秒	s
電流	アンペア	A
熱力学温度	ケルビン	K
物質量	モル	mol
光度	カンデラ	cd
平面角	ラジアン	rad
立体角	ステラジアン	sr

表2　SIと併用される単位

名称	記号
分，時，日	min，h，d
度，分，秒	°，′，″
リットル	l，L
トン	t
電子ボルト	eV
原子質量単位	u

1 eV＝1.60218×10^{-19} J

1 u＝1.66054×10^{-27} kg

表3　固有の名称をもつSI組立単位

量	名称	記号	他のSI単位による表現
周波数	ヘルツ	Hz	s^{-1}
力	ニュートン	N	m·kg/s^2
圧力，応力	パスカル	Pa	N/m^2
エネルギー，仕事，熱量	ジュール	J	N·m
工率，放射束	ワット	W	J/s
電気量，電荷	クーロン	C	A·s
電位，電圧，起電力	ボルト	V	W/A
静電容量	ファラド	F	C/V
電気抵抗	オーム	Ω	V/A
コンダクタンス	ジーメンス	S	A/V
磁束	ウェーバ	Wb	V·s
磁束密度	テスラ	T	Wb/m^2
インダクタンス	ヘンリー	H	Wb/A
セルシウス温度	セルシウス度	℃	
光束	ルーメン	lm	cd·sr
照度	ルクス	lx	lm/m^2
放射能	ベクレル	Bq	s^{-1}
吸収線量	グレイ	Gy	J/kg
線量当量	シーベルト	Sv	J/kg

表4　SIと共に暫定的に維持される単位

名称	記号
オングストローム	Å
バーン	b
バール	bar
ガル	Gal
キュリー	Ci
レントゲン	R
ラド	rad
レム	rem

1 Å＝0.1 nm＝10^{-10} m

1 b＝100 fm^2＝10^{-28} m^2

1 bar＝0.1 MPa＝10^5 Pa

1 Gal＝1 cm/s^2＝10^{-2} m/s^2

1 Ci＝3.7×10^{10} Bq

1 R＝2.58×10^{-4} C/kg

1 rad＝1 cGy＝10^{-2} Gy

1 rem＝1 cSv＝10^{-2} Sv

表5　SI接頭語

倍数	接頭語	記号
10^{18}	エクサ	E
10^{15}	ペタ	P
10^{12}	テラ	T
10^{9}	ギガ	G
10^{6}	メガ	M
10^{3}	キロ	k
10^{2}	ヘクト	h
10^{1}	デカ	da
10^{-1}	デシ	d
10^{-2}	センチ	c
10^{-3}	ミリ	m
10^{-6}	マイクロ	μ
10^{-9}	ナノ	n
10^{-12}	ピコ	p
10^{-15}	フェムト	f
10^{-18}	アト	a

（注）

1. 表1－5は「国際単位系」第5版，国際度量衡局 1985年刊行による。ただし，1 eVおよび1 uの値はCODATAの1986年推奨値によった。
2. 表4には海里，ノット，アール，ヘクタールも含まれているが日常の単位なのでここでは省略した。
3. barは，JISでは流体の圧力を表わす場合に限り表2のカテゴリーに分類されている。
4. EC閣僚理事会指令ではbar，barnおよび「血圧の単位」mmHgを表2のカテゴリーに入れている。

換算表

力	N(=10^5 dyn)	kgf	lbf
	1	0.101972	0.224809
	9.80665	1	2.20462
	4.44822	0.453592	1

粘度　1 Pa·s(N·s/m^2)＝10 P(ポアズ)(g/(cm·s))

動粘度　1 m^2/s＝10^4 St(ストークス)(cm^2/s)

圧力	MPa(=10 bar)	kgf/cm^2	atm	mmHg(Torr)	lbf/in^2(psi)
	1	10.1972	9.86923	7.50062×10^3	145.038
	0.0980665	1	0.967841	735.559	14.2233
	0.101325	1.03323	1	760	14.6959
	1.33322×10^{-4}	1.35951×10^{-3}	1.31579×10^{-3}	1	1.93368×10^{-2}
	6.89476×10^{-3}	7.03070×10^{-2}	6.80460×10^{-2}	51.7149	1

エネルギー・仕事・熱量	J(=10^7 erg)	kgf·m	kW·h	cal(計量法)	Btu	ft·lbf	eV
	1	0.101972	2.77778×10^{-7}	0.238889	9.47813×10^{-4}	0.737562	6.24150×10^{18}
	9.80665	1	2.72407×10^{-6}	2.34270	9.29487×10^{-3}	7.23301	6.12082×10^{19}
	3.6×10^6	3.67098×10^5	1	8.59999×10^5	3412.13	2.65522×10^6	2.24694×10^{25}
	4.18605	0.426858	1.16279×10^{-6}	1	3.96759×10^{-3}	3.08747	2.61272×10^{19}
	1055.06	107.586	2.93072×10^{-4}	252.042	1	778.172	6.58515×10^{21}
	1.35582	0.138255	3.76616×10^{-7}	0.323890	1.28506×10^{-3}	1	8.46233×10^{18}
	1.60218×10^{-19}	1.63377×10^{-20}	4.45050×10^{-26}	3.82743×10^{-20}	1.51857×10^{-22}	1.18171×10^{-19}	1

1 cal＝4.18605 J(計量法)

＝4.184 J　(熱化学)

＝4.1855 J　(15 °C)

＝4.1868 J(国際蒸気表)

仕事率　1 PS(仏馬力)

＝75 kgf·m/s

＝735.499 W

放射能	Bq	Ci
	1	2.70270×10^{-11}
	3.7×10^{10}	1

吸収線量	Gy	rad
	1	100
	0.01	1

照射線量	C/kg	R
	1	3876
	2.58×10^{-4}	1

線量当量	Sv	rem
	1	100
	0.01	1

(86年12月26日現在)